

Feasibility of Using Miniaturised Electromagnetic
Actuator in Small Air Pumps

By Lei Wang

A thesis submitted to



Auckland University of Technology

In fulfilment of the requirement of the degree of Master of
Engineering

May 2011

School of Engineering

Primary Supervisor: Professor Ahmed Al-Jumaily

STATEMENT OF ORIGINALITY

I hereby declare that this submission is my own work and that, to the best of my knowledge and belief, it contains no material previously published or written by another person nor material which to a substantial extent has been accepted for the qualification of any other degree or diploma of a university or other institution of higher learning, except where due acknowledgment is made'

_____ (Signed)

_____ (Date)

ACKNOWLEDGEMENTS

I would like to express my sincere thanks to my supervisor, Professor Ahmed Al-Jumaily for his incredible support, guidance and tremendously helpful suggestion to my research.

I would also like to express thanks to Mr. David white and Dr. Maximiano Ramos of IBtec at AUT for their valuable advice. I am grateful to Professor Olaf Diegel for his guidance, time and special support for manufacturing some of the components.

I must express my sincere thanks to the sixth floor Chemistry technicians for their assistance in providing the equipment and laboratory support. I also thank to the first and second floor mechanical workshop technicians for their support.

The studies performance could not have been complete without staffs of technical services group of school of engineering and colleagues of IBtec.

Finally, Thank to my wife without her this thesis would never have been written.

ABSTRACT

The feasibility of using an electromagnetic actuator as an important part in a portable diaphragm air pump is investigated. The ideal electromagnetic actuator will have capabilities of producing large deflection and high tuneable frequency. These two characteristics make the actuator very attractive for the present application. Much effort has been put into the development of the proposed diaphragm air pump because it is easily integrated into the complex system.

The characteristics of the magnetic field of the electromagnetic coils are thoroughly investigated in order to complete the design optimization for the proposed electromagnetic actuator. As the base of the design optimization for the proposed planar and cylindrical coils, the proposed model of magnetic field distribution for a circular current loop is developed. The design optimization for various parameters of planar coils was thoroughly investigated. Approximate approaches to determine the electromagnetic forces are discussed. Models for diaphragm deflection were determined. The fluid model for evaluation of flow rate from the output of diaphragm pump was developed.

The feasibility of using nozzle/diffuser elements as components of air pumps is investigated. The geometry of nozzle/diffuser elements was designed and the chamber configuration for the proposed electromagnetic air pump was determined.

The proposed air pumps, including the electromagnetic actuator, PDMS (polydimethylsiloxane) diaphragm, and chamber and nozzle/diffuser elements were built.

Several experiments were conducted to investigate the performances of the proposed electromagnetic actuator including the deflection of diaphragm and frequency characteristics. The flow rate of the proposed air pump was measured.

In conclusion this study supplies solid evidence of achievements using electromagnetic actuators in air pumps.

CONTENTS

ACKNOWLEDGEMENTS	ii
ABSTRACT	iv
TABLE OF FIGURES	ix
LIST OF TABLES	xii
NOMENCLATURE	xiii
CHAPTER 1 INTRODUCTION	1
1.1 Background	1
1.2 Pumping Technologies	2
1.2.1 Centrifugal pumps	2
1.2.2 Electrohydrodynamic pumps	3
1.2.3 Magnetohydrodynamic pumps	5
1.2.4 Electro-osmotic pumps	6
1.2.5 Rotary pumps	6
1.2.6 Piston pumps (Reciprocating Pumps)	7
1.2.7 Diaphragm pumps	7
1.3 Actuation schemes	8
1.4 Motivation	9
1.5 Research objective	10
1.6 Thesis structure	11
CHAPTER 2 MATHEMATICAL MODEL	12
2.1 Introduction	12
2.2 Electromagnetic model	13
2.2.1 Bio-Savart's law	13
2.2.2 Magnetic field of a circular current loop	14
2.3 Force generation model	18
2.4 Mechanical model	20
2.4.1 Small deflection of diaphragm	21
2.4.2 Large deflection of diaphragm	21

2.5 Fluid model	22
2.6 Summary	23
CHAPTER 3 DESIGN OPTIMISATION	24
3.1 Introduction.....	24
3.1.1 <i>Design optimisation procedure</i>	24
3.1.2 <i>Design consideration</i>	26
3.2 Air pump configuration	26
3.3 Optimization of electromagnetic actuation.....	27
3.4 Electromagnetic actuator	29
3.4.1 <i>Specification of electromagnetic coils</i>	30
3.4.2 <i>Optimised geometry of electromagnetic coil</i>	32
3.5 Driving circuit design	44
3.6 Diaphragm design.....	46
3.6.1 <i>Determining diaphragm materials</i>	46
3.6.2 <i>Dynamic properties of diaphragm</i>	47
3.7 Chamber configuration	47
3.8 Valve design	49
3.9 Summary.....	51
CHAPTER 4 AIR PUMP FABRICATION	52
4.1 Introduction.....	52
4.2 Air pump design	52
4.2.1 <i>Electromagnetic coils design</i>	52
4.2.2 <i>Small deflection of diaphragm</i>	54
4.2.3 <i>Large deflection of diaphragm</i>	57
4.2.4 <i>Chamber and nozzle element</i>	59
4.3 Air pump fabrication.....	61
4.3.1 <i>Electromagnetic coils fabrication</i>	61
4.4 PDMS Diaphragm	63
4.4.1 <i>Procedures of PDMS diaphragm</i>	63
4.4.2 <i>Diaphragm embedded with permanent magnet</i>	65
4.4.3 <i>Corrugated PDMS Diaphragm</i>	66
4.5 Chamber and valveless fabrication.....	68
4.5.1 <i>Chamber and nozzle/diffuser elements manufacture</i>	69
4.6 Air pump assembly	70

4.6 Summary	72
CHAPTER 5 TESTING AND RESULTS	73
5.1 Introduction.....	73
5.2 Experiment setup	73
5.2.1 Deflection of PDMS diaphragm.....	73
5.2.2 Flow rate	75
5.3 Air pump test	76
5.3.1 Deflection of PDMS diaphragm test	76
5.3.2 Corrugated diaphragm.....	82
5.3.3 Flow rate measurement.....	83
5.4 Summary	85
CHAPTER 6 DISCUSSION	86
6.1 Introduction.....	86
6.2 Force generation	86
6.2.1 Magnetic fields of circular planar coils.....	86
6.2.2 Electromagnetic coil fabrication.....	87
6.3 Diaphragm deflection	88
6.4 Flow rate of air pump	89
6.5 Configuration of chamber.....	89
6.6 General discussion	89
CHAPTER 7 CONCLUSION AND FUTURE WORK	91
7.1 Conclusion	91
7.2 Recommendations for Future Work	92
APPENDIX	94
A.1 Terminology.....	94
A.2 Coordinate system and transformation	94
A.3 Basic vector analysis.....	97
A.3.1 Unit vector operation.....	97
A.3.2 Vector cross product.....	98
A.4 Thin plate analysis	99
A.4.1 Small deflection of clamped plate.....	99
A.4.2 Large deflection of clamped plate	100
A.5 Driving circuit.....	100

A.6 Experimental data of flow rate measurement	101
A.6 Properties of PDMS	102
A.7 common materials and material properties	103
A.8 Matlab codes	104
<i>A.8.1 Matlab codes for magnetic field of a circular electromagnetic coils.....</i>	<i>104</i>
<i>A.8.2 Matlab codes for diaphragm deflection.....</i>	<i>105</i>
REFERENCE	108

TABLE OF FIGURES

Figure 1.1: Types of pumps.....	2
Figure 1.2: Impeller [6]	3
Figure 1. 3: Types of EHD pumps: (a) Induction type [5] (b)Injection type [12] (c) Ion-drag [13]	4
Figure 1. 4: Working principles of MHD pumps [19].....	5
Figure 1. 5: Operational principle of rotary ADU [19]	6
Figure 1. 6: Structure and operation of a typical diaphragm pump (a) Top view and section (b) operation principle [3]	7
Figure 1. 7: Operation of nozzle/diffuser-based pump with single chamber and diaphragm (a) Supply mode (b) Pump mode [29].....	8
Figure 2. 1: General structure of electromagnetic air pump.....	12
Figure 2. 2: Electromagnetic field of arbitrary point.....	14
Figure 2. 3: Source and field point in cylindrical coordinate system.....	15
Figure 2. 4: Electromagnetic force production in the Cartesian coordinate system.....	19
Figure 2. 5: Approximated calculation of electromagnetic force.....	19
Figure 2. 6: Load uniformly distributed along inter portion of a concentric circle.....	20
Figure 2. 7: Deflection of diaphragm in a cylindrical coordinate system	22
Figure 3. 1: Procedures of optimization	26
Figure 3. 2: Configuration of the proposed air pump.....	27
Figure 3. 3: Types of electromagnetic actuator	28
Figure 3. 4: A cylindrical magnet in the axis-symmetric field of coils (a) permanent magnet (b) optimal magnet [51].....	29
Figure 3. 5: Geometry of planar coils.....	31
Figure 3. 6: Geometry of Cylindrical coils.....	31
Figure 3. 7: Z component of magnetic flux density for a circular current loop	33

Figure 3. 8: Z component of magnetic flux density gradient for a circular current loop	35
Figure 3. 9: Magnetic field gradients of planar coils for z component at given z value	37
Figure 3. 10: Magnetic field gradients of planar coils for z component at given outer radius	39
Figure 3. 11: Magnetic field gradients of planar coils for z component at given inner radius	41
Figure 3. 12: Magnetic field gradient of planar coils for z component at given copper track width	43
Figure 3. 13: Driving circuit design	45
Figure 3. 14: Various configurations of pumps [58]	48
Figure 3. 15: Valve classification.....	49
Figure 3. 16: Geometry of a diffuser element [62].....	50
Figure 3. 17: A flat walled diffuser element	50
Figure 4. 1: Cutting of plastics [63]	68
Figure 4. 2: PDMS manufacturing procedure	64
Figure 4. 3: Experimental setup of diaphragm deflection measurement.....	74
Figure 4. 4: Experimental setup of flow rate measurement	75
Figure 5. 1: Sketch of the structure of the bobbin	54
Figure 5. 2: Numerical calculation of maximum deflection of diaphragm	56
Figure 5. 3: Numerical calculation of large deflection of PDMS diaphragm	58
Figure 5. 4: A chamber with nozzle/diffuse (explode view).....	59
Figure 5. 5: Configuration of single chamber	60
Figure 5. 6: Dimensions of a diffuser element (Unit: mm).....	60
Figure 5. 7: PCB planar coils	63
Figure 5. 8: Cylindrical coils.....	62
Figure 5. 9: Double chambers with one diaphragm	69
Figure 5. 10: Chamber with nozzle/diffuser under it	70

Figure 5. 11: PDMS diaphragm embedded with permanent magnet	66
Figure 5. 12: Corrugated PDMS diaphragm	67
Figure 5. 13: Tools for corrugated PDMS diaphragm (a) Cavity and (b) Core	67
Figure 5. 14: Single actuation air pump	71
Figure 5. 15: Double actuation air pump.....	71
Figure 5. 16: Measurement of diaphragm deflection	77
Figure 5. 17: Flow rate measurement.....	83
Figure 5. 18: Flow rate vs. amplitude of driving current for the proposed single acting air pump.....	84
Figure 5. 19: Flow rate vs. amplitude of driving current for the proposed double acting air pump.....	85
Figure A.1. 1: Differential volume element in Cartesian coordinates system.....	95
Figure A.1. 2: Variables in the Cartesian coordinate system and cylindrical system	96
Figure A.1. 3: Differential volume element in cylindrical coordinate system	97
Figure A.4. 1: (a) Line load P, (b) Load distributed along inner parts of a concentric circle [46]	99
Figure A.6. 1: Properties of PDMS (data from Dow Corning Corporation).....	103
Figure A.7. 1: Common material and material properties.....	103

LIST OF TABLES

Table 3. 1: Planar coils geometry.....	36
Table 3. 2: Planar coils geometry with various outer radius.....	38
Table 3. 3: Planar coils geometry with various values of inner radius.....	40
Table 3. 4: Planar coils geometry with various of copper track width.....	42
Table 5. 1: Planar coils design.....	53
Table 5. 2: Design parameters of the bobbin.....	54
Table 5. 3: Numerical calculation parameters of small deflection.....	55
Table 5. 4: Numerical calculation parameters for large deflection.....	57
Table 5. 5: Experimental results of diaphragm deflection.....	78
Table 5. 6: Experimental results of diaphragm deflection.....	79
Table 5. 7: Central Deflection of 30mm PDMS diaphragm.....	80
Table 5. 8: Central deflection of 50mm diaphragm.....	81
Table 5. 9: Central deflection of corrugated PDMS diaphragm.....	82

NOMENCLATURE

Symbol	Meaning	Unit
ADU	Air delivery unit	
A_{mag}	Surface area of magnet	m^2
B	Magnetic flux density	Teslas
B_r	Residual magnetic flux density	Gauss
B_x	X component of magnetic flux density	Teslas
B_y	Y component of magnetic flux density	Teslas
B_z	Z component of magnetic flux density	Teslas
D	Flexural rigidity of plate	$\text{N}\cdot\text{m}^2$
E	Young's modulus	Pa or N/m^2
F	Vector force	
F_z	Amplitude of force along z axis	N
H	Magnetic field intensity	A/m
H_z	Z component of magnetic field intensity	A/m
I	Current amplitude	A
P	Field point	
Q	Source point	
R	Radius of circular	m
R_i	Inter coils radius	m
R_o	Outer coils radius	m
V_m	Volume of magnet	m^3
a	Radius of plate	m
\mathbf{a}_x	Unit vector of Cartesian coordinate system	
\mathbf{a}_y	Unit vector of Cartesian coordinate system	
\mathbf{a}_z	Unit vector of Cartesian coordinate system	
b	Radius	m
$d\mathbf{l}$	Vector of differential element of current loop	m
f	Frequency	Hz
h	Thickness	m
\mathbf{r}'	Source point vector	
\mathbf{r}	Field point vector	
r	The central distance from any point	m

ν	Poisson's ratio	
w	Deflection	m
w_{\max}	Maximum deflection	m
μ_0	Permeability of free space	V·s/(A·m)
θ	Angle	radian
∇z	Gradient vector field along z axis	
ΔV	Volume change of chamber	m ³
η	Rectified efficiency of nozzle/diffuser	

CHAPTER1

INTRODUCTION

1.1 Background

Pump miniaturisation has been under development for more than two decades. The key characteristic of a small pump size is its manipulation of the small and precise volume of liquid or gas. This characteristic makes them able to serve in chemical, medical, and biomedical applications with great scientific and commercial potential. Drug delivery system is an example of its application when working with liquid [1], while the air delivery unit or air pump (terminology define see appendix A.1) is an example when working with gas.

A coherent system of categorisation is helpful for making sense of the diverse set of pumps that have been developed. Pump classification, illustrated in Figure 1.1, generally can be divided into two major categories [2]: (1) Dynamic pumps, which continuously add energy into the working fluid in a manner that increases either its momentum or its pressure directly; (2) Displacement pumps, which exert pressure force on the working fluid through one or more moving boundaries [3]. Such dynamic pumps include centrifugal pumps, which have only been miniaturisation to a limited extent, as well as pumps in which an electric or magneto-static field interacts directly with the working fluid to generate flow and pressure (electrohydrodynamic, magnetohydrodynamic and electroosmotic pumps). Displacement pumps on the other hand can be further classified as either rotary type or reciprocating type. A rotary pump is based on rotary elements, called gears or vanes. A reciprocating pump is based on reciprocating motion, such as a piston and diaphragm.

For many small-scale fluidic systems, a self-contained active small-scale pump, whose packaging size is comparable to the fluid volume to be pumped, is necessary or highly desirable [4]. A significant driving force underlying this pumping miniaturisation has been in the integration of the pumping mechanisms into micro total analysis systems, micro-dosing systems, and other small-scale electrometrical system [5].

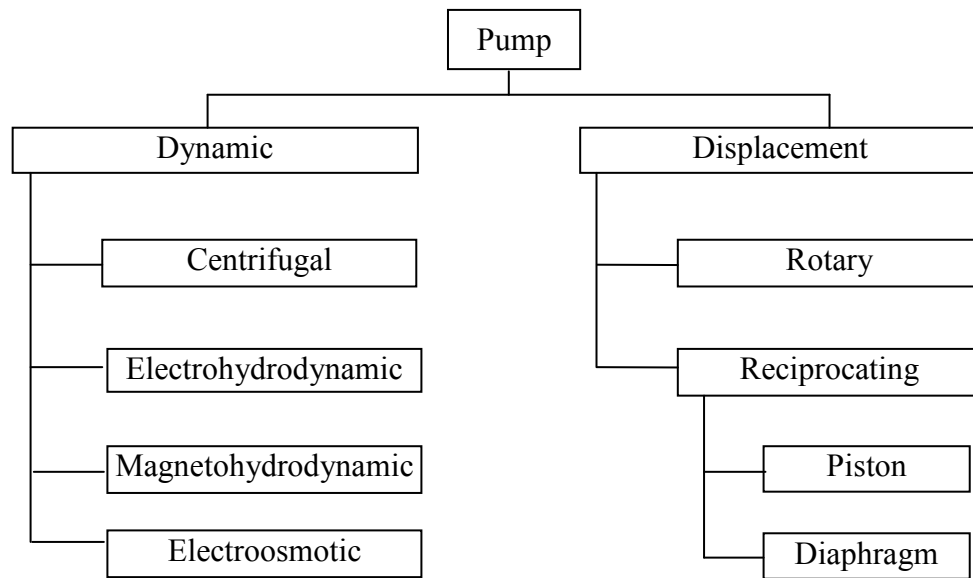


Figure 1.1: Types of pumps

1.2 Pumping Technologies

This literature review presents recent research on novel small-scale pumping techniques. It includes the basic working principle and critical features of the various kinds of pumps.

1.2.1 Centrifugal pumps

Centrifugal pumps are the most common type of traditional dynamic pump. A centrifugal pump is essentially composed of a casing, a bearing housing, the pump shaft and an impeller. The overhung impeller mounted on the shaft is driven via coupling with a motor. The impeller (refer to 3D-CAD Figure 1.2 for details) transfers the energy necessary to transport the fluid and accelerates it in the circumferential direction [6].

Studies were undertaken into the unsteady flow field of centrifugal pumps by some researchers [7-9]. Efforts also were put on the miniaturisation of the impeller of centrifugal pumps [10, 11].

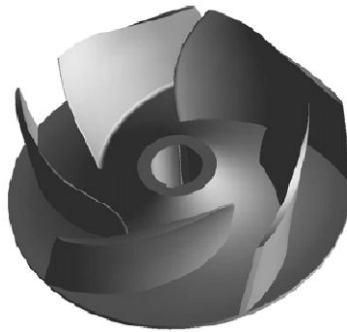
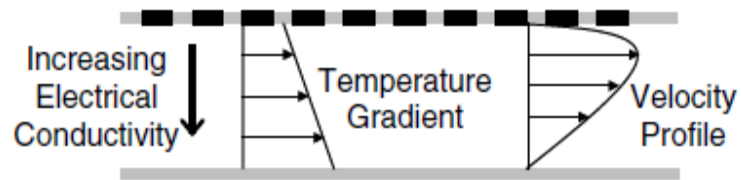


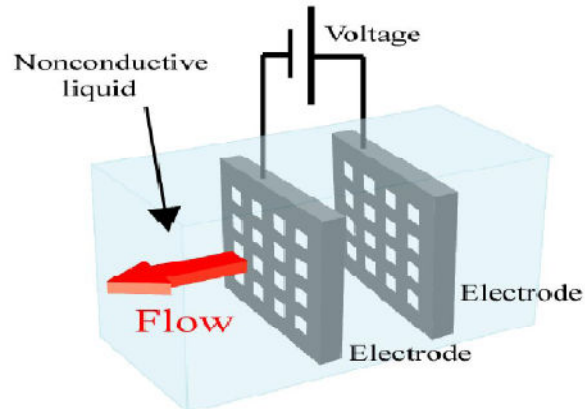
Figure 1.2: Impeller[6]

1.2.2 Electrohydrodynamic pumps

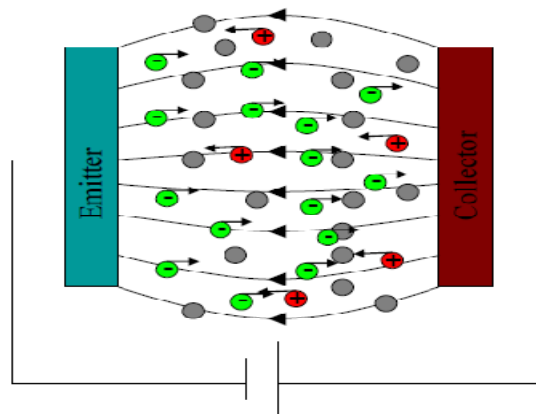
Electrohydrodynamic (EHD) pumps utilise electrostatic forces acting on dielectric fluids to generate flow. They directly convert electrical energy into fluid motion. There are several types of EHD pumps, and the distinction is based mainly on a method for the charged particle introduced into the fluid [5]. EHD pumps include three types: induction, injection and ion-drag (refer to Figure 1.3 for details). In induction EHD pumps, charge is induced in the working fluid by application of potential difference across them. In injection EHD pumps, electrochemical reactions at the electrode produce the injection of free ions into the working fluid. Ion-drag force drives the fluid in ion-drag pumps.



(a)



(b)



(c)

Figure 1. 3: Types of EHD pumps: (a) Induction type[5] (b)Injection type[12] (c) Ion-drag[13]

The working fluid for EHD pumps must be dielectric. The flow characterises induced by EHD pumps were studied [14-17]. Also the geometry of the electrodes as important components of EHD pumps were thoroughly investigated [12, 18].

1.2.3 Magnetohydrodynamic pumps

Magnetohydrodynamic (MHD) pumps exploit the Lorentz force that is generated when a current-carrying conductor is placed in a magnetic field. Figure 1.4 shows the basic structure of an MHD pump. An electric field is generated by the electrode on opposite walls of the channel. Permanent magnets are used to create a magnetic field across the depth of the channel in a direction perpendicular to that of the electric field.

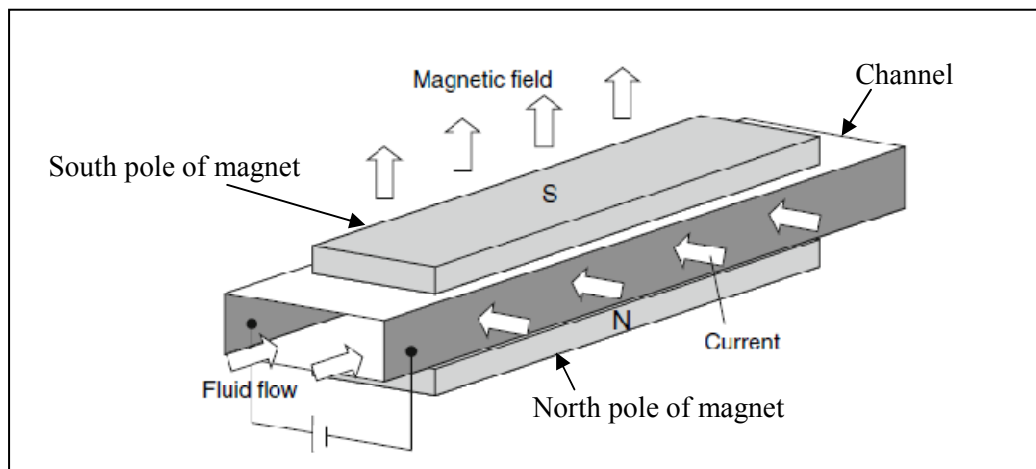


Figure 1. 4: Working principles of MHD pumps[19]

The interaction between the moving conducting fluids with electric and magnetic fields provides the magnetohydrodynamic (MHD) phenomenon. The flow mechanism in MHD pump was investigated by several researchers [20, 21]. MHD pumps were fabricated with a novel micro-fabrication process [22-24]. For the MHD pump, it provides several desired characteristics, including easy architecture and fabrication, no pulsation of fluid flow and bidirectional adjustability of fluid flow [4]. However, within the MHD pump the scaling of flow rate with the fourth power of hydraulic diameter makes miniaturisation challenging.

1.2.4 Electro-osmotic pumps

Electro-osmotic (EO) pumps utilise the surface charge that can spontaneously develop when a liquid comes in contact with a solid. The electro-osmotic pump is realised in a glass or SiO₂ capillary fitted with electrodes on two ends. Since this type of pumping technology is only suitable for the electrolyte solution, details of operation principle and main performance are not described at here.

1.2.5 Rotary pumps

The traditional rotary pump consists of a toothed gear rotating in a fluid chamber with an inlet and an outlet port. As shown in Figure 1.5, the pump consists of a circular chamber connected to an inlet and outlet channel. A rotor with eight poles is free to rotate inside the chamber while the stator coils lie outside the chamber.

Conventional rotary pumps are unsuitable for the purpose of miniaturisation due to their large size and power consumption [19]. A magnetic actuated rotary micro pump was discussed by Ahn and Allen [25]. The traditional rotating micro pump was reported to have achieved a high flow rate using micro fabrication technologies, namely photolithography, electroplating, and resist stripping [26]. However the micro fabrication of this pump is very complex and likely to be expensive.

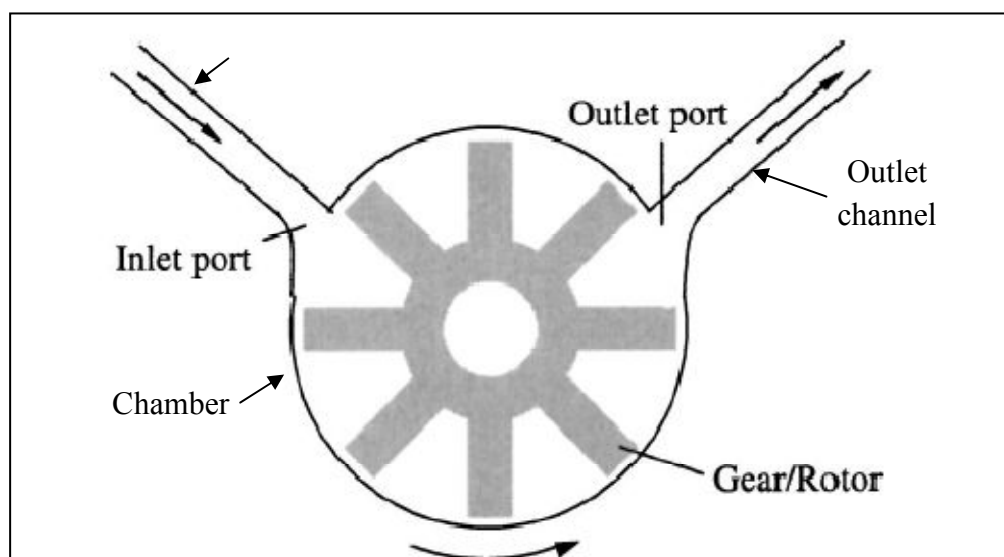


Figure 1. 5: Operational principle of rotary ADU [19]

1.2.6 Piston pumps (Reciprocating Pumps)

Piston pumping technology is traditional and space consuming. In addition, it needs a large power motor as driver. Some piston pumps need lubrication. Thus piston pumping technology might not be suitable for miniaturisation.

1.2.7 Diaphragm pumps

The name called “reciprocating pump” apply oscillatory or rotational motion on a part, such as a piston and diaphragm, to implement movement of the working fluid [27]. A typical diaphragm air pump includes four components: chamber, diaphragm, driver and valve or valve-less [1]. Valve-less pumps could be fitted with nozzle/diffuser or other non-moving part valve. The working principle of a diaphragm air pump with valve is illustrated in Figure 1.6 [3].

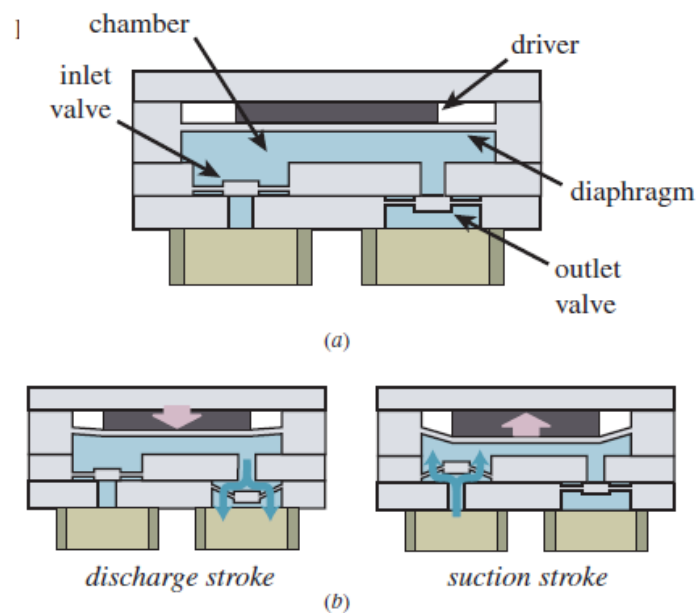


Figure 1. 6: Structure and operation of a typical diaphragm pump (a) Top view and section (b) operation principle [3]

During the operation of a diaphragm pump, the driver acts on the diaphragm to alternately increase and decrease the volume of the chamber. During the stage of the suction stroke or “supply mode”, air or fluid is drawn into the chamber. Fluid is forced out of chamber during the discharge stroke or “pump mode”. Figure 1.7 illustrates the working principle of an air pump with nozzle/diffuser [28].

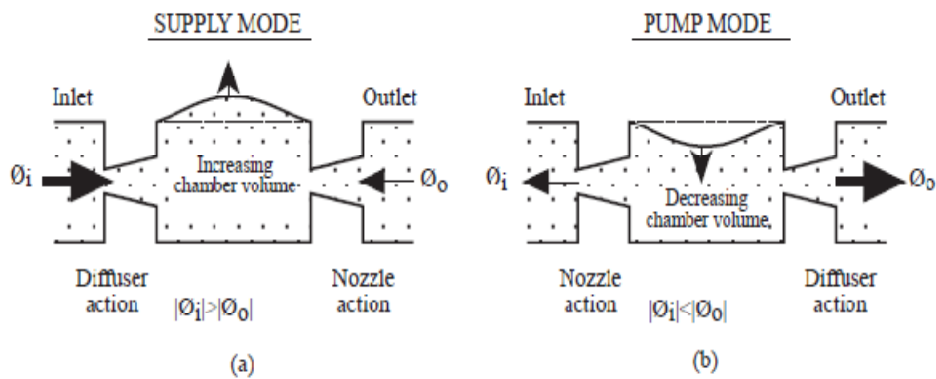


Figure 1. 7: Operation of nozzle/diffuser-based pump with single chamber and diaphragm (a) Supply mode (b) Pump mode [29]

The diffuser element is a fluidic channel which is able to make fluidic resistance in one direction higher than other direction. This characteristic causes a flow rate that is different in the two directions despite the same applied pressure [30]. The nozzle element has opposite characteristics. When fluid flows from left to right, the fluidic channel acts as a diffuser, but when fluid transportation is from the right to the left, it acts as a nozzle.

1.3 Actuation schemes

Ideally, actuators must be easy to construct, provide large force with a fast response time and run under low power consumption [1]. The choice of the type of actuator depends upon the specific requirement of the application.

Actuation schemes includes piezoelectric, thermal, electrostatic and electromagnetic actuation [1]. The advantages and disadvantages of these actuation schemes are described in the following section [5, 27].

Piezoelectric actuation provides a high actuation force and fast mechanical response. However, relatively high actuation voltages and the attachment of piezoelectric ceramic material can be regarded as disadvantages [31-33].

Thermal (Thermopneumatic and Shape Memory Alloys) actuation requires low input voltages. It can generate high pumping rates and actuation forces and can be very compact. A critical drawback of thermopneumatic actuation that has limited its use, is that it has a relatively long thermal time constant, especially during the cooling process [34, 35].

Electrostatic devices with high operating frequencies are characterised by extremely low power consumption and full integration capability. The major disadvantages are small actuation strokes and degradation of performance with time [36, 37].

The major advantage of an electromagnetic actuator is the generation of large deflection and high tuneable frequency capability. In addition, the electromagnetic field can be set up and disappear rapidly. Thus electromagnetic actuators are able to operate with very fast speed [1]. However, an electromagnetic actuator requires high power consumption. Although it is not well compatible with MEMS integration, this actuation concept can easily be adapted in a modular way and offers the benefit of a separate optimisation of micro-pump and actuation unit [27].

1.4 Motivation

Centrifugal pumps are well known and of significant economic importance in many areas of everyday life and industry. Their applications range from small pumps of a few watts, such as cooling air pumps for CPU, to blood pumps with power consumption below 100 watts. These pumps have several drawbacks. First the fluid flow in a centrifugal fan is highly turbulent and unsteady. It is well known that the flow pattern

and stability of the centrifugal fan depends on the geometry of its rotary blade and the shape of its channels [8]. The second negative property of the centrifugal fan is the noise which is caused by the rotating blade noise with a narrowband frequency and the turbulent noise with a broadband frequency spectrum [38]. Progress for extensive miniaturisation of centrifugal pump has been made. However, unfavourable scaling of efficiency with decreasing Reynolds number has been shown [3].

In order to overcome inherent drawbacks of the centrifugal and other moving part pumps, the research to the so-called “diaphragm pumps” is focused on. One of the main reasons for that is the suitability of the latter to miniaturisation and compact size device. The proposed pump consists of: an actuator, moving fluid, control valve and delivery element. The actuator is of electromagnetic nature, while other elements are of mechanical nature.

1.5 Research objective

The characteristics of the central deflection of a diaphragm are important factors impacting on the performance of air pumps. Configurations of electromagnetic coils have a great effect on the production of electromagnetic force. Due to the complex and nonlinear distribution of the magnetic field, design optimisation of electromagnetic coil is an essential part of the optimisation. To put there into context, the objective of this work can be summarised as the following:

1. Develop suitable models of the electromagnetic actuation based on the proposed diaphragm air pump.
2. Develop a mechanical model to determine the deflection of the diaphragm.
3. Develop the fluid model for flow rate based on the proposed type of diaphragm air pump.
4. Examine and investigate design optimisation of electromagnetic coils for enhancing electromagnetic force.

5. Numerical calculation of magnetic field distribution and the central deflection of diaphragm.
6. Investigate various configurations of the diaphragm air pump for better performance.
7. Determine the geometric parameters for the nozzle/diffuser as a component of the diaphragm air pump.
8. Fabricate the proposed electromagnetic coils, chamber and nozzle/diffuser.
9. Implement or assemble the proposed portable diaphragm air pump.
10. Investigate the characteristics of the proposed electromagnetic actuator.
11. Investigate performances of the proposed air pump.

1.6 Thesis structure

Modelling framework of electromagnetic air pumps is presented in Chapter 2. Four different models are used for analysis and design of electromagnetic air pumps. Based on the modelling formulation, chapter 3 describes the design optimisation methodology for electromagnetic air pumps. In this chapter two basic configurations of electromagnetic coils are designed. Details of model numerical calculation are presented in this chapter. Chapter 4 involves methods of fabrication and test for the electromagnetic air pumps. Utilising several experiments, characteristics of the proposed electromagnetic actuator and performances of the air pump are investigated in the chapter 5. Some discussions and conclusions are given in chapter 6 and chapter 7 separately.

CHAPTER 2

MATHEMATICAL MODEL

2.1 Introduction

Model developments and numerical calculations play important roles in research. Mathematical modelling for the electromechanical system has two purposes, first the implementation of design optimisation to guarantee customer requirements under physical and technological limitations, and second the assessment of performance and capability of the electromechanical system.

This chapter presents the electromechanical model developed in this study to quantify the relationship between the input and output of the proposed air pump. The model consists of (refer to Figure 2.1 for details) an electromagnetic model, followed by a force generation model, then a fluid model to quantify the values of the delivered flow rate and pressure.

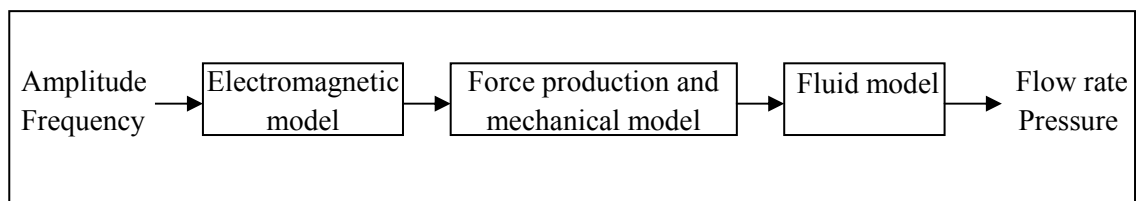


Figure 2. 1: General structure of electromagnetic air pump

The electromagnetic model describes the magnetic field distribution in space. The electromagnetic force is quantified by the force model. The mechanical model determines the behaviour of the central deflection of diaphragm. The flow rate model estimates the flow rate under various conditions of structure and geometry of the proposed air pump. Development of all the above models will be presented in the following sections.

2.2 Electromagnetic model

The electromagnetic model is based on the principle of electromagnetism. A static electromagnetic field is produced by charges moving with constant velocity [39]. The magnetic flux density (B) and magnetic field intensity (H) describes the characteristics of the electromagnetic field distributed in space. They both have amplitude and direction and best defined by a vector. For example, for three dimensional space there are x, y, z components representing the magnetic flux density B at any point in a Cartesian coordinate system (Figure 2.2). This can be written as

$$\mathbf{B} = B_x \mathbf{a}_x + B_y \mathbf{a}_y + B_z \mathbf{a}_z \quad (2.1)$$

Where \mathbf{a}_x , \mathbf{a}_y and \mathbf{a}_z are unit vector in the x, y, and z axis respectively. B_x , B_y , B_z are the magnetic flux density in the x, y, z direction respectively. The motion of electric charges with uniform velocity (direct current) or static magnetic charges (magnetic poles) produce magnetostatic fields or magnetic fields. Accelerated charges or time-varying currents usually generate the electromagnetic waves [40]. In this work we are proposing low frequency working actuation therefore Bio-Savart's law will be used [40].

2.2.1 Bio-Savart's law

Bio-Savart's law defines the magnetic flux density (B) of an arbitrary point in space. Figure 2.2 shows an arbitrary current loop. Typical source point and field point are located at Q and P respectively. It is assumed that the source point is a small element along the current loop and the field point is the specific point in space where the magnetic field intensity needs to be known. \mathbf{r} is the position vector of the field point, \mathbf{r}' is the position vector of the source point [41].

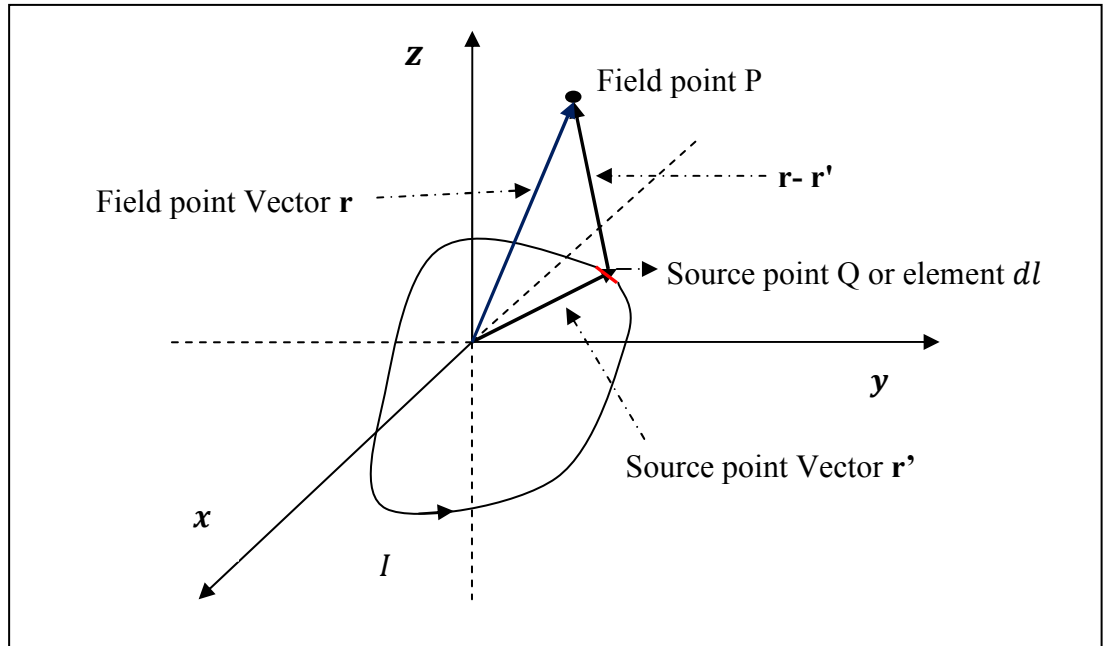


Figure 2. 2: Electromagnetic field of arbitrary point

For a differential element, Bio-Savart's law may be written as [40]:

$$\mathbf{B} = \frac{\mu_0 \cdot I}{4\pi} \oint \frac{d\mathbf{l} \times (\mathbf{r} - \mathbf{r}')}{|\mathbf{r} - \mathbf{r}'|^3} \quad (2.2)$$

Where B is the magnetic flux density. The cross product $d\mathbf{l} \times (\mathbf{r} - \mathbf{r}')$ gives the vector distance between the field point P and source point Q. $|\mathbf{r} - \mathbf{r}'|$ is defined as the magnitude of distance between the field point P and source point Q.

The direction of the magnetic field intensity is the progress of the right-handed screw turned from $d\mathbf{l}$ through the smaller angle to the line from differential element to field point P [41].

2.2.2 Magnetic field of a circular current loop

From Bio-Savart's law, the mathematical model of magnetic flux density distribution for any arbitrary shape of current loop can be obtained assuming of quasi-static field. The quasi-static condition allows for replacement of direct current in the mathematic

model of magnetic flux density distribution with alternating current. The mathematic expression for the magnetic field is for single current loop. However for multiple loops they should be considered summation.

Applying Bio-Savart's law, the magnetic field intensity \mathbf{B} at a point along the z axis of the circular current (shown in Figure 2.3) can be determined. Source point and field point are located at Q ($R \cos\theta, R\sin\theta, 0$) and P(0,0,z) respectively. The positive vector of the source point is $\mathbf{OQ} = \mathbf{r}'$. The positive vector of the field point is $\mathbf{OP} = \mathbf{r}$. The distance vector between the source and field point is $\mathbf{PQ} = \mathbf{r} - \mathbf{r}'$. In this case, the small element of the current loop $d\mathbf{l}$ is equal to $R \cdot d\beta$ in the cylindrical coordinate system. The unit vectors in the cylindrical coordinate system are \mathbf{a}_θ , \mathbf{a}_r and \mathbf{a}_z .

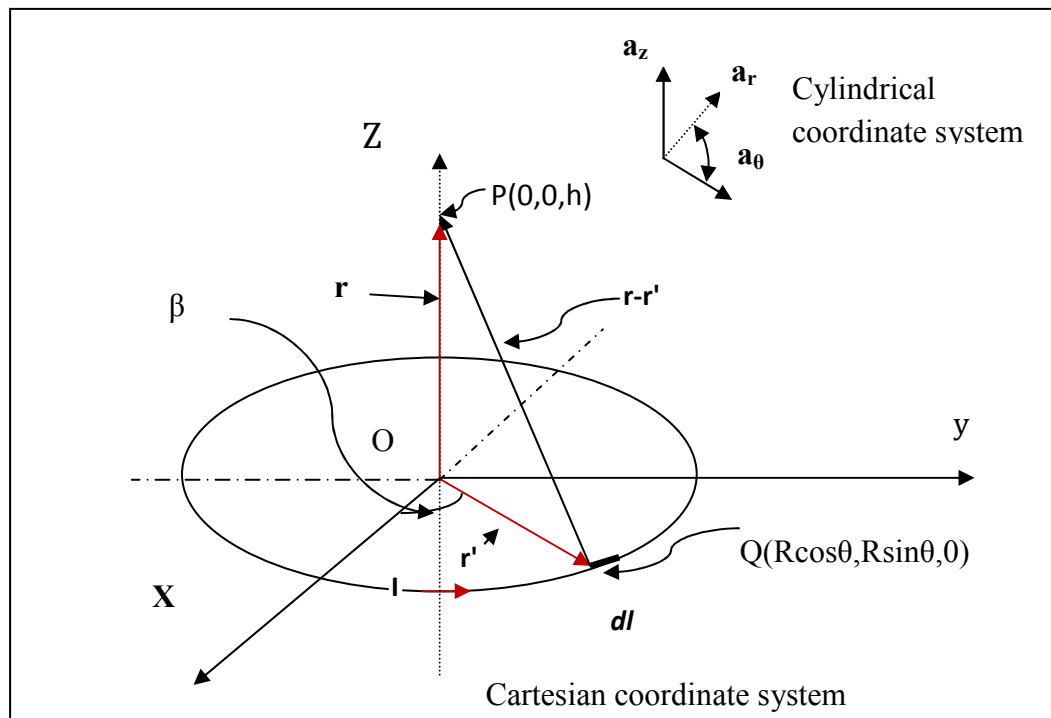


Figure 2. 3: Source and field point in cylindrical coordinate system

In cylindrical coordinate system, source point Q and field point P is represented as $(R, 0, 0)$ and $(0, \beta, h)$. The small element of current flow and the distance vector between the source and field point is written as equation

$$d\mathbf{l} = R \cdot d\theta \mathbf{a}_\theta \quad \text{and}$$

$$\mathbf{r} - \mathbf{r}' = \mathbf{PQ} = -R\mathbf{a}_r - \beta \mathbf{a}_\theta + h \mathbf{a}_z \quad (2.3)$$

The small element of current loop cross product with distance vector between the source and field point can be represented by:

$$(R \cdot d\theta \mathbf{a}_\theta) \times (-R\mathbf{a}_r - \beta \mathbf{a}_\theta + h \mathbf{a}_z)$$

Due to the rules of unit vector operation and vector cross product, z component of vector $(d\mathbf{l} \times \mathbf{PQ})$ can be written as:

$$(d\mathbf{l} \times \mathbf{PQ})_z = -R^2 d\theta \mathbf{a}_z$$

The length of vector \mathbf{PQ} can be written as:

$$|\mathbf{PQ}| = \sqrt{R^2 + h^2} \quad (2.4)$$

The magnetic flux density of z component under the condition of circular current loop can be written as equation [40]:

$$B_z = \frac{\mu_0 \cdot I}{4\pi} \int_0^\pi 2 \cdot \frac{R^2}{(\sqrt{R^2 + h^2})^3} d\theta \quad (2.5)$$

Or

$$B_z = \frac{\mu_0 \cdot I}{2} \cdot \frac{R^2}{(\sqrt{R^2 + h^2})^3} \quad (2.6)$$

Following the above method, the magnetic field density at any position around the z axis of circular current loop in Cartesian coordinate system can be obtained. We assume any field point P in space and any source point at a circular current loop of the radius R. They are represented as vector \mathbf{OP} and \mathbf{OQ} .

$$\mathbf{OP} = x \mathbf{a}_x + y \mathbf{a}_y + z \mathbf{a}_z \quad (2.7)$$

$$\mathbf{OQ} = R \cos\theta \mathbf{a}_x + R \sin\theta \mathbf{a}_y \quad (2.8)$$

The vector of distance between field point P and source point Q is calculated as:

$$\mathbf{OP} - \mathbf{OQ} = (x - R\cos\theta) \mathbf{a}_x + (y - R\sin\theta) \mathbf{a}_y + z \mathbf{a}_z \quad (2.9)$$

Thus magnetic field distribution for a small element of circular current loop is written as

$$dB_z = \frac{\mu_0 \cdot I}{4\pi} \cdot \frac{d\mathbf{l} \times \mathbf{PQ}}{|\mathbf{PQ}|^3} = \frac{[R^2 - xR\cos\theta - yR\sin\theta] \Delta\theta}{\left(\sqrt{[(x - R\cos\theta)]^2 + [(y - R\sin\theta)]^2 + z^2}\right)^3} \quad (2.10)$$

Consequently, the z component of the magnetic field distribution for a circular current loop is the result of integration of equation (2.10).

$$B_z = \frac{\mu_0 \cdot I}{4\pi} \int_0^{2\pi} \frac{[R^2 - xR\cos\theta - yR\sin\theta] d\theta}{\left(\sqrt{[(x - R\cos\theta)]^2 + [(y - R\sin\theta)]^2 + z^2}\right)^3} \quad (2.11)$$

Where I is amplitude of current (unit: A), μ_0 is the permeability of free space and equal as $4\pi \times 10^{-7} \text{ H}\cdot\text{m}^{-1}$ or $\text{N}\cdot\text{A}^{-2}$, B_z is amplitude of z component of magnetic flux density (unit: T).

The magnetic field gradient of the z component along z direction is written as the following:

$$\frac{\partial B_z}{\partial z} = -3Z \frac{\mu_0 \cdot I}{4\pi} \int_0^{2\pi} \frac{[R^2 - xR\cos\theta - yR\sin\theta] d\theta}{\left(\sqrt{[(x-R\cos\theta)]^2 + [(y-R\sin\theta)]^2 + z^2}\right)^5} \quad (2.12)$$

Above equation 2.12 will be used later when the total force generated from the coil is determined.

2.3 Force generation model

The electromagnetic model was developed as above. One possible application of the electromagnetic model is evaluation of electromagnetic force. The electromagnetic force can be written as [42] (see Figure 2.4).

$$F_z = B_r \oint_{V_m} \nabla_z H_z(\vec{r}) d^3 r \quad (2.13)$$

Where B_r is the remnant magnetic induction field given by manufacturers, V_m is volume of permanent magnet, $\nabla_z H_z$ is the z component of the magnetic field gradient along the z direction.

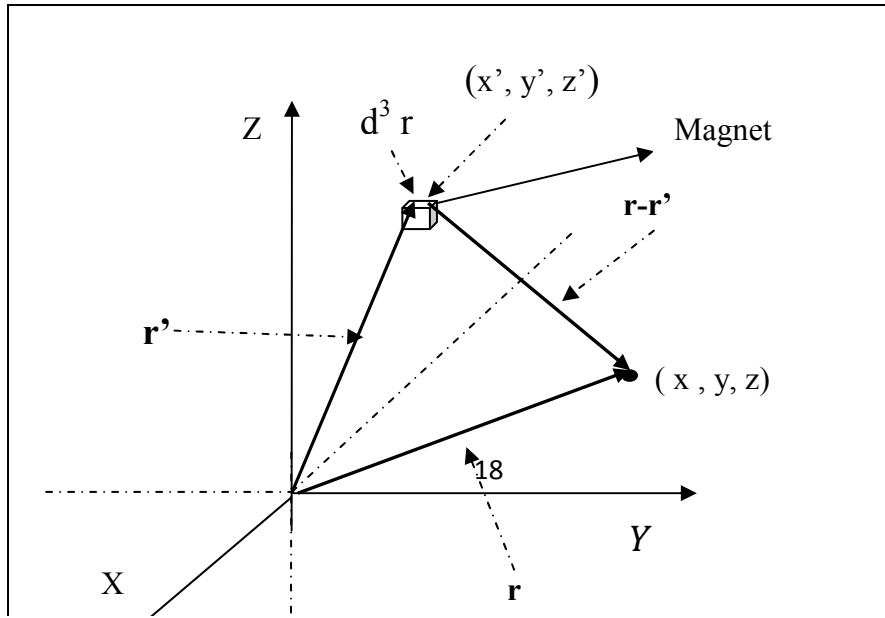


Figure 2. 4: Electromagnetic force production in the Cartesian coordinate system

One approximated method was suggested by D. de Bhailis [43] who tried to replace volume integration with surface integration in Equation (2.13).

$$F_z = B_r \times A_{\text{mag}} \int_z^{z+h} \frac{\partial H_z}{\partial z} dz \quad (2.14)$$

Where A_{mag} is the surface area of the permanent magnet, z is the distance between the current loop and the permanent magnet, and h is the thickness of the permanent magnet, as shown in Figure 2.5.

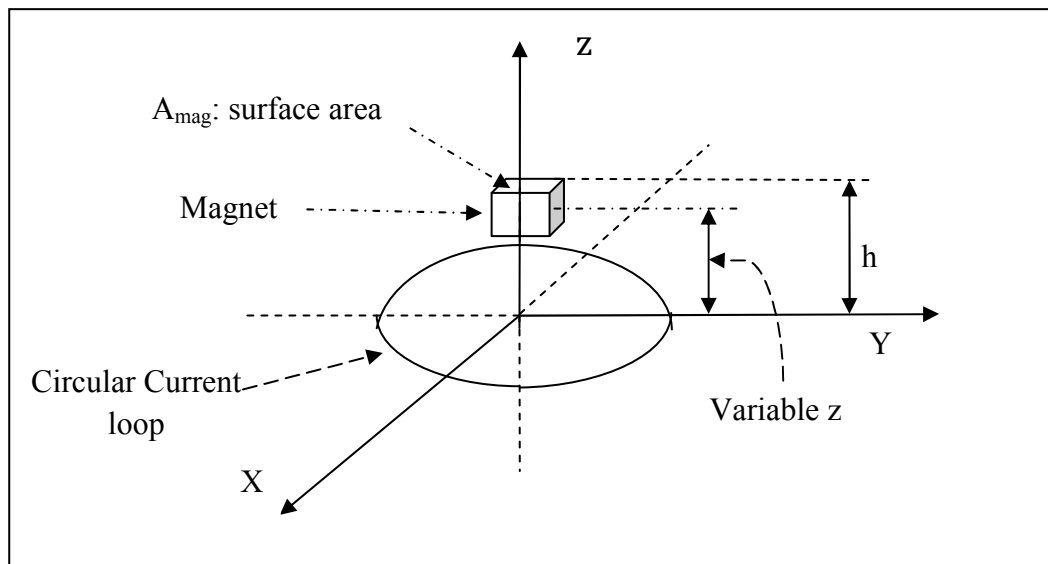


Figure 2. 5: Approximated calculation of electromagnetic force

Another approach is presented as to use cross multiplication as follow [44]

$$F_z = Br \times V_m \times \frac{\partial H_z}{\partial z} \quad (2.15)$$

V_m : Volume of magnet.

$\frac{\partial H_z}{\partial z}$: Differential of magnetic field intensity along z axis direction.

2.4 Mechanical model

The electromagnetic force generates displacement or deflection of the diaphragm in the proposed air pump. In the following section, the mode of diaphragm deflection is developed. Figure 2.6 shows a circular diaphragm with clamped edge. The load is assumed uniformly distributed along the inner portion of a concentric circle.

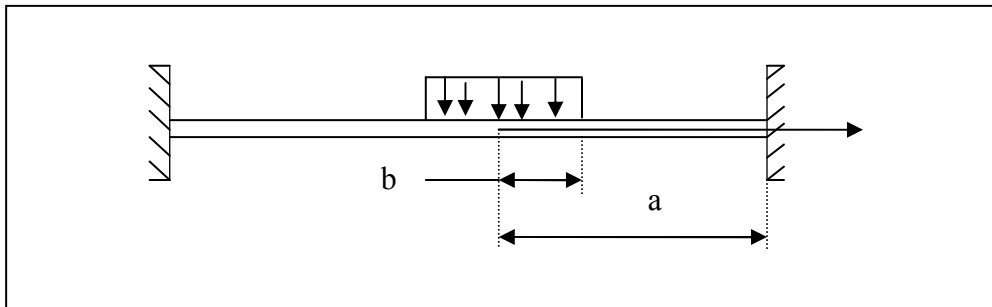


Figure 2. 6: Load uniformly distributed along inter portion of a concentric circle

Thin plate or small deflection theory is often used, and is appropriate for a small deflection of the plate in comparison with its thickness [45]. In the case of a PDMS diaphragm, when the deflection is three times smaller than its thickness and over ten times less than any other dimension such as the size of the diaphragm, the small deflection theory is applied. However, large deflection theory of membrane is used when the deflection is over three times of its thickness [45]. Since operation could be achieved in both ranges, the two theories are presented next.

2.4.1 Small deflection of diaphragm

Solutions for the small deflection theory are well known, but are repeated here for convenience. Deflection, w , of a clamped circular plate under the load uniformly distributed along the inner portion of a concentric circular is given by [46]:

$$w = \frac{pb^2}{16D} \left(a^2 - \frac{3}{4}b^2 + b^2 \log \frac{b}{a} \right) \quad (2.16)$$

Where w is maximum deflection of a diaphragm at the centre, p is the load density, b is radius boundary of load, a is diaphragm radius, and D is the flexural rigidity of plate.

D is given by equation

$$D = \frac{Eh^3}{12(1-\nu^2)} \quad (2.17)$$

Where E , ν , and h are PDMS young's modulus, Poisson's ratio and diaphragm thickness, respectively.

The details of driving equation (2.16) are presented in appendix A.2.

2.4.2 Large deflection of diaphragm

In contrast to small deflection theory, deflection in membrane theory is nonlinear when straining of the middle surface of plate is considered.

Many researchers have already developed models of large deflection of membrane under the action of uniformly distributed loads in its central portion, such as Chien Weizang [47], Sherbourne [48] and Kao R [49]. Because requirements of computational accuracy are not crucial for this study, the mathematical model of large deflection was treated as two parts: linear, which was solved with thin plate or small deflection theory; and nonlinear, in which strain of the middle plane due to stretching is calculated by the energy method [45].

Thus the large deflection of diaphragm at the centre can be written as:

$$2.51\pi Eh \frac{w^3}{12a^2(1-\nu^2)} + w = \frac{pb^2}{16D} \left(a^2 - \frac{3}{4}b^2 + b^2 \log \frac{b}{a} \right) \quad (2.21)$$

Where w is the maximum deflection of the diaphragm at the centre, p is the load density, b is the radius boundary of load, a is the diaphragm radius, and D is the flexural rigidity of plate.

2.5 Fluid model

The purpose of this flow model for air pumps allows engineers to understand the flow rate from the outlet theoretically and find approaches to improve performance of the air pumps. Prior to discussion of the expression of flow rate, the concept of volume change (see Figure 2.7) based on the circular shape of the chamber is explained.

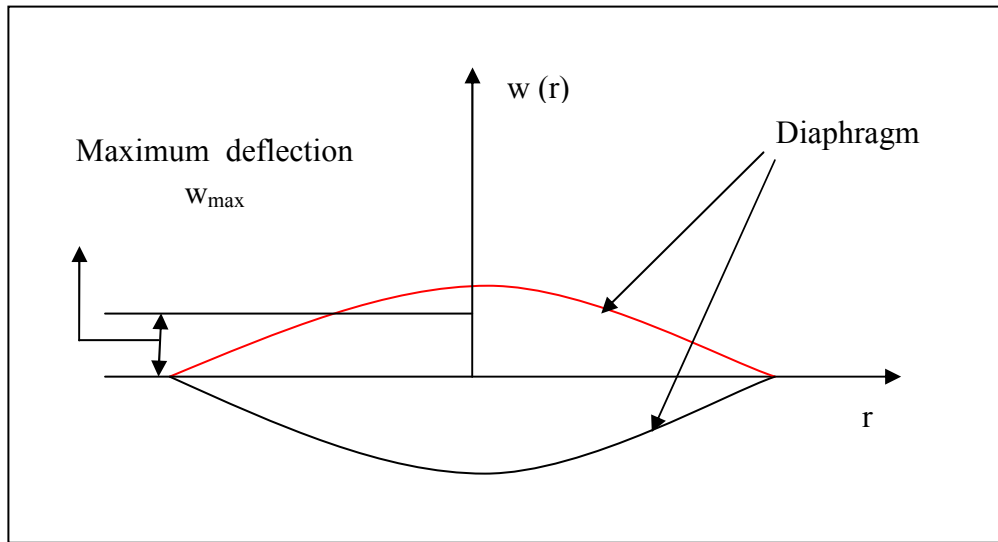


Figure 2. 7: Deflection of diaphragm in a cylindrical coordinate system

It is assumed that the stimulated signal is sinusoidal. In order to calculate the volume change of a circular pump chamber, the shape of diaphragm deflection must be considered. Thus the shape of deflected surface can be represented by the following expression [45]:

$$w(r) = W_{\max} \times \left(1 - \frac{r^2}{a^2} \right)^2 \quad (2.22)$$

Where r is radius variable, w_{\max} is the maximum deflection of the diaphragm, and a is the radius of the chamber.

Thus, the volume change of a pump chamber during half is the area under deflection curve given in Figure 2.7:

$$\Delta V = 2\pi \int_0^R r w(r) dr \quad (2.23)$$

Substituting equation (2.22) into equation (2.23) to obtain an expression of the volume change:

$$\Delta V = 2\pi \int_0^R r w(r) dr = 2\pi \int_0^R w_{\max} \times \left(1 - \frac{r^2}{a^2}\right)^2 r dr = \frac{\pi a^2}{3} w_{\max} \quad (2.24)$$

Therefore the fluid model of an air pump is defined as:

$$Q = 2 \times \Delta V \times f \times \eta \quad (2.25)$$

Where Q is the flow rate of the air pump, ΔV is the volume change during half of the operation cycle for the diaphragm pump, f is the operation frequency of the diaphragm pump, η is rectified efficiency of the operating valves or the system.

2.6 Summary

Through theoretical analysis, the operational mechanism of electromagnetic air pumps is developed. The magnetic field of the circular current loop for any point in space is described by the electromagnetic model. The force generation is used to approximate calculations. The mechanical models are used to investigate to the relationship between the force and deflection of the diaphragm. The proposed fluid model is used to describe the flow rate of the air pumps. Obviously, this flow rate depends on the volume change, the operation frequency and rectified efficiency of valves or valveless channels. The volume change is determined by two main factors including chamber dimensions and maximum central deflection of the diaphragm. The electromagnetic force and mechanical properties of the diaphragm must be known in order to calculate the

maximum central deflection of the diaphragm. Thus theoretical predicts for the defection of diaphragm is presented in chapter 4.

CHAPTER 3

DESIGN OPTIMISATION

3.1 Introduction

Before the system is designed, optimum design parameters must be determined. Using the relationship developed in chapter 2, one can determine the parameters and propose a feasible design.

3.1.1 Design optimisation procedure

In this research, the optimisation procedure for design is outlined in Figure 3.1. At the beginning of the optimisation procedure, a set of design parameters of the models are identified and determined. Then results of numerical calculation are obtained using MATLAB (codes see Appendix A.8). Evaluations for these are carried out to determine the optimal possible design. Among a set of possible optimal designs, the final design is determined with capabilities and limitations of fabrication technologies.

It is impossible to achieve an absolute accuracy from the mathematical models, but they are expected to be adequate to meet the demand of designer. In the numerical calculation, balance between the computational time and accuracy must be considered. The techniques of approximate solutions for integration and differentia are utilised.

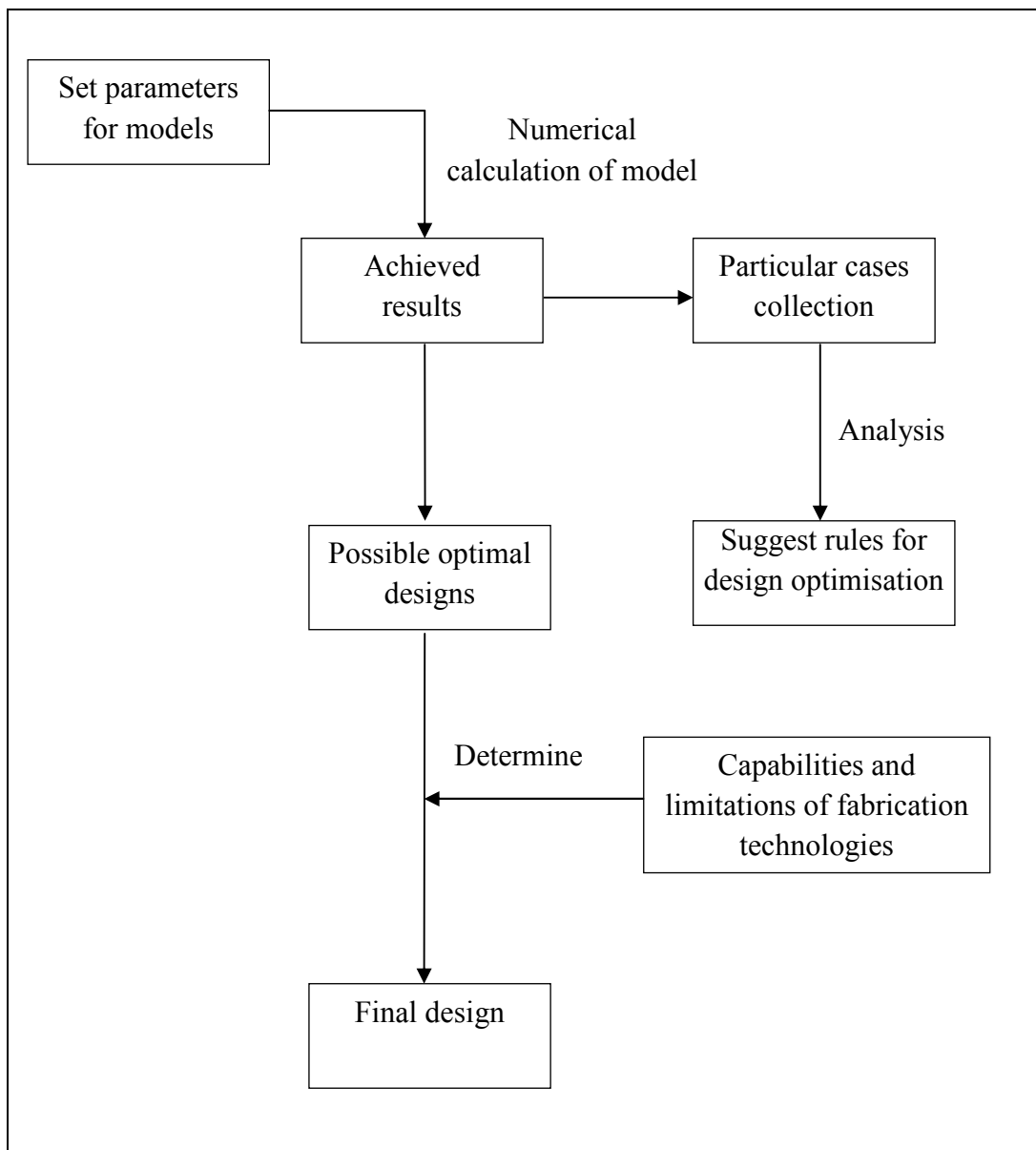


Figure 3. 1: Procedures of optimization

3.1.2 Design consideration

The principle of a diaphragm pump states that the diaphragm moving backward and forward generate pressure and flow rate at some range of operating frequency [3]. Several crucial factors impact on the generation of flow rate. These include but are not limited to:

- a) Volume change, the difference between maximum and minimum volume of pumping chamber over the course of a pump cycle;
- b) Air pump operating frequency;
- c) Characteristics of inlet and outlet valve , thus whether these inlet/outlets are designed with valve or valveless;
- d) Properties of the working fluids;
- e) Air pump dead volume.

From the fluid model, three approaches to raise the amounts of flow rate delivered from the air pump are considered. These are:

- (1) Raise the amount of volume change
- (2) Increasing the operation frequency
- (3) Improve the rectifier efficiency
- (4) Improve the design of the inlet and outlet of valve

The later two points of the valve or valveless rectifier for the efficiency are beyond the scope of this work. The first and second methods are considered.

3.2 Air pump configuration

The schematic diagram Figure 3.2 illustrates the propose air pump including four components. These are: electromagnetic actuator, diaphragm, chamber, and fluid channel.

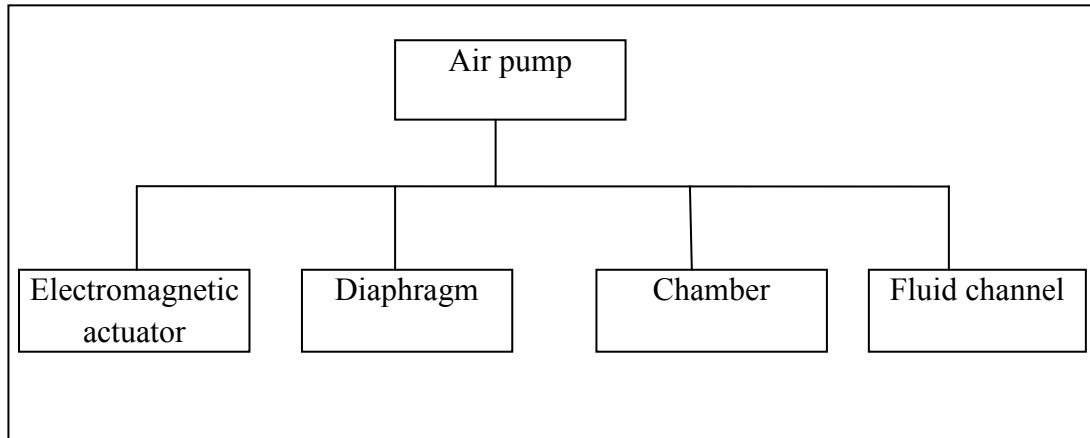


Figure 3. 2: Configuration of the proposed air pump

The electromagnetic air pump with circular chamber was proposed by considering advantages of the electromagnetic actuation scheme and approaches of increasing the amounts of flow rate. The design optimisation for electromagnetic actuator is discussed in section 3.3. The nozzle/diffuser element is selected as the fluid channel due to its ease of integration into the air pump. The physical dimensions for the other three components, namely the diaphragm, chamber and nozzle/diffuser elements are also designed.

3.3 Optimization of electromagnetic actuation

There are several scenarios to consider. The schematic diagram Figure 3.3 shows different type of electromagnetic actuator.

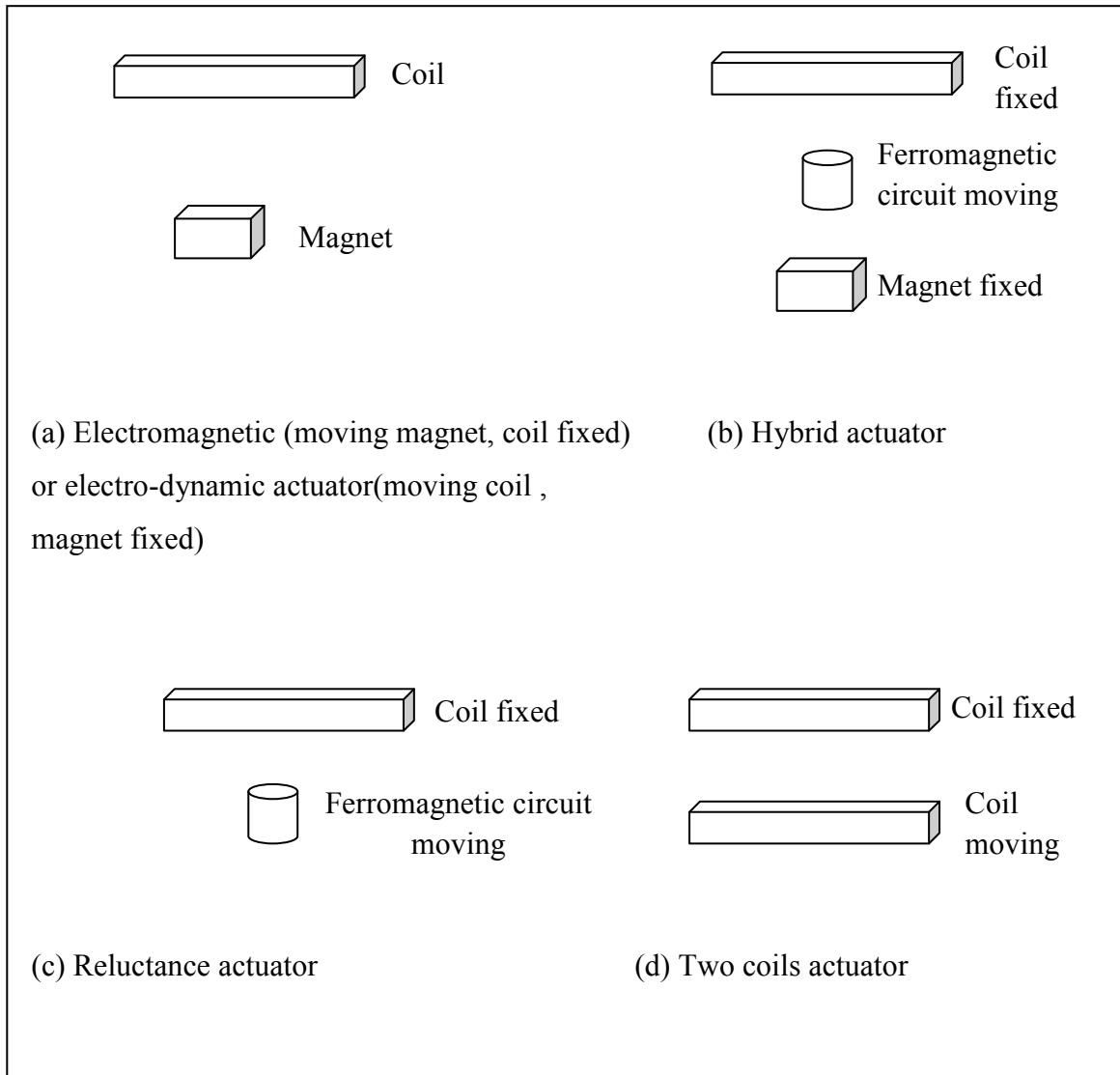


Figure 3. 3: Types of electromagnetic actuator

The electromagnetic actuator is made up of three parts: magnet, electromagnetic coil and a ferromagnetic circuit. They are grouped into several categories as follows [50]:

- 1) Electromagnetic actuator: moving magnet, coil fixed.
- 2) Electro-dynamic actuator: moving coil, magnet fixed.
- 3) Hybrid actuator: coil and magnet fixed, ferromagnetic circuit moving
- 4) Reluctance actuator: coil fixed ferromagnetic circuit moving, no magnet.
- 5) Two coils actuator: interaction between two coils.

If only the actuation force is considered, the electromagnetic and electro-dynamic system is regarded as equal. A hybrid actuator has the problem of magnet adhesion. The reluctance actuator and two coils actuator both have big power consumption. Thus in this study, the electromagnetic actuator is used and further investigated.

3.4 Electromagnetic actuator

It is possible to design and implement an electromagnetic actuator by two methods. The first is by having an embedded magnet into the diaphragm. The other is by having embedded coils into the diaphragm. There are some disadvantages for embedded coils into the diaphragm. Namely, the thickness of the conductor is required to be very thin which results in the lack of the capability of carrying relatively large current. In addition, coils must occupy relatively large area of the diaphragm to produce the required force. This introduces some limitations on the mechanical fluctuation and deflection of the diaphragm. Thus the method of the embedded magnet into diaphragm is chosen in this study.

Both the coil and magnet in an electromagnetic actuator could be individually optimisation. The general configuration of coils and magnet in electromagnetic actuator is present in the following Figure 3.4.

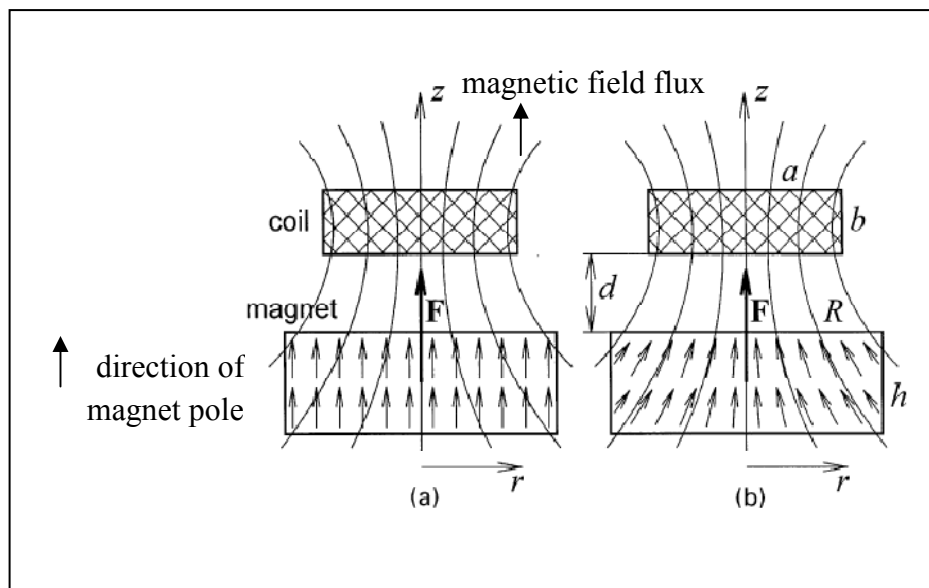


Figure 3. 4: A cylindrical magnet in the axis-symmetric field of coils (a) permanent magnet (b) optimal magnet [51]

To make fabrication convenient, as well as to balance the mass and force, practical electromagnets usually have axial symmetry [51]. The force is greatest if the magnet is magnetised along the field flux lines [52]. The optimisation of magnet orientation of permanent magnet for actuators has been studied extensively [51-53]. However, research on optimising coils is not well documented. Thus in this study, the optimisation of electromagnetic coils must be investigated. Optimum design is achieved when the magnetic field flux follows the direction of the magnet pole (the large curve and small arrows in Figure 3.4(b)).

According to the electromagnetic and force model, electromagnetic force is directly proportional to the current amplitude and the magnetic field gradients. Due to the structure and working principles of diaphragm air pump, one object of optimisation of coils is to obtain maxima magnetic field gradient at central area of the chamber. Before we discuss the design optimization of coils, their geometrical specification must be described.

3.4.1 Specification of electromagnetic coils

Most applications of electromagnetic coils require having a capability to generate a high magnetic field gradient. Considering the structure of electromagnetic air pumps, the maximisation of the magnetic field gradient along z axis direction must be considered. Many features of coils, such as geometry and material, contribute to the enhancement of the magnetic field gradient. Other quantities involved in the force production, such as current capacity of wire or copper track, must also be considered.

Figure 3.5 and figure 3.6 show some design parameters of planar coils and cylindrical coils, such as inner coil radius and outer coil radius. The height of coils is a parameter only for the cylindrical type. The space between two copper tracks is another important parameter for planar coils when it is manufactured by print circuit board technology. R is the central distance for any position and R_o is the outer coils radius.

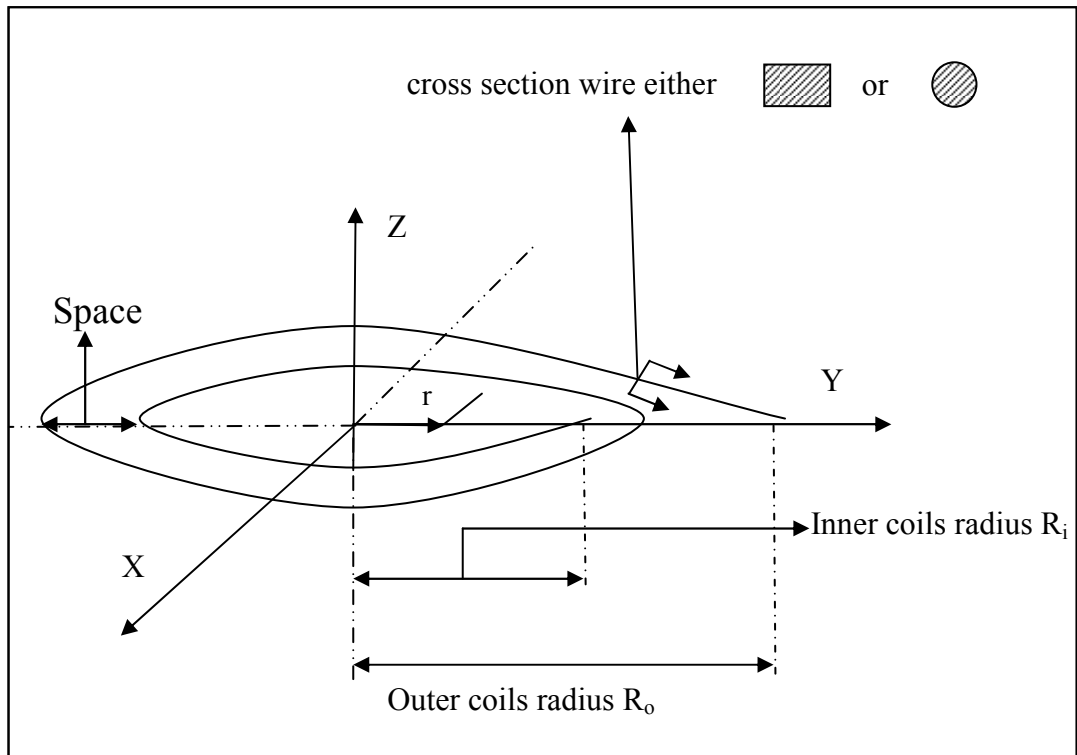


Figure 3. 5: Geometry of planar coils

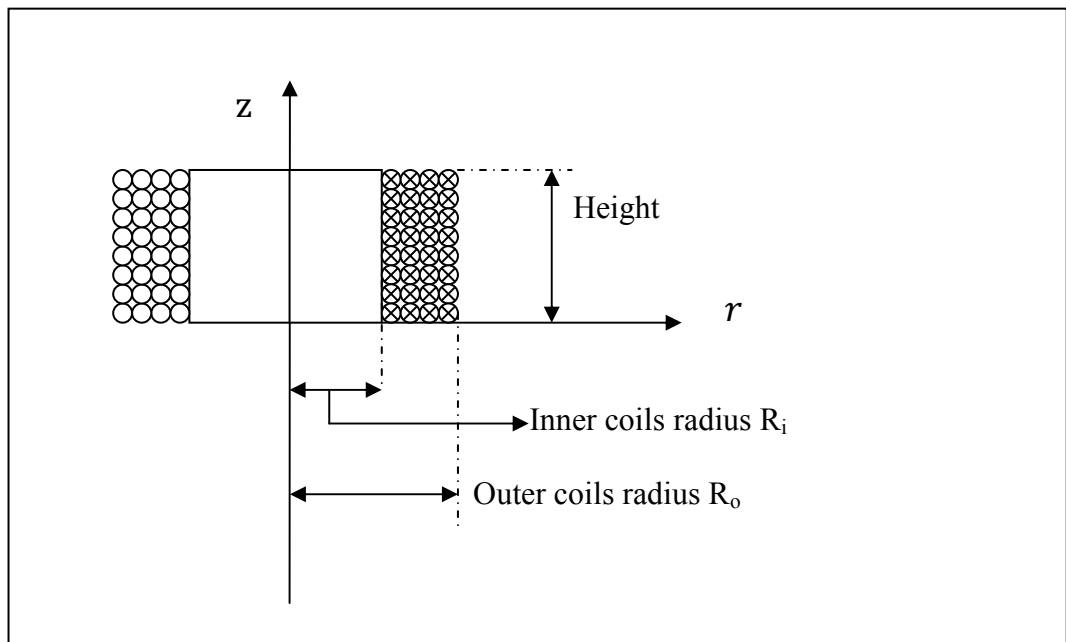


Figure 3. 6: Geometry of Cylindrical coils

The application of a diaphragm air pump requires the maximum force loading in the central area along the z direction. Since the electromagnetic force is a function of

current amplitude and magnetic field gradients ($F \propto I, \partial B_z / \partial z$), each is considered separately. According to the electromagnetic model, the amplitude of current is positive linear and proportional to the force generation. The relationship between the magnetic field gradient and electromagnetic force is non linear. Thus the configuration of the coils is an absolute requirement to be optimised.

3.4.2 Optimised geometry of electromagnetic coil

It is useful for a designer is able to calculate the desired system performance (also called objective function) by determining the system model parameters (also called design variable). Objective function in this work is to maximise the B_z by means of determination for the geometry of electromagnetic coils.

The three-dimensional representations of the magnetic field can give comprehensive positional information about amplitude and orientation. The advantage of using MATLAB is the ability to perform very fast matrix operation. To graph a function of two variables, the *meshgrid()* function is used. There are several three-dimensional plot types available. *Surf()*, which plots the surface of the function, is used here.

The magnetic field intensity B_z of z component is a function of three variables, x, y and z. Due to the application of magnetic field in this study, the amplitude of function B_z distributed along the x and y axis for the given z value is of interest. For optimum design condition, we would like to have a graph of B_z in order to determine an appropriate value of design. For example, the amplitude of B_z for the circular current loop (10mm radius) is plotted as in Figure 3.7 for given z valve ($z=3\text{mm}$). It is assumed that the amplitude of current in the circular loop is 1 Ampere.

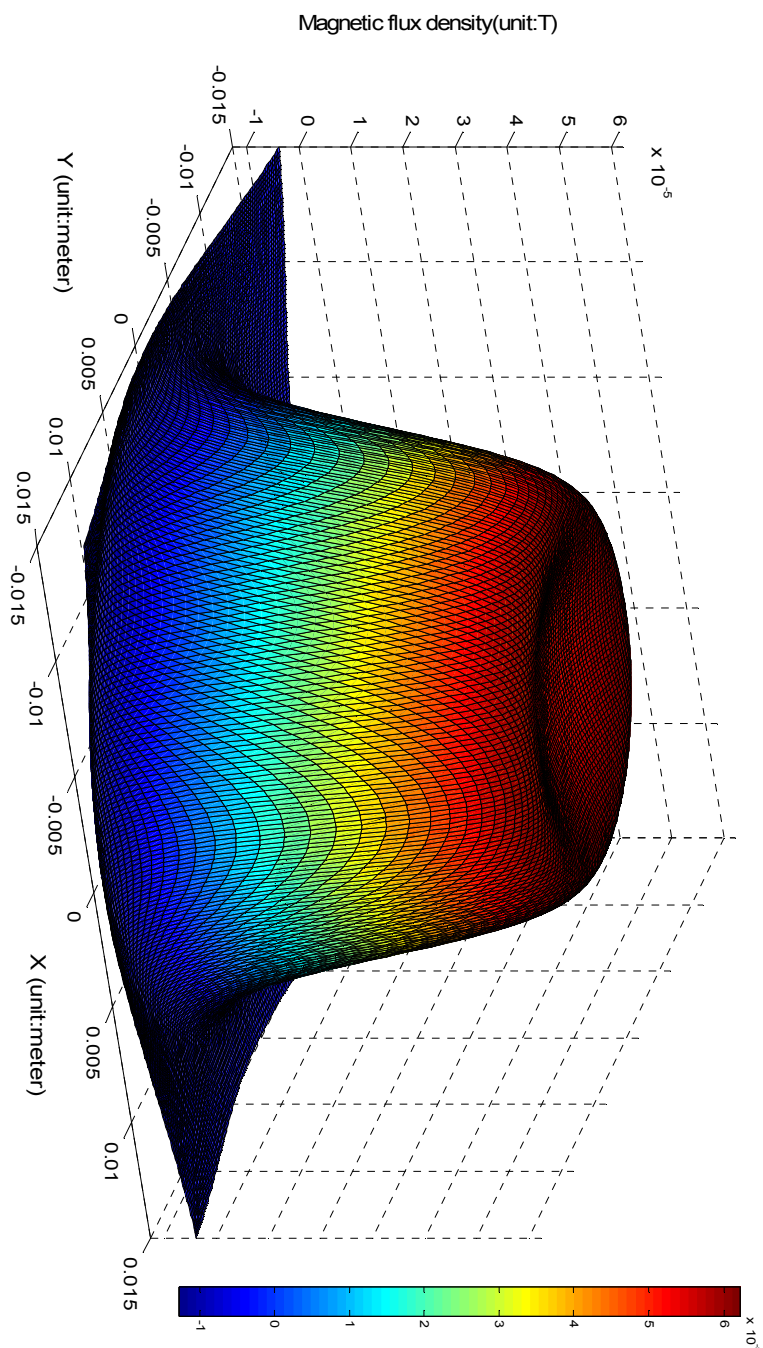


Figure 3. 7: Z component of magnetic flux density for a circular current loop

The original point of the coordinate system represents the centre of the circular current loop. X and Y are coordinates representing the spatial position. Z axis refers to the amplitude and orientation of magnetic field intensity of z component. Figure 3.7 shows that the distribution of magnetic field intensity for z component is asymmetric with the centre line of the circular current loop. The maximum value of B_z is not located at the centre but the $2/3$ part of radius of the circular current loop. The magnetic field intensity of z component has relatively large amplitude around the centre line of the circular current loop.

The $\partial B_z/\partial z$ is defined as the magnetic field gradient of z component along z direction for any point in space. The amplitude of $\partial B_z/\partial z$ for a circular current loop (10mm radius) is presented as 3D Figure 3.8 for the given z value ($z=3\text{mm}$). In Figure 2.5, the z axis refers to the amplitude of magnetic field gradients. The magnetic field gradient is relatively small around centreline of the circular current loop. Distribution of magnetic field gradient $\partial B_z/\partial z$ is also asymmetrical with the centre line of the circular current loop.

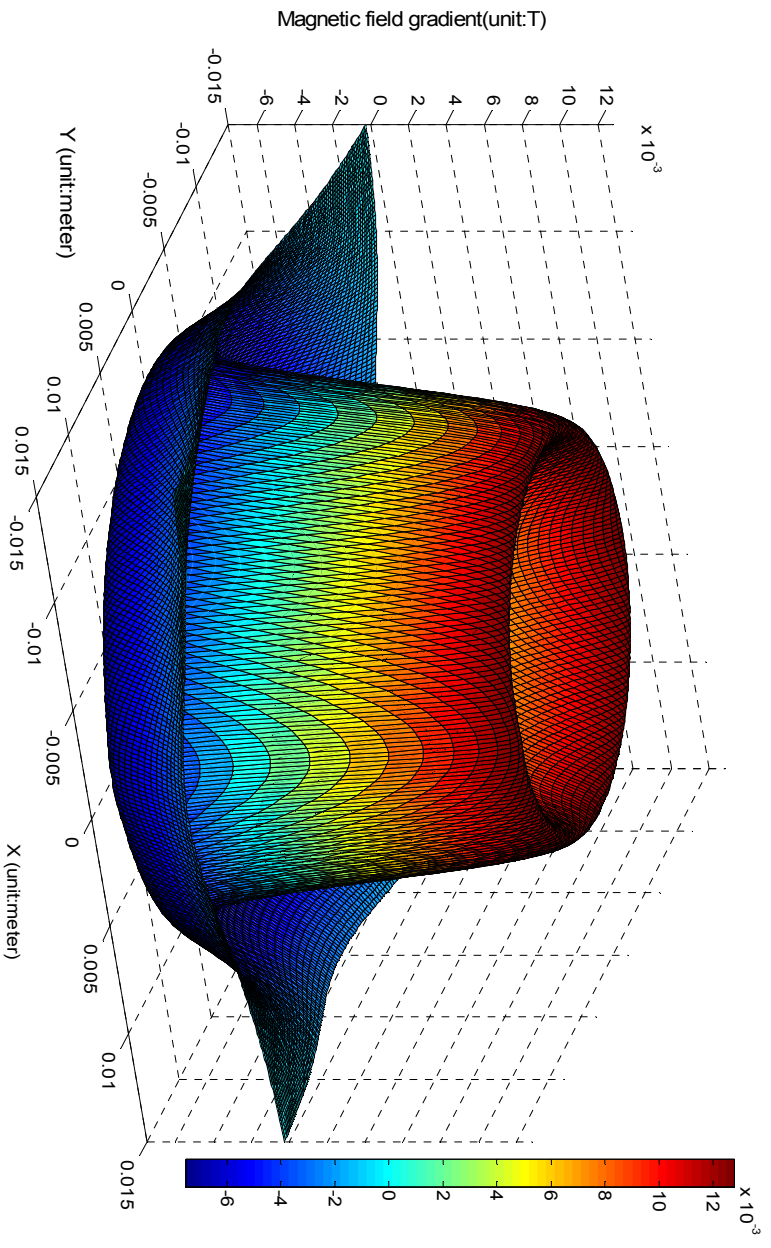


Figure 3. 8: Z component of magnetic flux density gradient for a circular current loop

3.4.2.1 Magnet-coil distance

After several attempts, it is convenient to fix the amplitude of current as 100mA for numerical calculation. It is important to know the distribution of magnetic field gradients on the specific plane under the coils. The distance between the specific plane and coils is a key factor for maximisation of the magnetic field gradient. Investigation of cases in which the inter coils radius and outer coils radii are 2mm and 16mm respectively are shown in Table 3.1.

Table 3. 1: Planar coils geometry

Inter coils radius	Outer coils radius	Space or pitch	Copper track width	Turn	Distance between coils and specific plane
2mm	16mm	0.4mm	0.4mm	20	0.5mm, 1mm, 3mm, 5mm

Figure 3.9 illustrates the z component of the magnetic field gradients along the z axis direction which is the numerical calculation done using electromagnetic model for several cases $z=0.5\text{mm}$, 1mm , 3mm , 5mm .

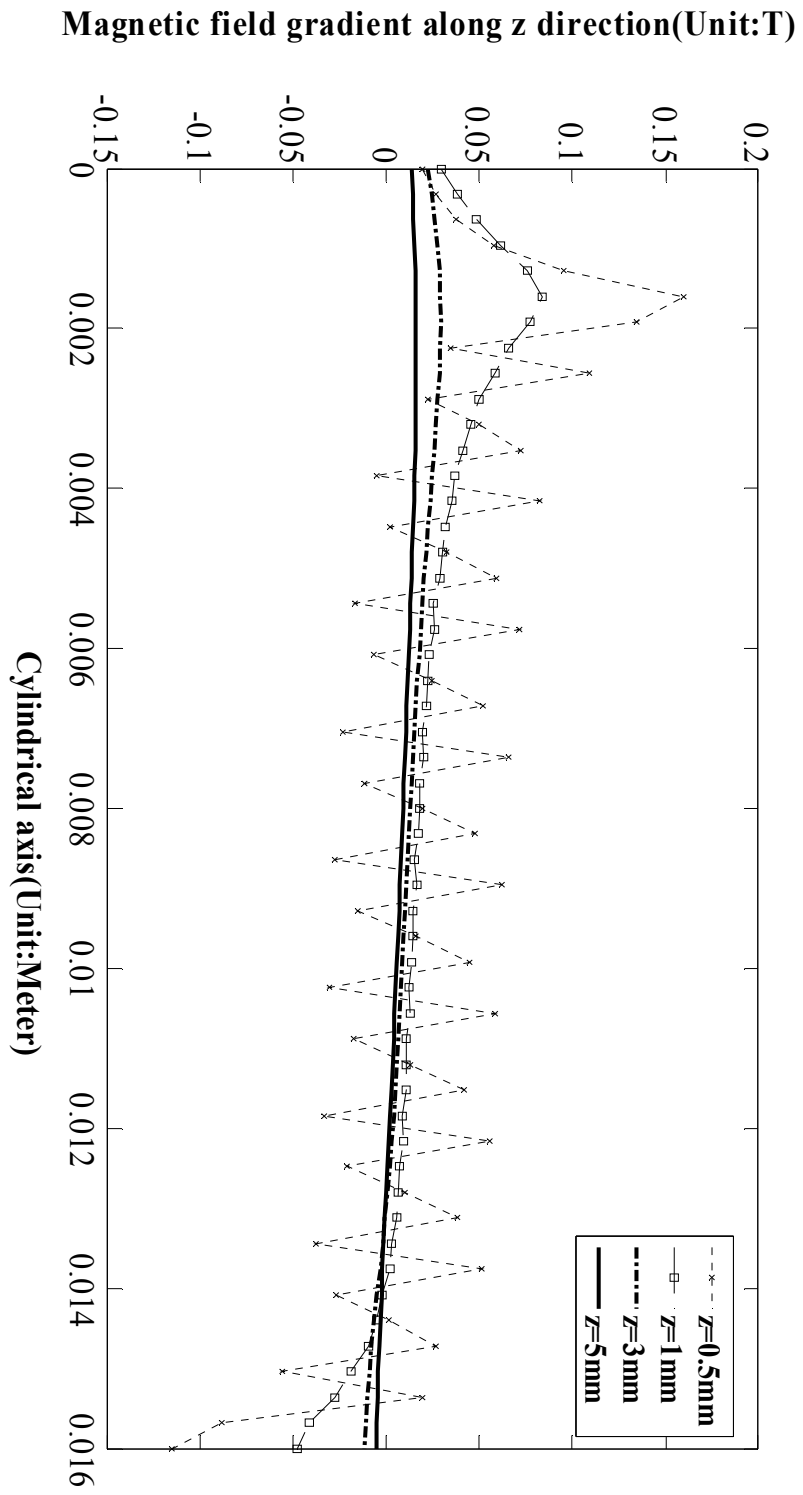


Figure 3. 9: Magnetic field gradients of planar coils for z component at given z value

The cylindrical axis indicates the distance from the centre of planar coils in Figure 3.9. The vertical axis is represented as the amplitude and orientation of $\partial B_z/\partial z$. Readings are taken on the $y=0$ plane at $z=0.5, 1, 3, 5$ mm. The four colours and line styles represent each curve separately. Figure 3.9 shows that the magnetic field gradients ($\partial B_z/\partial z$) decreases dramatically with an increase in z . For a given z value ($z=0.5$ mm), the amplitude of magnetic flux gradient for the z component is relatively small in the centre area of multiple-circular current loops but large values are distributed away from the central area.

3.4.2.2 Outer coils radius

Optimisation design for the outer coils radius must be considered. The parameters of planar coils have to be set before numerical calculation. These are listed in Table 3.2.

Table 3. 2: Planar coils geometry with various outer radius

Inter coils radius	Coil and magnet distance	Space or pitch	Copper track width	Outer radius/inner radius or R_o/R_i (turn)
2mm	3mm	0.4mm	0.4mm	5 (11 turns), 8 (18 turns), 12 (28 turns)

Figure 3.10 illustrates numerical calculation curves which describe the z component of magnetic field gradients along z axis direction for different outer radius. Outer radius of coils are 10 mm, 16 mm, 24 mm respectively. The inner radius of coils is 2 mm.

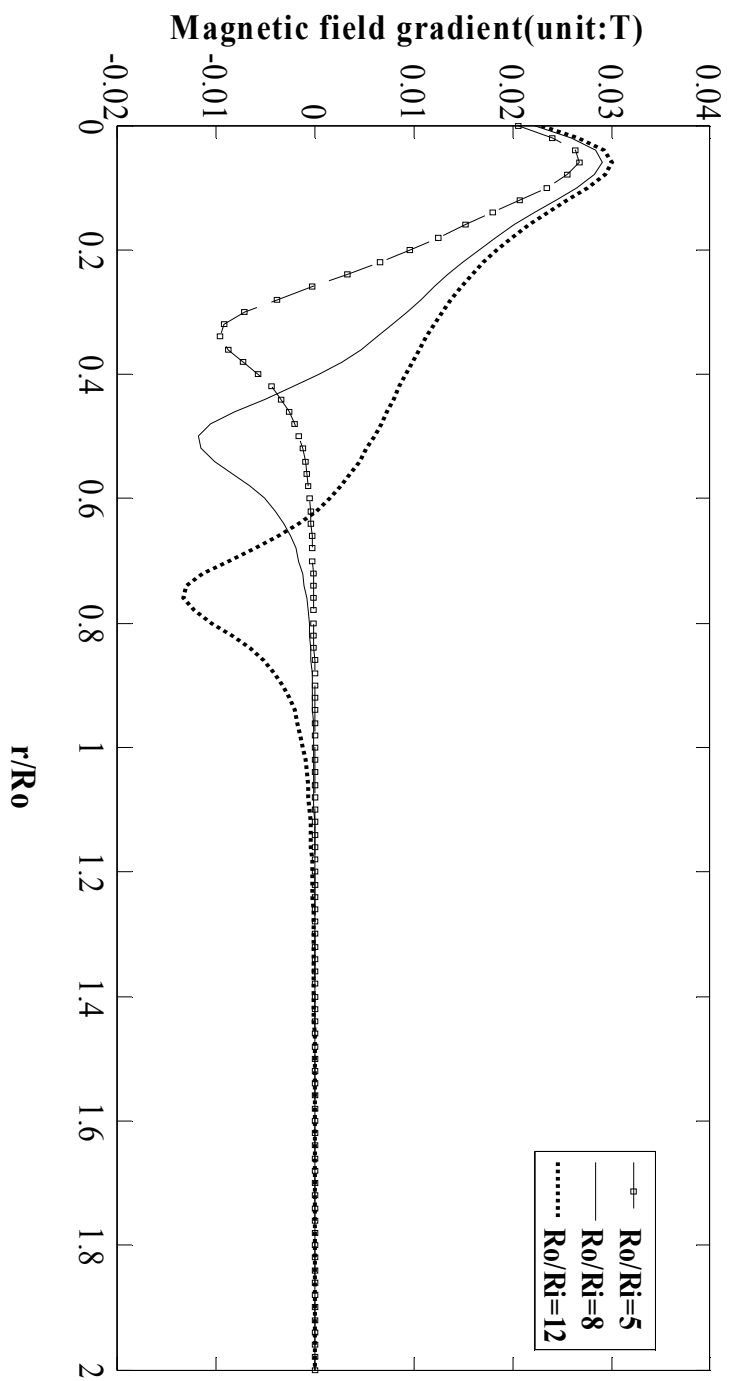


Figure 3. 10: Magnetic field gradients of planar coils for z component at given outer radius

Figure 3.10 shows the magnetic field vs. r / R_o . Readings are taken on the $y=0$ plane at $z=3\text{mm}$ below the surface of planar. Each curve in Figure 3.10 describes the z component of the magnetic field gradients as a function of the distance radius from the centre of the planar. They are represented by three colours and line styles. It shows that the magnetic field gradients become strong in the small central area of planar coils when the outer radius coils is enlarged. The magnetic field gradients increase when the ratio of inner radius and outer radius increase from 5 to 8. There is, however, no marked increase in the magnetic field gradient when the ratios of inner radius and outer radius is 12.

3.4.2.3 Inner coils radius

Inner radius of coils is an important parameter that should be considered. In order to find the design rules of inner radius, the numerical calculation of magnetic field gradients for inner radius is performed. The numerical calculation parameters are listed in Table 3.3.

Table 3. 3: Planar coils geometry with various values of inner radius

outer coils radius	coils and magnet distance	Space or pitch	Copper track width	inner radius/Outer radius or R_i/R_o (turn)
16mm	3mm	0.4mm	0.4mm	0.05 (20 turns), 0.1 (19 turns), 0.3 (15 turns), 0.5 (11 turns)

Figure 3.11 illustrates the properties of the magnetic field gradient along the z axis direction of z component at various r value.

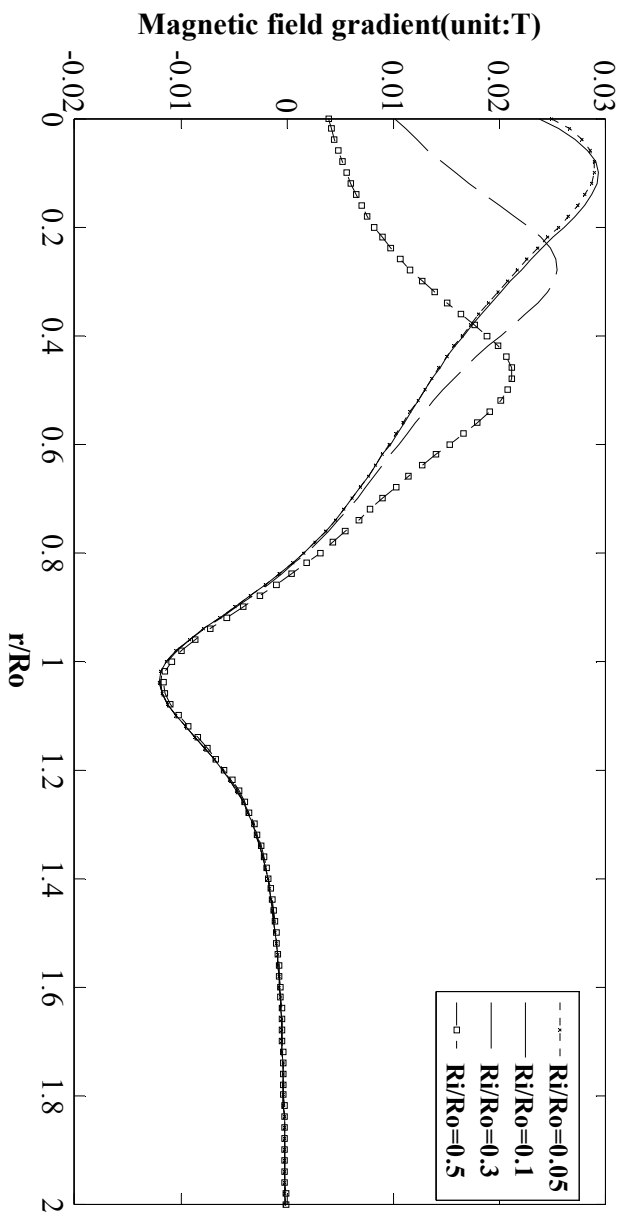


Figure 3. 11: Magnetic field gradients of planar coils for z component at given inner radius

The horizontal axis represents as ratio between the inner radius and outer radius in Figure 3.11. The vertical axis represents the amplitude and orientation of the magnetic field gradient. Each curve is presented as a function of the z component of magnetic field gradients with the distance radius from the centre of the planar. Four curves are drawn under condition of four inner radius for given $z=3\text{mm}$ and outer radius= 16mm . It is observed (Figure 3.11) that the magnetic field gradient has a large drop when the ratio of inner radius and outer radius decreases from 0.1 to 0.3. At the same time, the location of the maximum value of $\partial B_z/\partial z$ shifts from radius of coils/ $R_o=0.1$ to 0.3. The magnetic field gradient is not sensitive to reduction of the inner radius when the ratio of inner radius and outer radius is below 0.1.

3.4.2.4 Copper track width

The copper track width is the same as the wire diameter for circular wires and the width for rectangular a cross-sectional area wire. Numerical calculation parameters for examining copper track width are listed in Table 3.4.

Table 3. 4: Planar coils geometry with various of copper track width

inter coils radius	outer coils radius	inner radius/ width(turn)	Space or pitch	Copper track width	coils and magnet distance
2mm	16mm	5 (18 turns), 10 (24 turns), 15 (27 turns), 20 (29 turns)	0.4mm	0.4mm	3mm

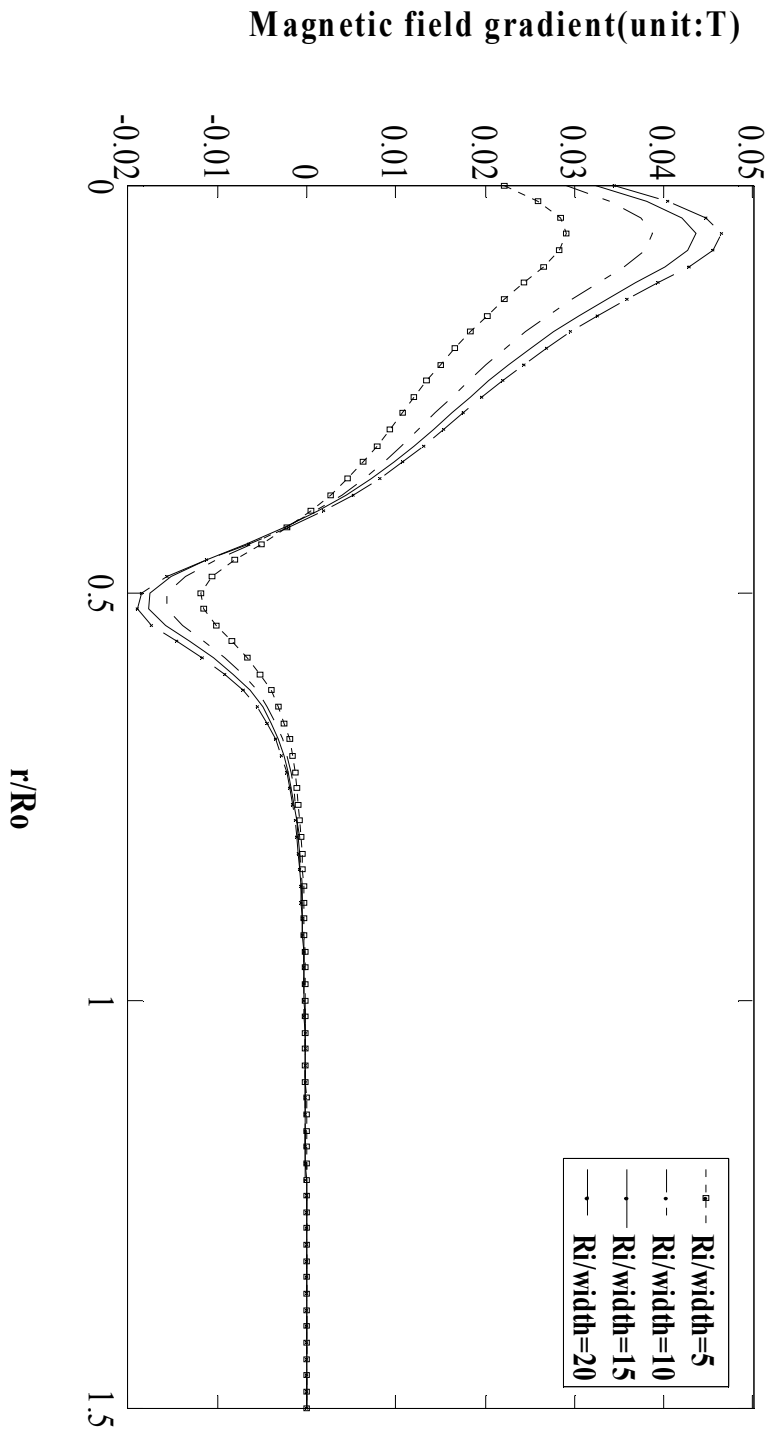


Figure 3. 12: Magnetic field gradient of planar coils for z component at given copper track width

Figure 3.12 shows the magnetic field gradient vs. r to outer radius. The vertical axis indicates the amplitude and orientation of the magnetic field gradient. This figure shows that a reduction of width of conductor increases the z component of magnetic field gradient.

3.5 Driving circuit design

The purpose of the driving circuit for electromagnetic actuator is the supply of the tuneable current to generate the magnetic field. It is well known that design parameters of driving circuits can vary from case to case because of the coil impedance. The operational or maximum current and voltage for the electronic component is calculated based on the coil configuration. The performance of a driving circuit is decided by the circuit layout and the quality of the components. Achieving a good dynamic performance of driving circuits is also challenging. The simple audio amplifier is selected to complete the function of the driving circuit. Figure 3.13 shows an example of the driving circuit design.

The magnetic field created by a changing the current in the circuit itself induces a voltage in the same circuit. The self-inductance voltage is defined by the ratio of the magnetic flux linkage to the current through circuit [40]. The flux linkage is directly proportion to the number of turns of coils, cross sectional area of conductor, current and multiplicative inverse of coils radius [41]. Because the thickness of the conductor is negligible as compared to the radius of the coils, the self inductance voltage is not a factor in this study.

3.6 Diaphragm design

The choice of pump diaphragm material can be particularly important. Desired properties of pumping diaphragm are large deflection and good sealing. In addition, to improve the achievable flow rate, a material that will allow the deflected membrane to efficiently match and conform to the pumping chamber geometry is needed. For an electromagnetic air pump driven by a low-frequency and/or low force actuator, a low young modulus diaphragm material generally allows the volume change to be maximised.

The vibration characteristic of a diaphragm is determined by the geometry and material properties as well as boundary conditions. The diaphragm geometry is specified by its shape and dimensions. And the material properties parameters influencing resonant frequency include the density, residual stress, elastic modulus, and Poisson's ratio [54].

3.6.1 Determining diaphragm materials

The choice of diaphragm material demands consideration of the frequency of vibration, which is often dependent on the actuation method. Because of low working frequency for electromagnetic diaphragm pumps, low-modulus diaphragm materials are better choices to generate the maximum change in volume. Silicone rubber has low Young's modulus and durometer, as well as high elongation. These properties make it an excellent choice for this task. Flexible diaphragms with large deflection amplitudes, such as PDMS, are becoming more common as materials in diaphragm pumps.

Recently, PDMS material is receiving an increasing amount of attention from researchers [55, 56]. It provides several advantages:

- a) Bio- and chemical compatibility and safety;
- b) At low temperature and short time periods, it acts like a viscous liquid. After a long time periods curing, it acts like an elastic solid, similar to rubber;
- c) Suitable and cheap material for encapsulation.

3.6.2 Dynamic properties of diaphragm

The dynamic characteristics of diaphragm deflection impact on the amounts of flow rate production by the air pump. Dynamic properties of diaphragm vibrating are suggested by Doebelin [57]. For a clamped edge diaphragm vibrating in a fluid, the lowest natural frequency is given by the following equation (3.1) [57]:

$$\omega = \frac{10.21}{C R^2} \sqrt{\frac{E t^2}{12 \rho_d (1 - \nu^2)}} \text{ rad/s} \quad (3.1)$$

$$C = \sqrt{1 + 0.669 \frac{\rho_f R}{\rho_d t}} \quad (3.2)$$

Where ρ_f is the density of the fluid, ρ_d is the mass density of the diaphragm material, R is the radius of diaphragm, t is the thickness of diaphragm, E is Young's module of diaphragm, ν is Poisson's ratio.

As per equations (3.1) and (2.23), it is possible to understand in theoretically that the volume change is increased with the diameter of the diaphragm but the trade-off is reducing the natural frequency. Numerical calculation of maximum defection of diaphragm was made according to the electromagnet, force produce and mechanical models and given in next chapter.

3.7 Chamber configuration

A pump chamber (bounded on one side by the pump diaphragm) is the basic component of air pump. Chamber configuration will influence the pressure characteristics, volume stroke, and valveless channel or nozzle-diffuser loss coefficients significantly [1].

Most air pumps have a single chamber. In order to improve the performance of air pumps, two and three-chamber configurations have been introduced in the Figure 3.14.

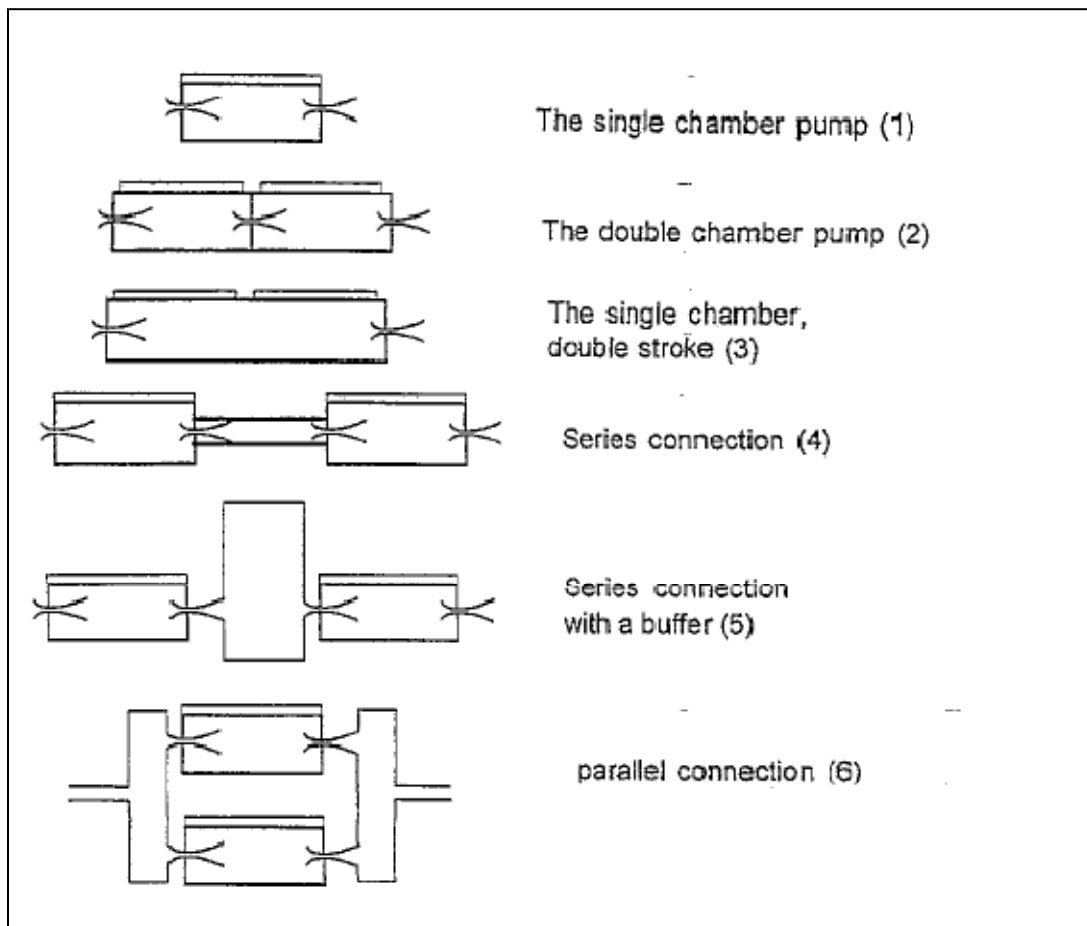


Figure 3. 14: Various configurations of pumps [58]

In order to understand the best operational chamber configuration for pumps, Ullmann [58] developed a model for the performance of a single and double-chamber pump. Analysis and comparison of different combination modes also were explained, including a single chamber pump (1), a double-chamber pump (2), a single chamber with two times the stroke volume (3), a series connection of two single chamber pumps (4), a series connection of two single chamber pumps with a middle buffer (5) and a parallel connection of two single pumps (6).

Most of diaphragm air pumps have a single pump chamber. However, two pump chambers arranged in parallel was intended to reduce oscillation in the pump output due to periodic driver operation [59-61].

3.8 Valve design

Valves are among the most important elements of a diaphragm air pump and the promising flow control devices. Valve classification, illustrated in Figure 3.15, generally can be classified into two categories: (1) Active valve, the closure and opening of active elements is operated by means of an active external control; (2) Passive valve, meaning that they do not include any actuation. The directional effect can be obtained from the mechanical motion of an opening/closing element or from dynamic flow directionality of the fluidic conduit, in the case of fixed elements.

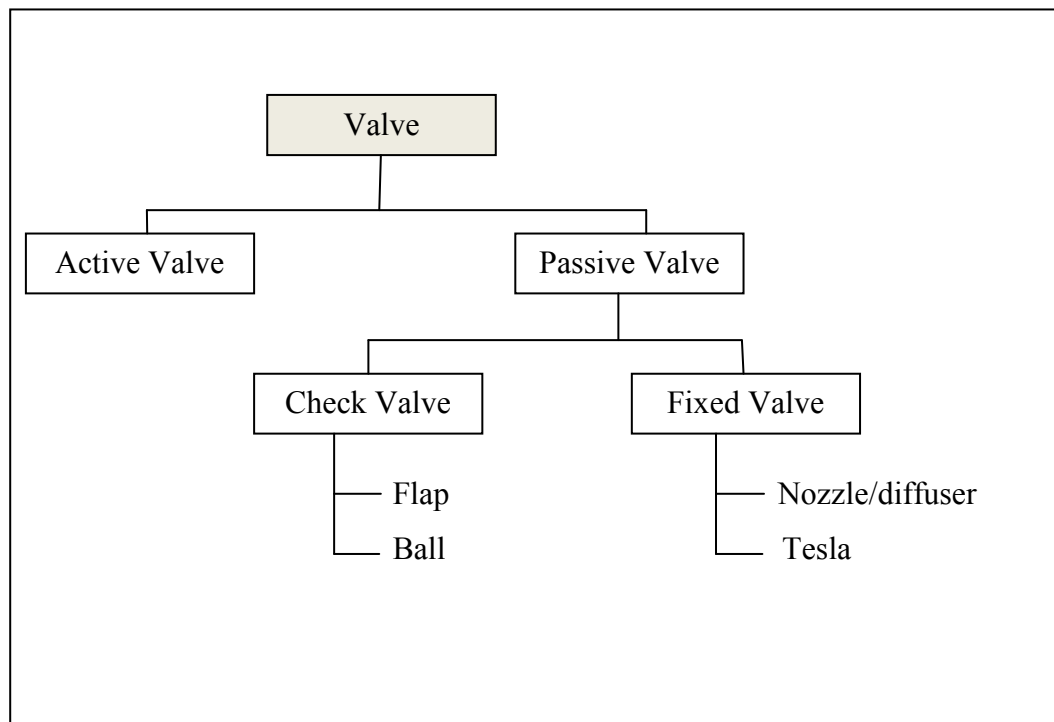


Figure 3. 15: Valve classification

The first valveless miniature pump was presented in 1993 by E.Stemme. Pumps with movable valves, and other pumps with movable parts such as rotating pumps, may suffer from problems such as a high pressure drop across the valves and wear and fatigue of the movable parts. This may result in reduced lifetimes and reliability. There is also the risk that the valve action may cause damage to sensitive fluids. Therefore there is a need for pumps with no movable parts valve [29].

The geometry of the nozzle/diffuser is a very important factor impacting on the amount of flow rate from the air pump. The determination of geometry for nozzle/diffuser is complex and was not covered in this study. Much research on this topic has been published [62]. Figure 3.16 shows the dimensional parameters of a flat-walled diffuser element.

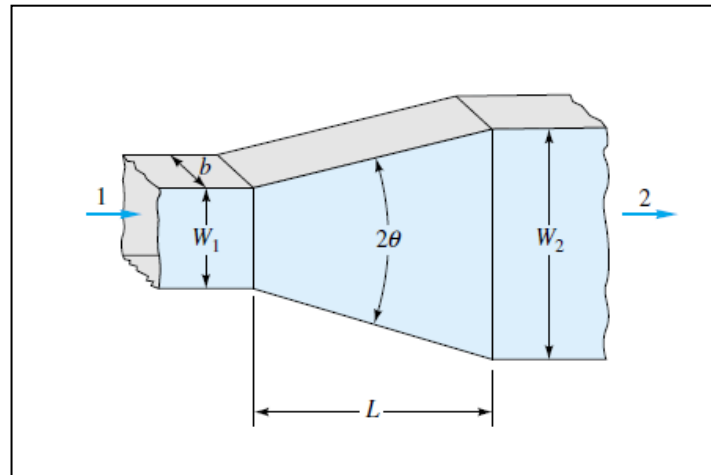


Figure 3. 16: Geometry of a diffuser element [62]

There are four important geometric parameters:

- a. Area ratio $AR = A2/A1$
- b. Divergence angle 2θ
- c. Slenderness $L/W1$ or L/D
- d. Aspect ratio $AS=b/W1$

After careful consideration, this research was the system given in Figure 3.17 because of smoothness of the flow.

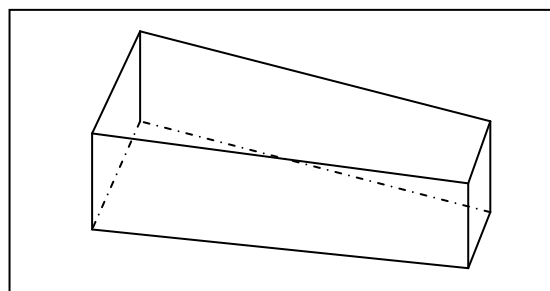


Figure 3. 17: A flat walled diffuser element

3.10 Summary

In the above work, the optimal design for electromagnetic coils has been done based on electromagnetic and force production model. The results of numerical calculation allow a chance to assess the design before physical building. An interesting property of the distribution of the magnetic field gradient is symmetry. The height of cylindrical coils could be considered as Cartesian coordinate translation. The methods for the air pumps design including the electromagnetic coils, diaphragm, chamber configuration and valveless channel are presented. Methods of fabrication and test for air pumps are discussed in the next chapter.

CHAPTER 4

AIR PUMP FABRICATION

4.1 Introduction

Chapter 2 describes the analytical models of the various components of a diaphragm air pump. Using these models, some computations were conducted for design optimisation and presented in the chapter 3. This chapter discusses fabrications of the air pumps. The fabrication process of the air pump is detailed and the procedure of manufacturing of electromagnetic coils, the chamber and the diaphragm are given. Generally, the methods of fabrication used in the prototype and commercially may be different. Cost and quality are the priorities to be considered in commercial manufacturing. However researches would like to take notice of rapid and flexibility.

4.2 Air pump design

Details for air pump design using methods presented in the chapter 3 will be outlined in the following section. The physical dimensions of two types of electromagnetic coils, flat planar and cylindrical, are determined. The shape and size of chambers are developed. According to the model, presented in the chapter2, the maximum central deflection of diaphragm is calculated. The geometry of nozzle element is developed.

4.2.1 Electromagnetic coils design

According to numerical calculation results of design optimisation for the electromagnetic actuation, two types of electromagnetic coils were designed.

4.2.1.1 Flat planar coils

A flat planar coil was proposed to be designed to produce the required magnetic field gradients along the z axis direction. Minimising power consumption is also considered. To utilise the full range of the power amplifier (1-2A), the planar coil was designed to carry 3 Amps peak current. This was limited by the capability of the printed circuit board. Employing traditional PCB technology, the complex pattern of planar could be transformed on the PCB with small package size. In addition, they are easy to integrate into an air pump. This planar coil on PCB is designed by CAD software (Altium designer winter 09). The main design parameter is presented as in Table 4.1.

Table 4. 1: Planar coils design

PCB material and type	Internal Radius	External Radius	Space or pitch	Copper track width
FR4,singal side	1.6mm	16.4mm	0.4mm	0.4mm

4.2.1.2 Cylindrical coils

Conventional cylindrical coils can generate strong magnetic field gradients, but less current consumption. Configurations of cylindrical coils were optimally designed to be in accordance with the numerical calculation results of the electromagnetic model. The particular bobbin is needed for the special case of coil configurations. Bobbin was designed using CAD software the Solidwork 2009. The 0.25mm diameter enamelled copper wire was selected to carry a maximum 0.5mA current. A sketch of the structure of bobbin is presented in Figure 4.1. Geometric parameter of the special bobbin is shown in Table 4.2.

Table 4. 2: Design parameters of the bobbin

A	B	C	D	H
60mm	8mm	10mm	14mm	2mm

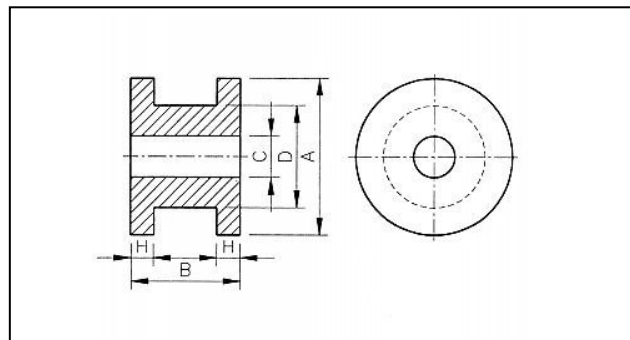


Figure 4. 1: Sketch of the structure of the bobbin

4.2.2 Small deflection of diaphragm

Using equations (2.15, 2.16 and 2.17) built in chapter2, numerical calculations were conducted by Matlab. Figure 4.2 shows the relationship between the amplitude of current and the maximum central deflection of PDMS diaphragm as a linear function. Conditions of numerical calculation are listed in Table 4.3.

Table 4. 3: Numerical calculation parameters of small deflection

Electromagnetic planar coils				
inter coils radius	outer coils radius	Space or pitch	Copper track width	turn
1.6mm	16.4mm	0.4mm	0.4mm	20
Permanent magnet(cylindrical shape)				
diameter	thickness	coils and magnet distance		
12mm	2mm	3mm		
Circular PDMS diaphragm^[1]				
thickness	Young's modulus^[2]	Poisson's ratio^[3]	diameter	
0.23mm	0.8×10^6	0.5	32mm	

^[1] Boundary condition is clamping.

^{[2][3]} Young's modulus and Poisson's ratio depend on fabrication process [64] .

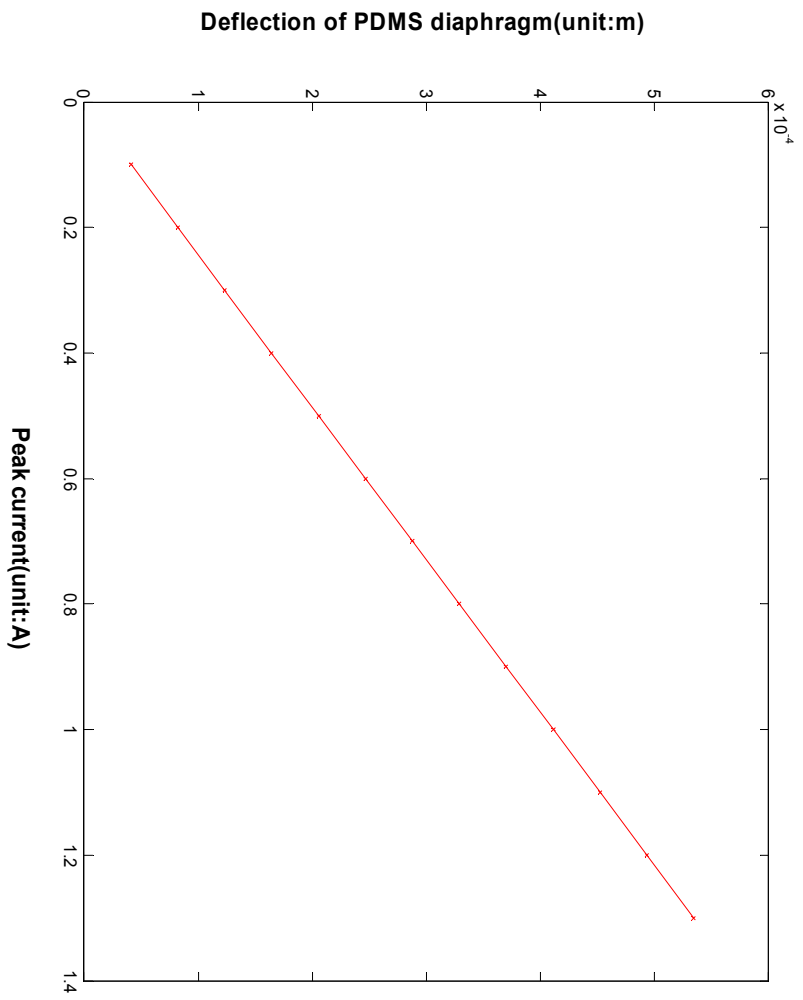


Figure 4. 2: Numerical calculation of maximum deflection of diaphragm

4.2.3 Large deflection of diaphragm

Using equations (2.15, 2.17 and 2.21) in chapter2, numerical calculations were made by Matlab. Figure 4.3 shows the relationship between the amplitude of current and the maximum central deflection of PDMS diaphragm. Numerical calculation parameters for the large deflection of diaphragm are listed in Table 4.4.

Table 4. 4: Numerical calculation parameters for large deflection

Electromagnetic cylindrical coils				
inter coils radius	outer coils radius	Space or pitch	Copper track width	height
7mm	24mm	0	0.27mm	8mm
Permanent magnet (square shape)				
Diameter	Thickness	coils and magnet distance		
6mm	4mm	1mm		
Circular PDMS diaphragm^[4]				
thickness	Young's modulus	Poisson's ratio	Diameter	
0.23mm	0.8×10^6	0.5	50mm	

^[4] Boundary condition is clamping.

Using equations (2.15), (2.17) and (2.19), numerical calculations were made by Matlab. Results are shown in Figure 4.3.

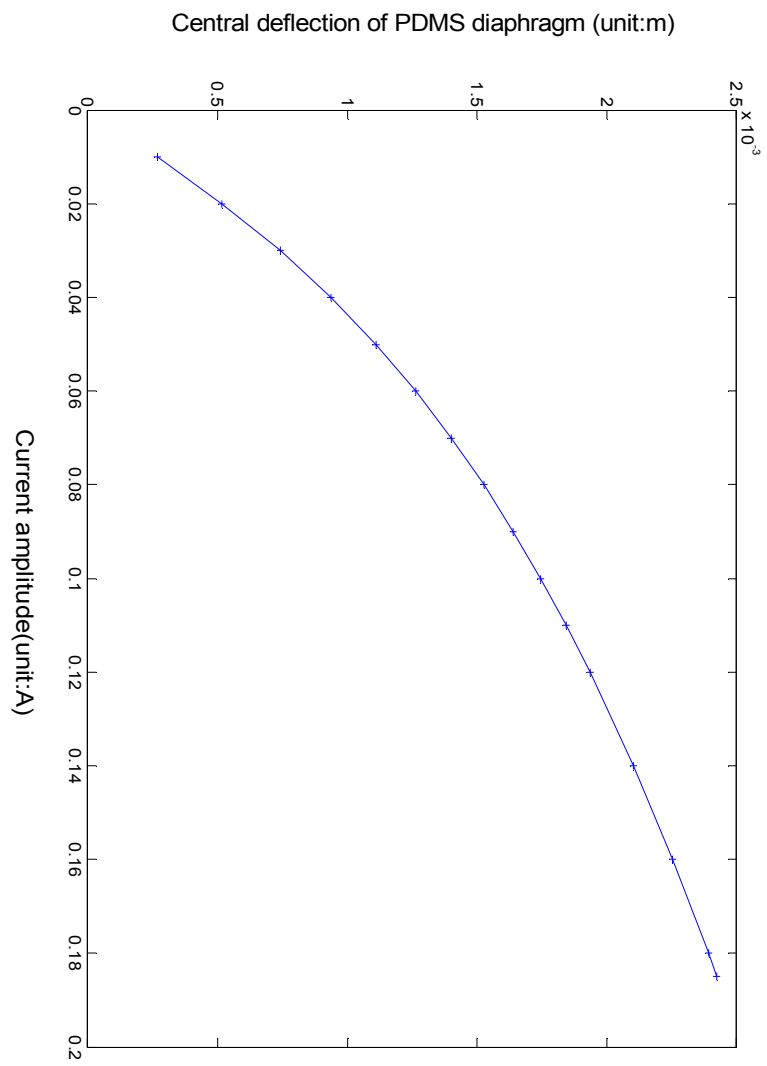


Figure 4. 3: Numerical calculation of large deflection of PDMS diaphragm

Figure 4.3 shows the relationship between the load and maximum deflection of diaphragm as a non-linear function. The deflection of the diaphragm increase rapidly when the load is enlarged from zero to 0.005 N. The increase of the deflection for diaphragm is not significant when the load is over 0.01N.

4.2.4 Chamber and nozzle element

A circular shape of a double chamber with one diaphragm was considered. The diameter of the chamber is 32mm. The sketch of structure this type of air pump is shown in Figure 4.4.

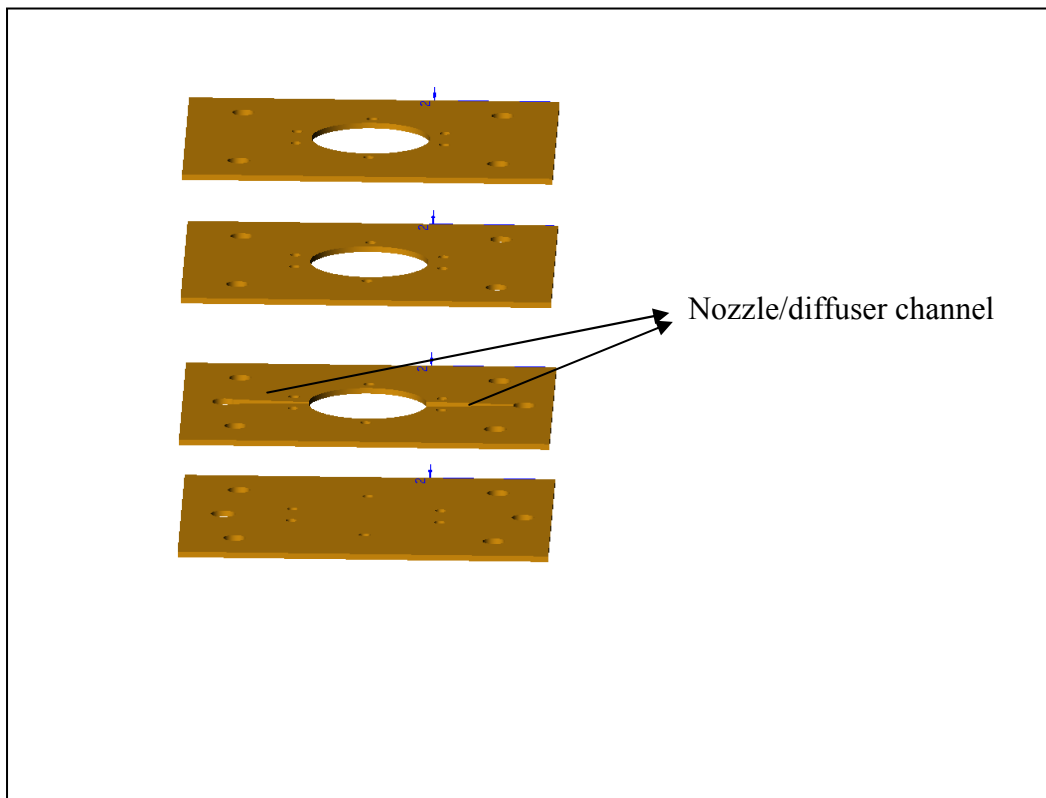


Figure 4. 4: A chamber with nozzle/diffuse (explode view)

A circular shape of single chamber with 50mm diameter was designed. The sketch of arrangement for electromagnetic coils, chamber and nozzle/diffuser channel components is presented in Figure 4.5. Typical value of flow rectification efficiency of diffuser is in the range of 0.01----0.05.

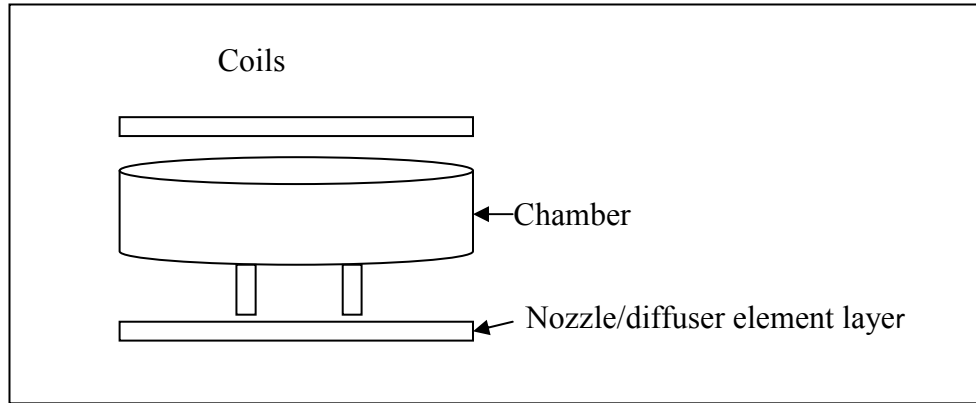


Figure 4. 5: Configuration of single chamber

The dimensions of the propose diffuser element in this study is shown in Figure 4.6.

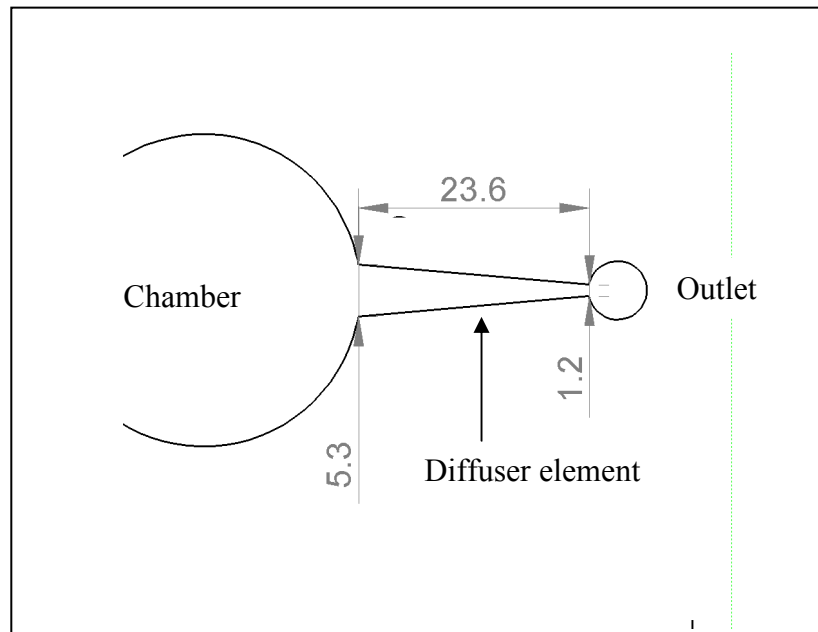


Figure 4. 6: Dimensions of a diffuser element (Unit: mm)

4.3 Air pump fabrication

Last section shows details of air pump design involved in some components such as electromagnetic coils, chamber and nozzle/diffuser element. Fabrication for the air pumps will be presented in the following section. It includes that fabrication of electromagnetic coils, PDMS diaphragm, chamber, nozzle/diffuser elements as well as assembly of the air pumps.

4.3.1 Electromagnetic coils fabrication

In general, there are two methods for wire winding, conventional wire-winding and printed circuit board technology, which can be utilised for fabrication of electromagnetic coils. These methods will be discussed shortly.

4.3.1.1 Conventional wire-winding

Conventional wire-winding technology for fabrication of coils is simple. According to the electromagnetic coils design, the shape and dimension bobbin must be determined. After bobbin construction, the suitable diameter of enamelled copper wire will be wind around it by manual or winder machine.

The cylindrical coils utilise the traditional technology. Some drawbacks of this technology are space occupation and heat dissipation. It is obvious that this technology has less capability to built complex patterns of electromagnetic coils. However, it is available and easy to use.

4.3.1.2 Cylindrical coils

A special bobbin was manufactured by the rapid prototype technology—3D printing. Cylindrical coils were manufactured by the Marque Magnetic Company (see Figure 4.7). The cylindrical coils consist of the standard enamelled copper wire (AWG 30).

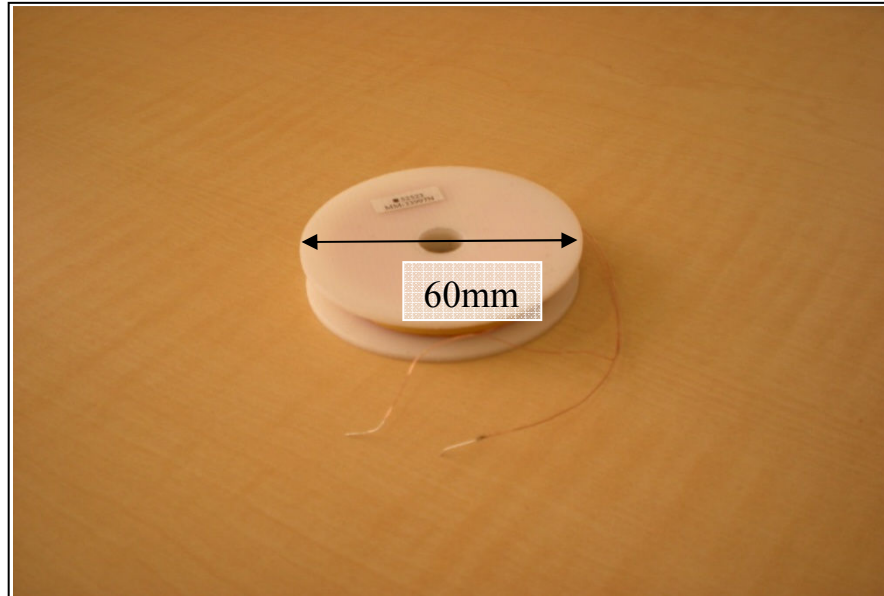


Figure 4. 7: Cylindrical coils

4.3.1.3 Printed circuit technology

A printed circuit board, or PCB, is used to mechanically support and electrically connect electronic components using conductive pathways, tracks or signal traces etched from copper sheets laminated onto a non-conductive substrate. The major steps involved in the fabrication process of electromagnetic coil on the single-sided PCBs are pattern transform, electroplating, etching. The PCB technology is more affordable and has the capability to transform complex pattern of 2D planar coils.

4.3.1.4 PCB planar coils

PCB technology uses printed circuit boards consisting of epoxy laminate (FR4) with copper coating on one side (Figure 4.8). The copper track space is 0.4mm and it can be manufactured locally. The connected wire was soldered by hand.

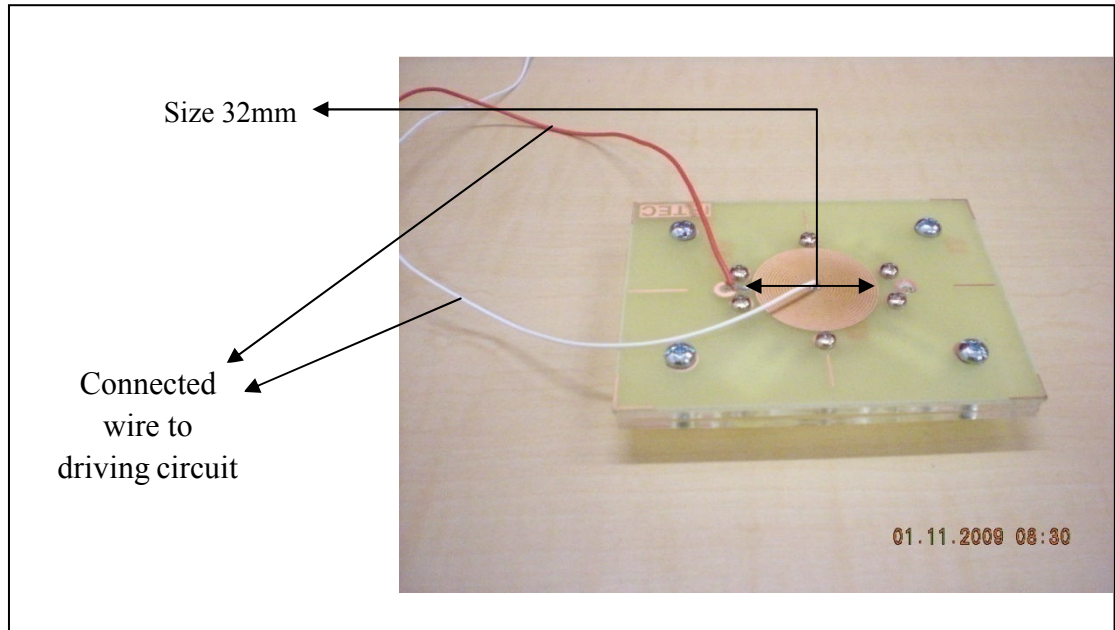


Figure 4. 8: PCB planar coils

The inner radius and outer radius of the planar coils are 1.6mm and 16mm respectively. These boards are structured by drilling and milling (for the whole board) and by etching for the copper plating. These boards and the treatment are standard in the electronic industry and are inexpensive.

4.4 PDMS Diaphragm

The following section shows the procedure of thin PDMS diaphragm made. Also the PDMS diaphragm embedded with magnet as well as corrugated diaphragm are presented in the section.

4.4.1 Procedures of PDMS diaphragm

The schematic procedure for fabrication of thin PDMS (Sylgard@ 184, silicone elastomer kit) diaphragm is shown in Figure 4.9.

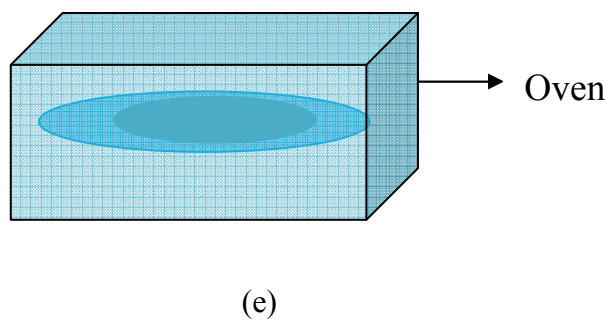
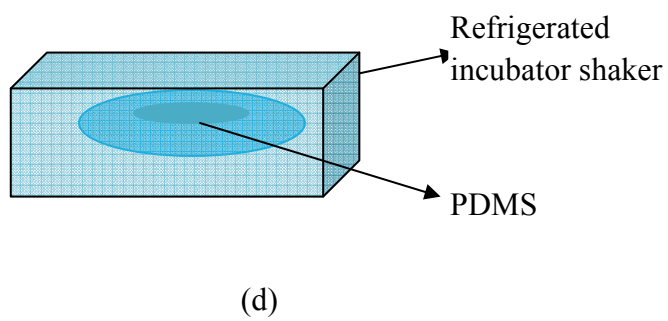
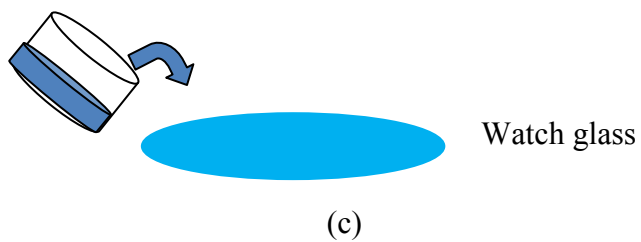
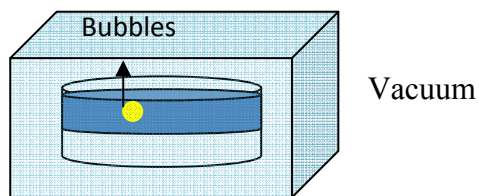
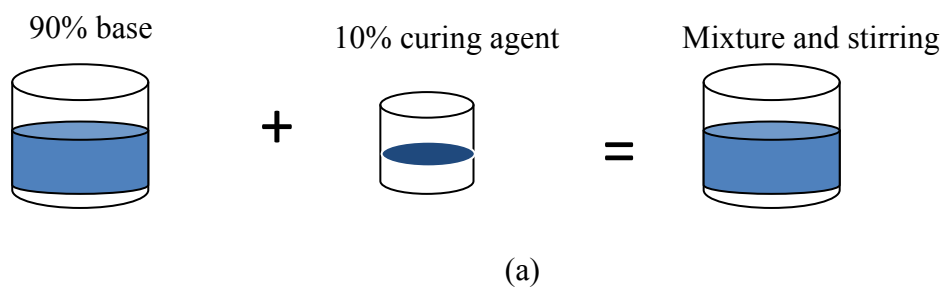


Figure 4. 9: PDMS manufacturing procedure

Fabrication procedures of PDMS diaphragm are described in the following steps:

Step 1: Pour the required amount of curing agent into a clear container on the electronic balance. Keep in mind that PDMS base added should be 10 times this weight.

Step 2: Carefully pour the required amount of PDMS base – this is 10 times the weight of the curing agent already measured.

Step 3: Thorough mixing with glass stick ensuring that the curing agent is uniformly distributed – this will ensure that the final PDMS mould is uniformly cross linked.

Step 4: The mixture must be vacuumed to eliminate the trapped air bubbles.

Step 5: Once a clear, bubble free PDMS mixture is obtained, it is poured over the watch glass or moulds.

Step 6: Place the watch glass or moulds into low temperature oven.

Step 7: Curing is done by placing the PDMS with watch glass or moulds in an oven at 70°C. Duration of heating is between 6-8 hours. Cured PDMS cease to be sticky – and this can be tested by prodding with a sample holder.

Step 8: Wait for the PDMS to cool. After this, tweak around the edges with a sharp knife, trying to get a grip of the PDMS at an edge. If the PDMS is suitably cured, application of a steady pressure should help peel off the PDMS completely with ease.

4.4.2 Diaphragm embedded with permanent magnet

Figure 4.10 shows the PDMS diaphragm embedded with a permanent magnet.

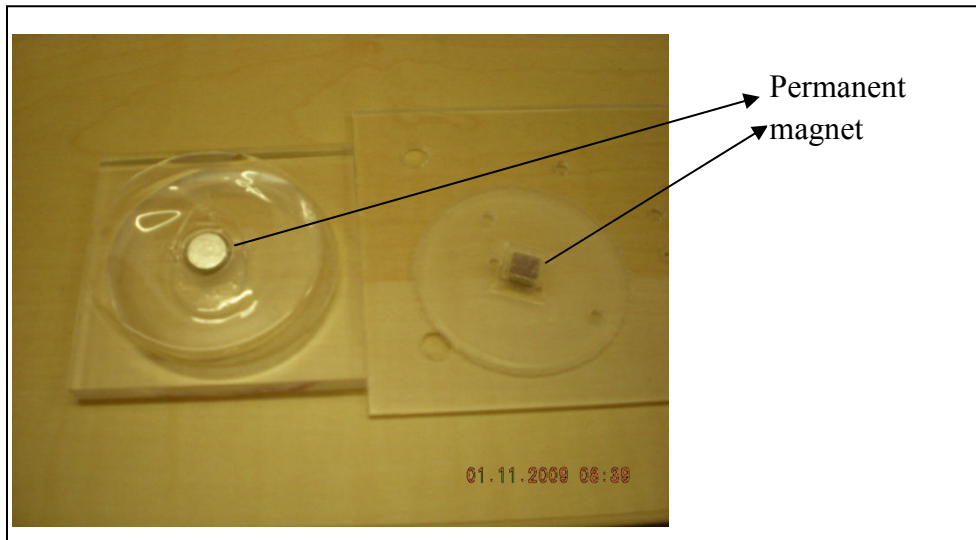


Figure 4. 10: PDMS diaphragm embedded with permanent magnet

In this work the electromagnetic actuator is with moving magnet. In order to achieve the large deflection of diaphragm, the magnet has to be embedded at the diaphragm centre.

4.4.3 Corrugated PDMS Diaphragm

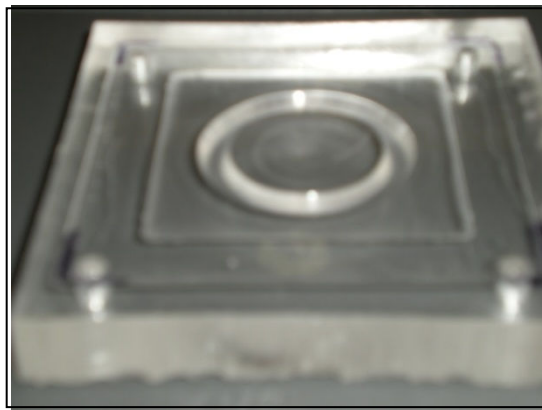
Preliminary investigation has indicated that the deflection of the diaphragm given above are relatively small. To improve this corrugation diaphragm is proposed.

The thin PDMS diaphragm is corrugated as shown in Figure 4.11.

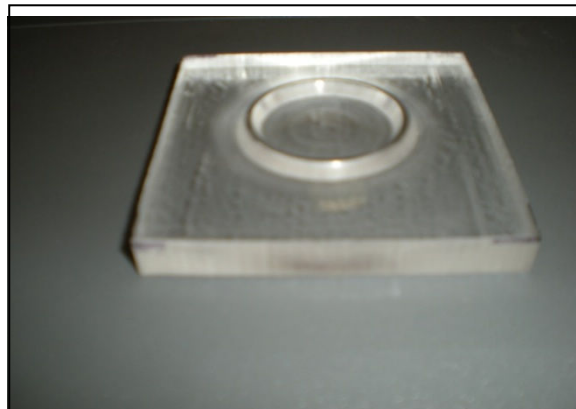
Figure 4.12 shows mould tools. The material of the moulds tools is acrylic. The mould tools are designed by the solidwork2009, and built by the CNC machine.



Figure 4. 11: Corrugated PDMS diaphragm



(a)



(b)

Figure 4. 12: Tools for corrugated PDMS diaphragm (a) Cavity and (b) Core

4.5 Chamber and valveless fabrication

Lasers may be used to cut or shape a wide variety of materials. By cutting, we mean vaporization of material along a line, so as to separate the work piece into separate parts. Lasers have been widely used for cutting of plastics. The resulting edge quality may vary greatly, depending on the exact composition of the material and the parameters of the cutting operation [63]. Figure 4.13 illustrates how the edges of some common plastics typically respond to the laser cutting operation. A number of plastics can be cut well, but others often yield discoloured or charred edges.

<p>Plastics that are easily cut with good edge quality:</p> <ul style="list-style-type: none">• Acrylic• Polyethylene• Polypropylene• Polystyrene <p>Plastics that are subject to edge deterioration, ranging from mild discoloration to burning, depending on the exact parameters of the cutting operation:</p> <ul style="list-style-type: none">• Cellulosics• Fluoropolymers• Nylon• Polyesters• Silicones• Polyurethane <p>Plastics for which the edge is always charred to some degree:</p> <ul style="list-style-type: none">• ABS• Epoxy• Phenolics• Polycarbonate• Polyimide• Polyvinyl chloride
--

Figure 4. 13: Cutting of plastics[63]

Acrylic glass is a suitable material to build the chamber and the nozzle/diffuser channel. Acrylic glass is a widely used polymer in the industry because of its low price and good chemical resistance to many products. This material is well adapted to many biochemical applications, and is of particular interest to fluid applications. In this research acrylic glass was chosen to build the chamber and the nozzle/diffuser channel

for its good mechanical properties, good optical properties and well-known chemical properties.

Laser cutting is used to form the proposed design from acrylic glass sheets. It vaporises to gaseous compounds upon laser cutting, so a very clean cut is made, and cutting is performed very easily.

4.5.1 Chamber and nozzle/diffuser elements manufacture

The complete air pump is fabricated from several acrylic glass layers. The PDMS diaphragm was clamped between two acrylic glass layers. The nozzle/diffuser channel was built in an acrylic glass layer.

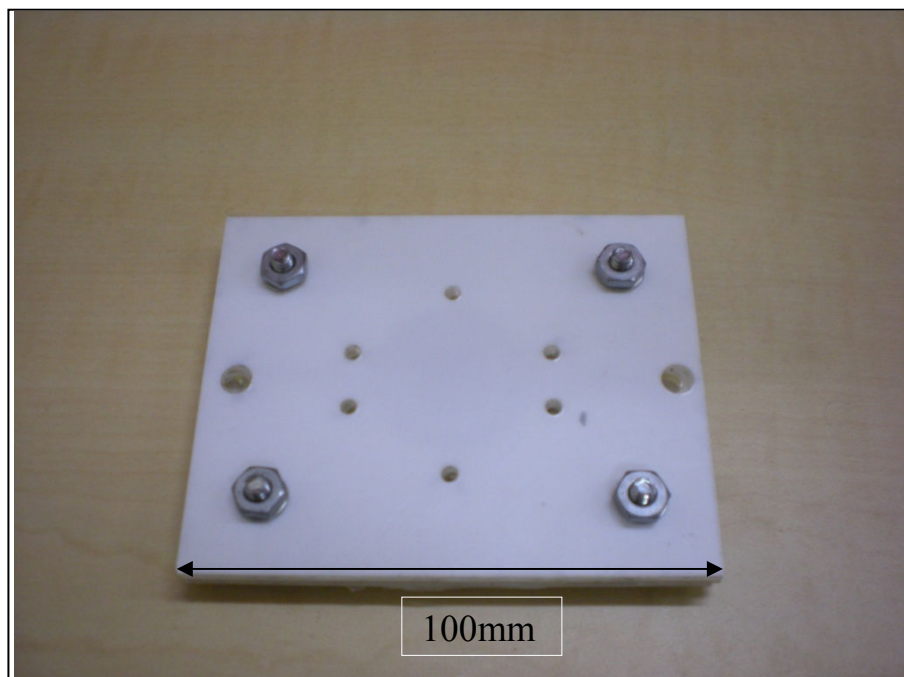


Figure 4. 14: Double chambers with one diaphragm



Figure 4. 15: Chamber with nozzle/diffuser under it

Two types of chambers with nozzle/diffuser elements were designed and built in this project. One is double chambers (32mm diameter) with one diaphragm in the middle and nozzle/diffuser along two sides (see Figure 4.14). The other is one chamber (50mm diameter) with nozzle/diffuser elements under it (see Figure 4.15). All acrylic glass layers were fabricated by a laser cutting machine.

4.6 Air pump assembly

Two types of electromagnetic air pumps are assembled without driving circuit. The proposed air pump type single actuation (see Figure 4.16) is assembled by cylindrical coils and single chambers. The proposed air pump type double actuation (see Figure 4.17) is assembled by cylindrical coils and double chambers with one diaphragm.

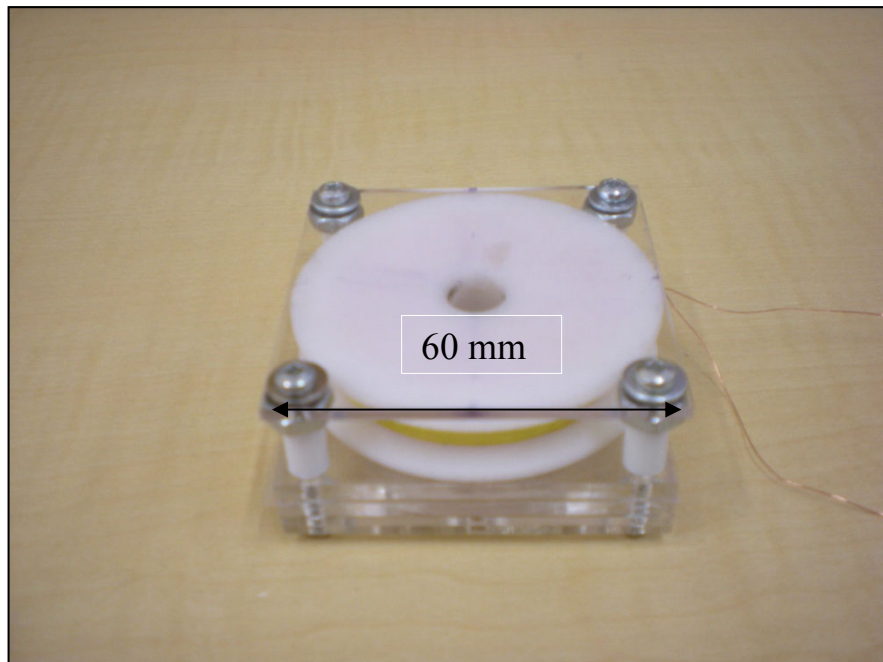


Figure 4. 16: Single actuation air pump

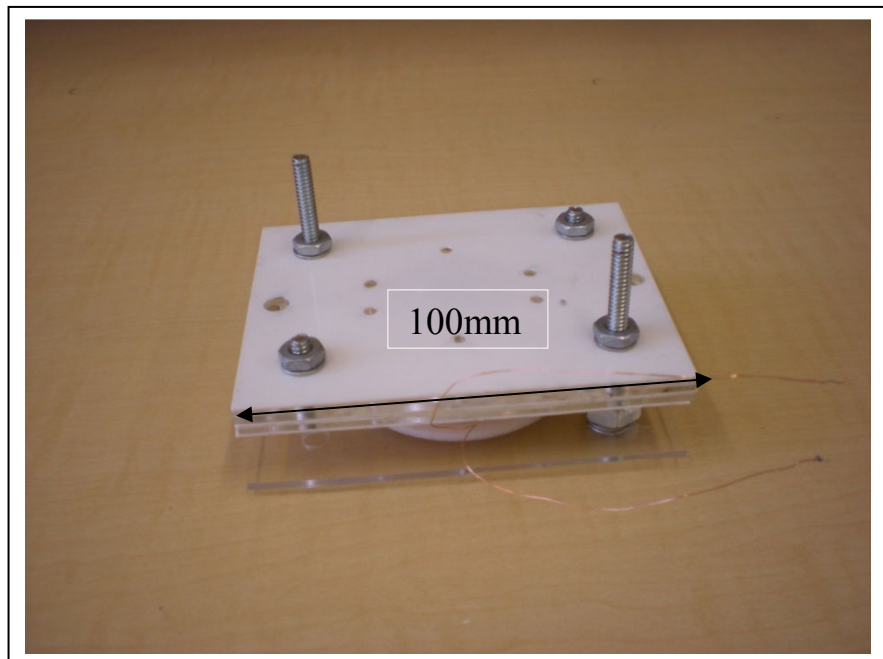


Figure 4. 17: Double actuation air pump

4.6 Summary

Outcomes of this chapter are fabrications of all components of an air pump, such as electromagnetic actuator, chamber and nozzle/diffuser elements. The technology of fabrication for electromagnetic coils, chamber and valveless are outlined in this chapter. The next chapter will present experimental investigation for the entire of the fabricated pump with valveless.

CHAPTER 5

TESTING AND RESULTS

5.1 Introduction

This chapter presents test setups and experimental results. It includes two sections, first section shows details of the experimental setups and instrumentations utilised in this work for evaluating the characterises of the actuator and air pump, the second section analyses the experiment results.

5.2 Experiment setup

Air pump performance was assessed by measuring the deflection of PDMS diaphragm at the centre, as well as measuring the flow rate at the output of the air pump. The configurations of the measurement setups for the deflection of PDMS diaphragm and flow rate of the air pump are presented in the following section.

5.2.1 Deflection of PDMS diaphragm

Figure 5.1 shows a schematic diagram of the experimental investigation used to measure the central deflection of the PDMS diaphragm. It consists of two sections: namely actuation and measurement. The actuation section consists of a function generator (HP 33120A) which supplies a signal to an amplifier (LDS 25E). After the voltage signal is amplified, it goes through the electromagnetic coils. The measurement section consists of a Laser Doppler vibrometer (OFV-5000) which detects the central deflection of the PDMS diaphragm. The output signal of Laser Doppler vibrometer is sent into the oscilloscope (TDS1012). The current through the electromagnetic coils is monitored by a precision digital multi-meter (HP33401A).

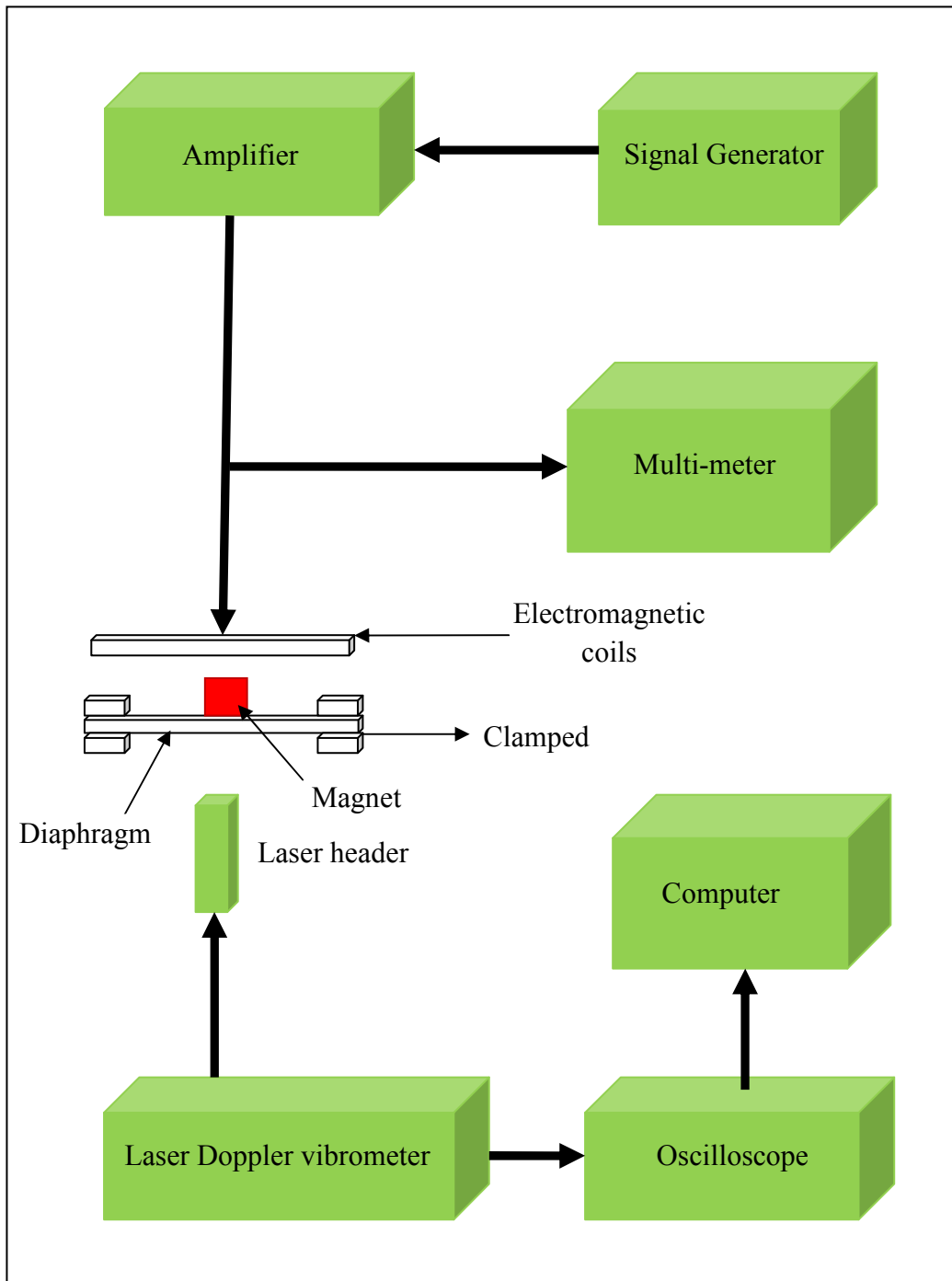


Figure 5. 1: Experimental setup of diaphragm deflection measurement

5.2.2 Flow rate

Figure 5.2 shows a schematic diagram of the experimental setups for measurement of the air pump flow rate. In the actuation section, configurations and instrumentation of the experimental setups are similar to those used for the central deflection of PDMS diaphragm measurement. In the measurement section, the flow rate from the output of the air pump is detected by the flow meter (wavefront THOR D22/5B). The detected signal from the flow meter is sent to a computer to be collected and recorded.

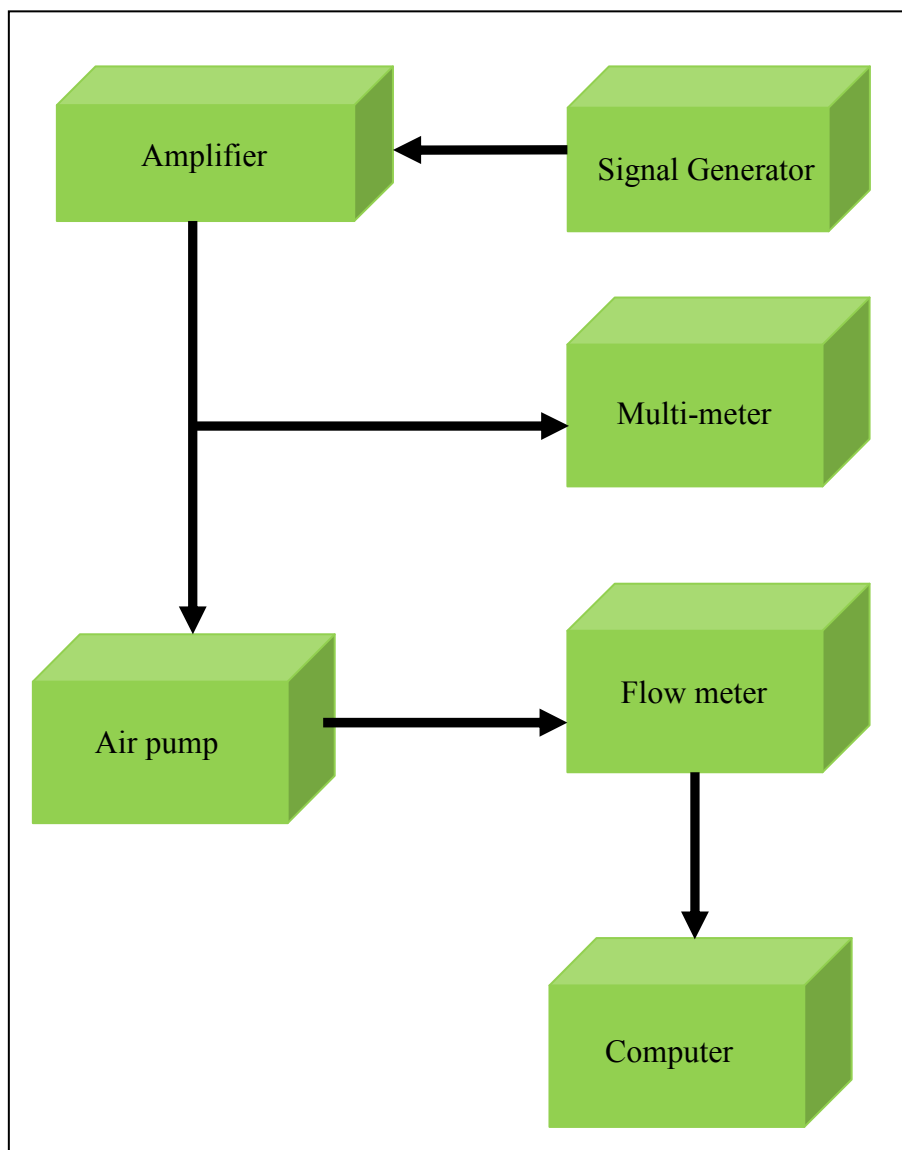


Figure 5. 2: Experimental setup of flow rate measurement

5.3 Air pump test

The main purpose of the experimentation is to determine the performance of the air pump in terms of PDMS diaphragm deflection, frequency of oscillation and air flow rate delivery. The performance for two types of air pumps, single-acting and double-acting is investigated.

5.3.1 Deflection of PDMS diaphragm test

Two types of tests using the experimental setups introduced in Figure 5.1 were conducted. The first was to investigate the central deflection of PDMS diaphragm at various amplitudes of driving current (fixed frequency) supplied to the electromagnetic coils. The second was to measure the central deflection of PDMS diaphragm at various frequencies of the driving current (fixed amplitude).

Each electromagnetic actuator was fixed on the solid support (see details in Figure 5.3). The function generator (HP 33120A) supplies a sine signal to the amplifier (LDS 25E) which produces the driving current to the electromagnetic coils. A high precision multi-meter (HP33401A) is connected in series to the electrode of the electromagnetic coils. The laser beam of LDV (OFV-5000) is aligned and focused to the centre of PDMS diaphragm.



Figure 5. 3: Measurement of diaphragm deflection

5.3.1.1 Fixed frequency of driving current

The central deflection of two PDMS diaphragms of different size (32mm and 50mm diameter) was tested using the experimental setups presented in Figure 5.1.

PDMS diaphragm (32mm diameter)---- Fixed frequency

The central deflection of PDMS diaphragm (diameter 32mm) was measured in the range of the amplitude of the driving current increased from 0.1A to 1.3A while the frequency is fixed at 45 Hz. This frequency is selected to be around the resonance frequency, and the amplitude of current is limited by the safe operation allowed by the driving circuit. Table 5.1 gives the central deflection of PDMS diaphragm at various amplitudes of driving current with fixed frequency.

Table 5. 1: Experimental results of diaphragm deflection

Peak current (unit: A)	Peak to peak voltage (unit: V)	LDV measurement range (unit: $\mu\text{m/s/V}$)	Current frequency (unit: Hz)	Maximum deflection (unit: mm)
0.1	0.148	640	45	0.004
0.2	0.296	640	45	0.093
0.3	0.436	640	45	0.141
0.4	0.592	640	45	0.189
0.5	0.78	640	45	0.233
0.6	0.88	640	45	0.2816
0.7	1.06	640	45	0.346
0.8	1.2	640	45	0.384
0.9	1.42	640	45	0.448
1	1.72	640	45	0.512
1.1	1.74	640	45	0.55
1.2	1.86	640	45	0.595
1.3	2.02	640	45	0.646

PDMS diaphragm (50mm diameter) ---- Fixed frequency

For the central deflection of the 50mm diameter PDMS diaphragm, the test procedure was repeated and the experimental results are shown in Table 5.2.

Table 5. 2: Experimental results of diaphragm deflection

Peak current (unit :A)	Peak to peak voltage (unit: V)	LDV measurement range (unit: um/s/V)	Current frequency (unit: Hz)	Maximum deflection (unit: mm)
0.01	0.66	0.64	43	0.2112
0.02	0.576	1.28	43	0.36864
0.03	0.92	1.28	43	0.5888
0.04	1.26	1.28	43	0.8064
0.05	0.82	2.56	43	1.0496
0.06	0.96	2.56	43	1.2288
0.07	1.06	2.56	43	1.3568
0.08	1.18	2.56	43	1.5104
0.09	1.26	2.56	43	1.6128
0.1	1.34	2.56	43	1.7152
0.11	1.42	2.56	43	1.8176
0.12	1.48	2.56	43	1.8944
0.14	1.58	2.56	43	2.0224
0.16	1.72	2.56	43	2.2016
0.18	1.8	2.56	43	2.304
0.185	1.84	2.56	43	2.3552

5.3.1.2 Fixed amplitude of driving current

The central deflection of two PDMS diaphragms of different size (32mm and 50mm diameter) was measured at various of frequencies of driving current with fixed amplitude.

PDMS diaphragm (32 mm diameter) ----Fixed current amplitude

The central deflection of PDMS diaphragm (diameter 32mm) was tested by applying driving current in the range of 40 Hz to 60 Hz while the amplitude is fixed at 1 A as per Figure 5.16. Table 5.3 gives the central deflection of PDMS diaphragm at various frequencies.

Table 5. 3: Central Deflection of 30mm PDMS diaphragm

Peak current (unit :A)	Peak to peak voltage (unit: V)	LDV measurement range (unit: um/s/V)	Current frequency (unit: Hz)	Maximum deflection (unit: mm)
1	1.17	640	40	0.374
1	1.24	640	42	0.397
1	1.6	640	46	0.512
1	2	640	49	0.64
1	2.08	640	50	0.66
1	2.24	640	54	0.717
1	1.44	640	60	0.46

PDMS diaphragm (50 mm diameter) ----Fixed current amplitude

Utilising the same experimental setups (see Figure 5.16), the central deflection of the PDMS diaphragm (diameter 50 mm) was measured in the range of frequency from 20 Hz to 160 Hz while the amplitude of applied driving current is fixed at 0.058 A. Table 5.8 gives the central deflection of PDMS diaphragm applied the driving current with a variety of frequency. Table 5.4 shows that the first and second natural frequencies are about 30 Hz and 50 Hz respectively.

Table 5. 4: Central deflection of 50mm diaphragm

Peak current (unit :A)	Peak to peak voltage (unit: V)	Peak to peak voltage (unit: V)	Current frequency (unit: Hz)	Maximum deflection (unit: mm)
0.058	0.64	2.02	20	0.6464
0.058	0.64	2.08	25	0.6656
0.058	0.64	2.48	30	0.7936
0.058	2.56	0.768	35	0.98304
0.058	2.56	0.496	40	0.63488
0.058	2.56	0.608	45	0.77824
0.058	2.56	0.632	46	0.80896
0.058	2.56	0.648	47	0.82944
0.058	2.56	0.656	48	0.83968
0.058	2.56	0.608	49	0.77824
0.058	2.56	0.368	50	0.47104
0.058	2.56	0.14	60	0.1792
0.058	2.56	0.083	70	0.10624
0.058	0.64	0.432	80	0.13824
0.058	0.64	0.32	90	0.1024
0.058	0.64	0.256	100	0.08192
0.058	0.64	0.264	110	0.08448
0.058	0.64	0.32	120	0.1024
0.058	0.64	0.368	130	0.11776
0.058	0.64	0.416	140	0.13312
0.058	0.64	0.464	150	0.14848
0.058	0.64	0.088	160	0.02816

5.3.2 Corrugated diaphragm

The central deflection of the corrugated PDMS diaphragm with 0.8mm thickness and 50 diameters was measured with a range of amplitudes of driving current while the frequency is fixed at 30 Hz. The amplitude of the driving current is increased from 0.2 A to 1A. Table 5.9 gives the central deflection of corrugated diaphragm for various amplitudes of driving current.

Table 5. 5: Central deflection of corrugated PDMS diaphragm

Peak current (unit :A)	Peak to peak voltage (unit: V)	LDV measurement range (unit: mm/s/V)	Current frequency (unit: Hz)	Maximum deflection (unit: mm)
0.2	1.12	0.64	30	0.36864
0.3	1.56	0.64	30	0.5888
0.4	2.02	0.64	30	0.8064
0.5	2.6	0.64	30	1.0496
0.6	1.6	1.28	30	1.2288
0.7	1.92	1.28	30	1.3568
0.8	4.16	0.64	30	1.5104
0.9	2.32	1.28	30	1.6128
1	2.48	1.28	30	1.7152
1.1	2.68	1.28	30	1.8176

5.3.3 Flow rate measurement

The maximum flow rate of two types of the air pump (single and double action) was measured using the experimental setups (see Figure 5.2). The flow rate of the output of the air pump was detected by the flow meter (wavefront THOR D22/5B). The detected signal was collected and recorded by computer (see Figure 5.4).

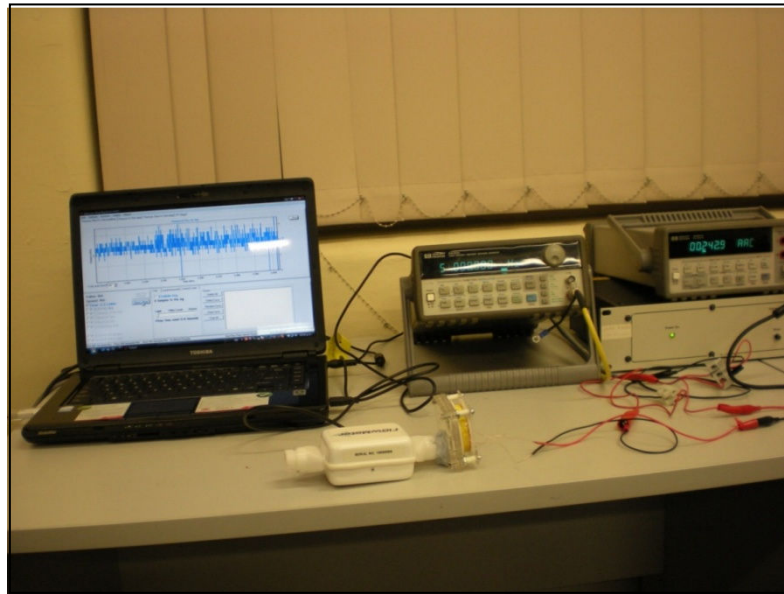


Figure 5. 4: Flow rate measurement

5.3.3.1 Single acting air pump

Utilising the same experimental setup of flow rate measurement (details see the Figure 5.4), the flow rate of the output of the proposed single acting air pump was measured. The amplitude of driving current is increased from 0.1 A to 0.23 A while the frequency is fixed at 50 Hz. The flow rate of the output of the proposed single acting air pump is measured by the flow meter (wavefront THOR D22/5B). Figure 5.5 shows the

experimental data which indicate the relationship between the amplitude of current and flow rate of the output of the proposed single acting air pump.

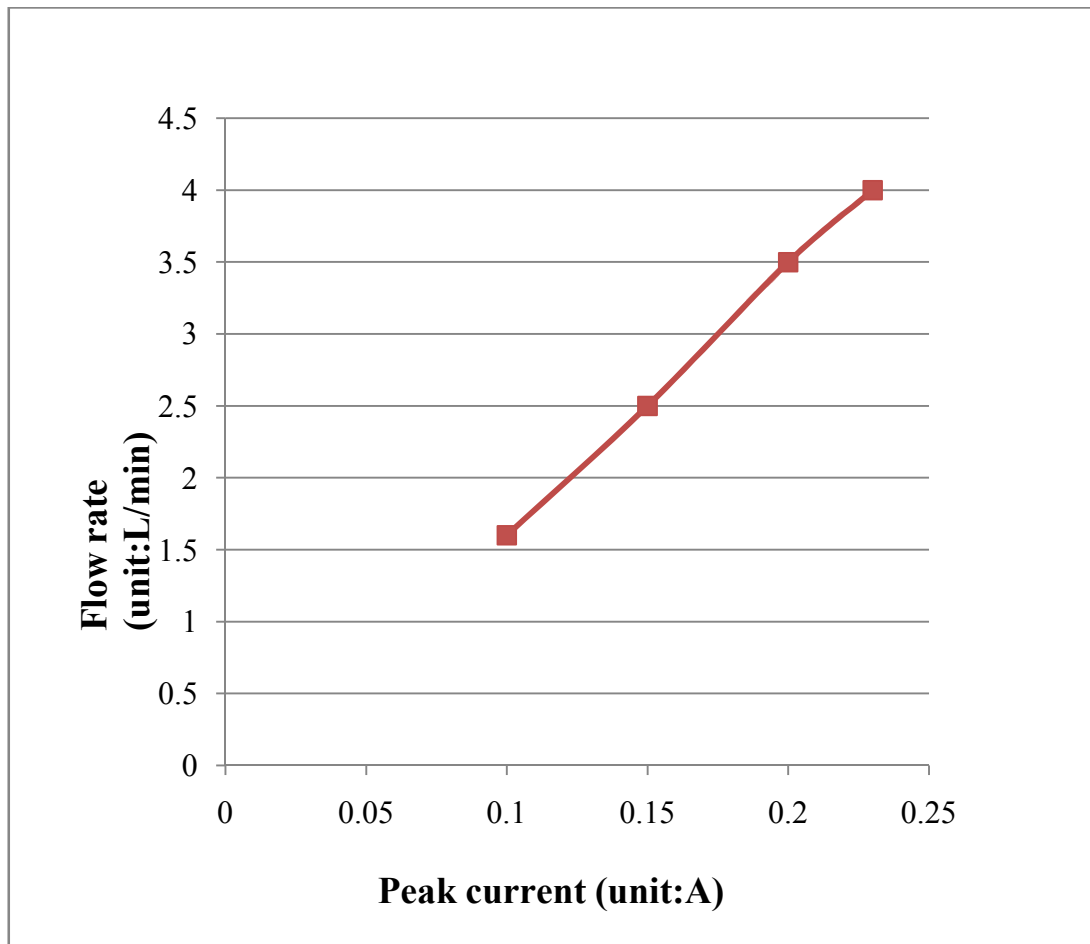


Figure 5. 5: Flow rate vs. amplitude of driving current for the proposed single acting air pump

5.3.3.2 Double acting air pump

Utilising the same experimental setup of flow rate measurement, the flow rate of the proposed double acting air pump was measured. The amplitude of the driving current is increased from 0.02 A to 0.23 A while the frequency is fixed at 60 Hz. Figure 5.6 shows the experimental data which describes the relationship between the amplitude of current and flow rate of the output of the proposed single acting air pump.

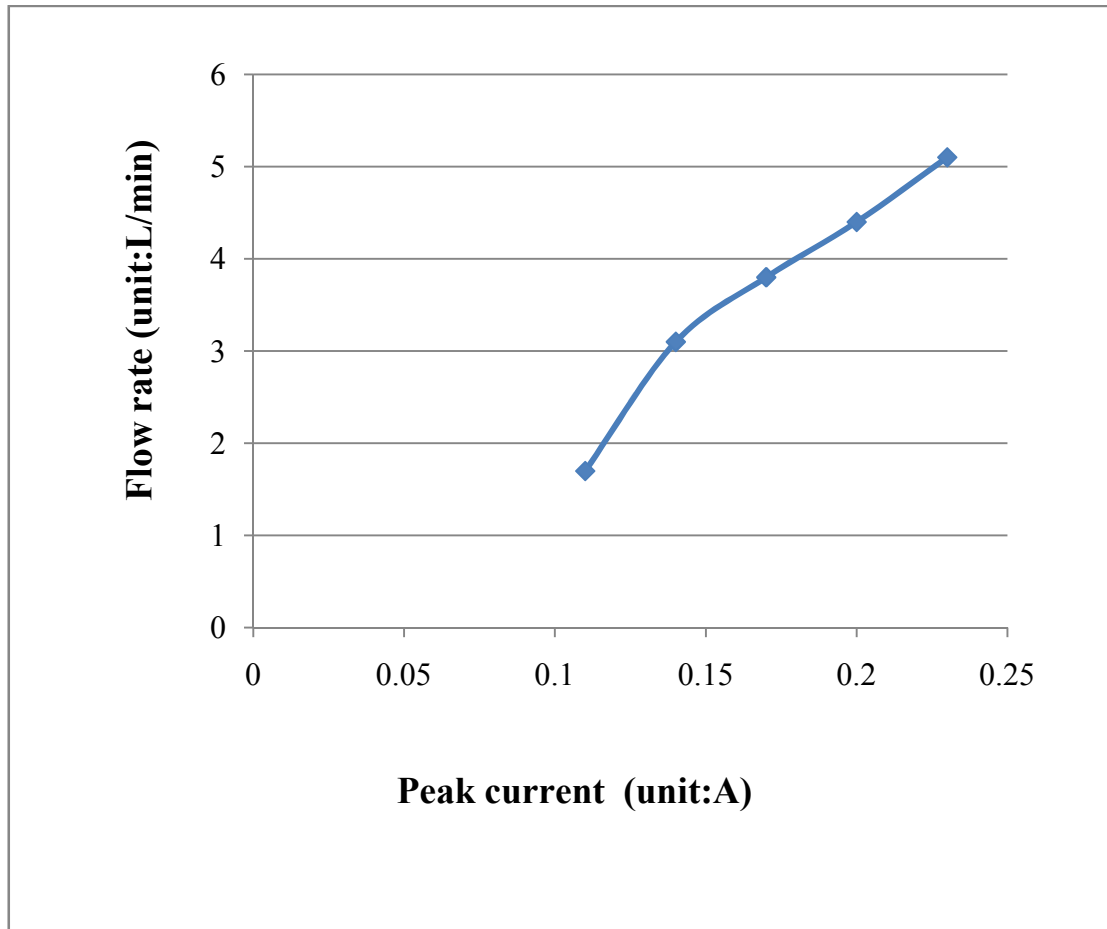


Figure 5. 6: Flow rate vs. amplitude of driving current for the proposed double acting air pump

5.4 Summary

The characteristics of the central deflection of PDMS diaphragm were experimentally investigated in this chapter. Also the performance of two types of the proposed air pump was evaluated by the experimental method. In this chapter, the details of experiment is presented and experimental results is listed.

The next chapter examines those results and draws conclusion about the feasibility of using electromagnetic actuator in small air pump.

CHAPTER 6

DISCUSSION

6.1 Introduction

In this chapter, the experimental results are analysed and compared with the numerical calculation of the models. Some discussions including the magnetic field, electromagnetic force, deflection of diaphragm and configuration of chamber are presented in the following section.

6.2 Force generation

The force on a magnetic cylinder or cube due to a planar or cylindrical coil depends on the magnetic field gradient and the amplitude of the driving current.

6.2.1 Magnetic fields of circular planar coils

From the numerical calculations for distribution of magnetic field (refer to Figures 3.7 and 3.8), some points are presented. It is seen that the value of magnetic field gradients (∇B_z) of z component decreases with increasing z value (coils and magnet distance). The maximum amplitude of magnetic field gradients (∇B_z) is not located at the original centre for a given z value. The amplitude of magnetic field gradients (∇B_z) starts from a relatively large value to a maximum value, then reduces gradually with an increase of x for a given z value.

The amplitude of the magnetic field falls off toward the outer rim of planar coils and the value of B_z eventually becomes negative, indicating the bending of the field flux lines.

Increasing the cross-section area of a conductor allows higher current intensities, resulting in increased magnetic flux intensity. Conversely, reducing the conductor width produces high field gradients due to more turns of coils. The magnetic field gradients (∇B_z) increase linearly with the amplitude of current and inversely with size (radius) of the planar.

It is intuitive that increasing the number of turns of planar coils would increase the overall magnetic field gradient. Through investigations of distribution for magnetic field gradient vs. geometric parameters of planar coils, referring to design optimisation in the chapter 3, some views are discussed here. It has been observed in this study that adding an extra turn to the planar coils at its periphery has a progressively reduced impact on magnetic field gradient. In addition, the magnetic field gradient along the centreline of the planar coils increases with reducing inner radius. However, the influence on the magnetic field gradients decreases rapidly when inner radius of planar is reduced to smaller than the specified value.

Strong strength of a magnetic field gradient distributed inside a magnetic cube produces large force. Due to the effects of the number of turns, the cylindrical coils produce the large amounts of force than the planar as the same driving current.

6.2.2 Electromagnetic coil fabrication

Increasing the amplitude of the driving current for enlarging force always have some limitations such as the capability of carrying current for the coils, heat dissipation and conductor insulation.

Common coil materials are copper, aluminium and silver (material properties list in appendix A.8). Copper is best material to built electromagnetic coils.

The conventional wire winding technology for fabrication of electromagnetic coils have a large advantage of space saving. However, there is a disadvantage of this technology involving in bad the heat dissipation.

Distribution and strength of the magnetic field depend on the geometrical pattern and dimension of electromagnetic coils. Thus, it is important for electromagnetic coils can be built with complex pattern (refer to Figure 4.8). The PCB technology of fabrication of coils has an advantage of complex pattern transformation. In addition, the capability of carrying current for copper track depends on their thickness. Generally, the copper track on the PCB can afford more amount of current than same size of copper wire.

6.3 Diaphragm deflection

Characteristics of diaphragm deflection including deflection shape, maximum deflection and natural frequency are keys of performance of actuators and air pumps. Diaphragm deflection depends on the electromagnetic force, mechanical properties of diaphragm, geometry of diaphragm and edge conditions.

The shape of PDMS diaphragm deflection is a hemispherical dome under the concentric load. The boundary condition is also an important factor impacting on the deflection of PDMS diaphragm.

Referring to the experimental results (see Table 5.1), they indicate that the relationship between the force and small deflection of diaphragm is linear. Comparison between the experimental results and numerical calculations of a small deflection of PDMS diaphragm (see Figure 4.2) at centre shows close agreement. However, experiment results (see Table 5.2) show that adding force to the PDMS diaphragm has a progressively reduced influence on its large deflection. Thus the theory of membrane deflection could be a suitable method of analysis. A primary indication of membrane deflection is given by the ratio *radius / thickness* falling between 80 and 100.

Refer to experimental results (see Tables 5.3 and 5.4), the maximum deflection at the centre increases with the increasing size (radius) of diaphragm under the concentric load. At the same time, the first natural frequency of diaphragm deflection is decreased.

The experimental results (see Table 5.5) supply strong evidences of advantage for corrugated diaphragm utilisation. If the thin diaphragm is corrugated, the deflection of diaphragm will be greater flexibility and sensitivity to the load variation.

The shape of the radial cross-section of the diaphragm is called its profile and the load-deflection characteristic is influenced by the profile. Corrugation results in stress largely due to bending rather than tension. The deflection at the centre will be as much as 2% of the diameter of the diaphragm, and the characteristic can also be made non linear by the choice of the profile [65].

6.4 Flow rate of air pump

The experimental results (see Tables 5.5 and 5.6) show that the relationship between the amplitude of driving current and flow rate of the proposed air pump is linear. These results give strong evidence that the flow rate of the proposed air pump is controllable. It is feasibility to design open loop control system for a diaphragm air pump using the internal system variable, such as amplitude of current.

6.5 Configuration of chamber

The proposed type double acting air pump has two chamber arranged in parallel. This configuration was intended to reduce oscillation of flow in the pump output due to periodic driver operation.

Approach of enlarging signal chamber size is not a good strategy to increase the flow rate of air pumps, because large size of chamber trade off less operation frequency. Configuration of multiple chambers is best way to increase flow rate of air pumps.

6.6 General discussion

Two types of air pumps were fabricated in this work to serve as models verifications of air pumps. Through assessments by experiments, two types of air pumps show their

capabilities of producing relative large flow rate. From air pumps built in this work, design and fabrication of air pump have been demonstrated. Therefore the results from this work have shown sufficient feasibility of using electromagnetic actuator in small air pumps. It is well known that diaphragm air pump using electromagnetic actuator is not simple system due to it involving in three working mechanism such as electric, mechanic and fluid. Some suggestions for future work are presented in the chapter 7.

CHAPTER 7

CONCLUSION AND FUTURE WORK

7.1 Conclusion

The main aim of this work is to develop an electromechanical air pump. This includes studying the performance and design for an electromagnetic actuator with less power consumption and small sizes. In this study the proposed electromagnetic actuator were developed and their performances were investigated. The performance of the proposed electromagnetic air pumps (types of single acting and double acting) was also investigated. This project has accomplished the objectives set out initially as listing in the following:

1. Develop relative accurate models for diaphragm air pumps using electromagnetic actuator.
 - a) The electromagnetic model was used to investigate magnetic field distribution of planar coils.
 - b) The mechanical model to determine the deflection of diaphragm was validated against experimental data and show good agreement.
 - c) The fluid model used to investigate the flow rate of air pump was validated against experiment data.
2. Investigate design methods for diaphragm air pump using electromagnetic actuator.
 - a) Design optimization of planar coils was validated by the agreement between the numerical calculation and experimental data.
 - b) Geometry of nozzle element design was met the objective.

3. Fabricate of air pumps and investigate the fabrication of electromagnetic coils methods of air pumps.
 - a) Two types of air pumps were built and met with the objectives of this work.
 - b) This research has also investigated two technologies for electromagnetic coils fabrication.

7.2 Recommendations for Future Work

In this study the initial focus of the research effort was to develop the models of actuation behaviour of the electromagnetic actuator and to explore how this may be exploited in an air pump application. The present work has been successful in miniaturisation of the air pump by design optimisation for the electromagnetic actuation. However, further work is needed which may include the following:

- a) The theoretical model of the magnetic field produced by the current in a square spiral
- b) The theoretical model of the magnetic field produced by a current-carrying N-sided (for example: N=4, 5, 6) planar polygon coils
- c) The small size of coils is constructed from an array of circular loops joined to each other. The theoretical models of the magnetic field produced by this type of coils might be of interest because it is possible to manipulate the magnetic field intensity for the specific zone.
- d) The fabrication approach of miniaturising the cylindrical coils.
- e) The development of an analytic expression of the magnetic field distribution of the cylindrical or rectangular permanent magnet.

- f) The investigation of the magnetic field produced by the electromagnetic coils and magnet has merit to be explored for its application into electromagnetic NDT and MRI technique.

- g) The air pump could be integrated with other component, such as fluidic channel and detect element, to create an analysis system using PCB technology.

These brief statements are provided merely as a guide to future work. Any work to further develop the air pump will likely be undertaken with regards to the consideration of specific application.

Appendix

A.1 Terminology

Sometimes the words "pump" and "compressor" are used interchangeably, but there is a difference. A pump is a machine that moves a substance (either liquid or gas) from one place to another. A compressor is a machine that squeezes a gas into a smaller volume and pumps it somewhere else at the same time. While pumps can work on either liquids or gases, compressors generally work only on gases. That is because liquids are very difficult to compress.

Pumps

- A pump is a machine for raising a liquid - a relatively incompressible fluid - to a higher level of pressure or head.

Compressors

- A compressor is a machine for raising a gas - a relatively compressible fluid - to a higher level of pressure.

Air pumps or air delivery units

- An air pump or air delivery unit (ADU) is a machine for moving volumes of a gas with low increase of pressure.

A.2 Coordinate system and transformation

In general, the electromagnetic field is produced in space when the charges are moving with constant velocity. This requires using a suitable coordinate system to define all the points in space uniquely. In the following section, the Cartesian coordinate system and circular cylindrical coordinate system will be used to represent a point or vector.

- 1) Cartesian coordinates system (x, y, z)

A vector \mathbf{A} in Cartesian coordinate can be represented as:

$$(A_x, A_y, A_z) \quad \text{or} \quad A_x a_x + A_y a_y + A_z a_z \quad (\text{A.1.1})$$

Where a_x , a_y , and a_z are unit vectors along the x, y, and z direction.

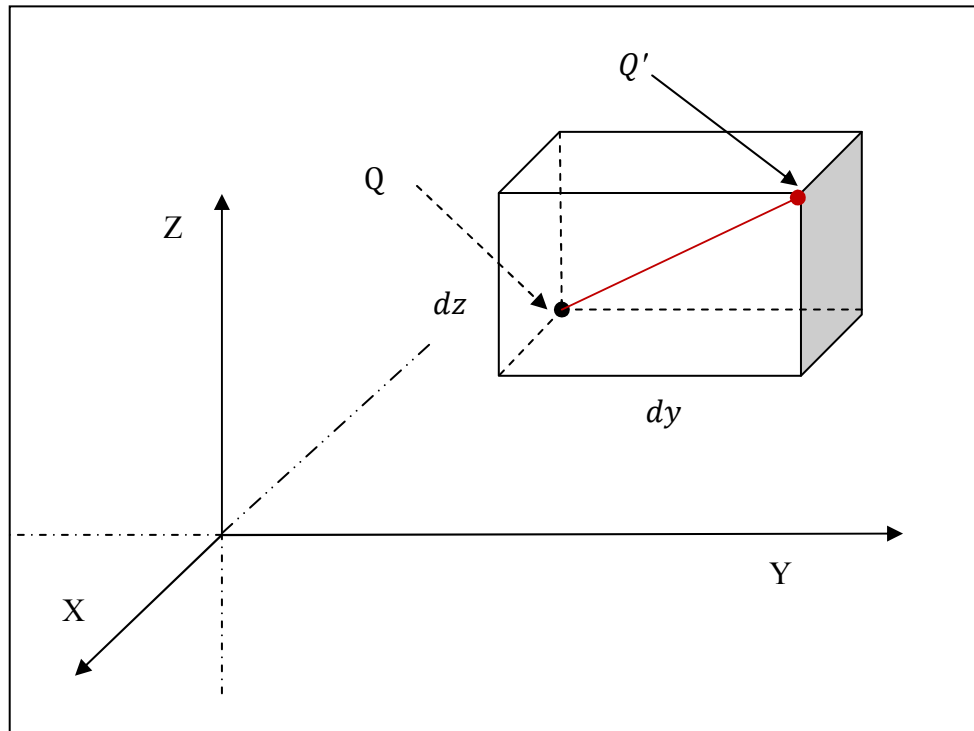


Figure A.1. 1: Differential volume element in Cartesian coordinates system

Each coordinate value of the point Q whose the coordinate are x, y, and z, can be increased by the differential amount and obtained the point Q' whose the coordinate are $x+dx$, $y+dy$, and $z+dz$. This differential element has volume: $dx \cdot dy \cdot dz$ and surface area $ds: dx \cdot dy; dx \cdot dz; dy \cdot dz$. The distance between the point Q and Q' is $\sqrt{dx^2 + dy^2 + dz^2}$.

1) Circular cylindrical coordinate system

A Q point in a cylindrical coordinate system is represented as (r, θ, z) and is illustrated in the following Figure A.1-2

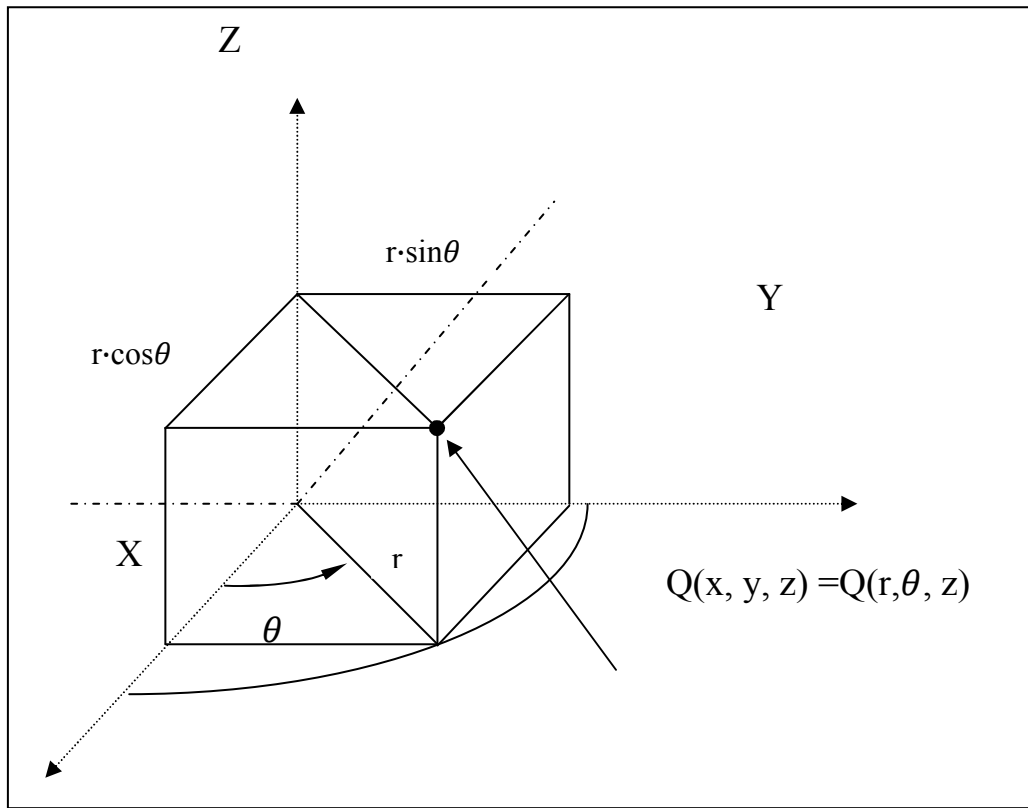


Figure A.1. 2: Variables in the Cartesian coordinate system and cylindrical system

A vector \mathbf{A} in cylindrical coordinates can be written as:

$$(A_r, A_\theta, A_z) \quad \text{or} \quad A_r \mathbf{a}_r + A_\theta \mathbf{a}_\theta + A_z \mathbf{a}_z \quad (\text{A.1.2})$$

A point from the Cartesian coordinate system (x, y, z) can be transformed to the cylindrical system (r, θ, z) and vice versa obeying the following rules:

$$r = \sqrt{x^2 + y^2}, \quad \theta = \tan^{-1} \frac{y}{x}, \quad z = z \quad (\text{A.1.3})$$

Or

$$x = r \cdot \cos\theta, \quad y = r \cdot \sin\theta, \quad z = z \quad (\text{A.1.4})$$

The differential volume element in a circular cylindrical coordinate system might be obtained by increment dr , $d\theta$, and dz . The differential element volume is $r \cdot dr \cdot d\theta \cdot dz$.

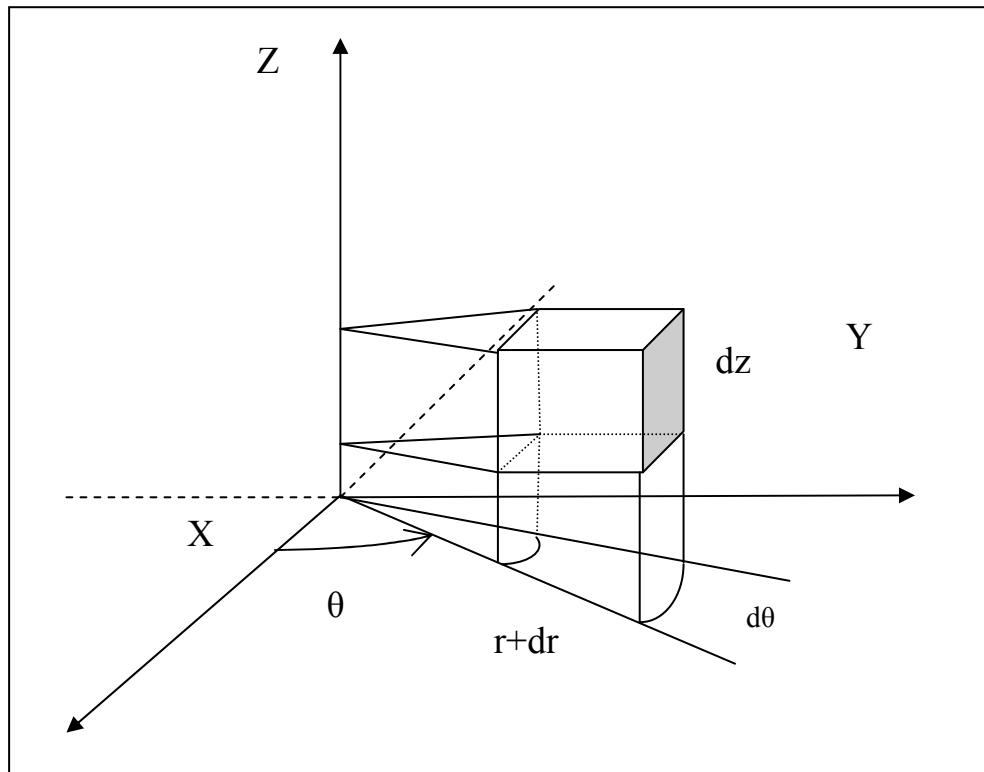


Figure A.1. 3: Differential volume element in cylindrical coordinate system

A.3 Basic vector analysis

A.3.1 Unit vector operation

Unit vector operation is one of the instructions that must be obeyed for obtaining the component when a vector cross product is done. In the Cartesian coordinates system, unit vector operation is carried out as:

$$\mathbf{a}_x \cdot \mathbf{a}_x = \mathbf{a}_y \cdot \mathbf{a}_y = \mathbf{a}_z \cdot \mathbf{a}_z = 1 \quad (\text{A.2.1})$$

$$\mathbf{a}_x \cdot \mathbf{a}_y = \mathbf{a}_x \cdot \mathbf{a}_z = \mathbf{a}_y \cdot \mathbf{a}_z = 0 \quad (\text{A.2.2})$$

$$\mathbf{a}_x \times \mathbf{a}_y = \mathbf{a}_z \quad (\text{A.2.3})$$

$$\mathbf{a}_y \times \mathbf{a}_z = \mathbf{a}_x \quad (\text{A.2.4})$$

$$\mathbf{a}_z \times \mathbf{a}_x = \mathbf{a}_y \quad (\text{A.2.5})$$

In the circular cylindrical coordinate system, the rules of unit vector operation are as following:

$$\mathbf{a}_r \cdot \mathbf{a}_r = \mathbf{a}_\theta \cdot \mathbf{a}_\theta = \mathbf{a}_z \cdot \mathbf{a}_z = 1 \quad (\text{A.2.6})$$

$$\mathbf{a}_r \cdot \mathbf{a}_\theta = \mathbf{a}_\theta \cdot \mathbf{a}_z = \mathbf{a}_r \cdot \mathbf{a}_z = 0 \quad (\text{A.2.7})$$

$$\mathbf{a}_r \times \mathbf{a}_\theta = \mathbf{a}_z \quad (\text{A.2.8})$$

$$\mathbf{a}_\theta \times \mathbf{a}_z = \mathbf{a}_r \quad (\text{A.2.9})$$

$$\mathbf{a}_z \times \mathbf{a}_r = \mathbf{a}_\theta \quad (\text{A.2.10})$$

A.3.2 Vector cross product

If we assume vector \mathbf{A} cross product vector \mathbf{B} , the rules of cross product can be shown as the following equation in the Cartesian coordinates system and Circular cylindrical coordinate system:

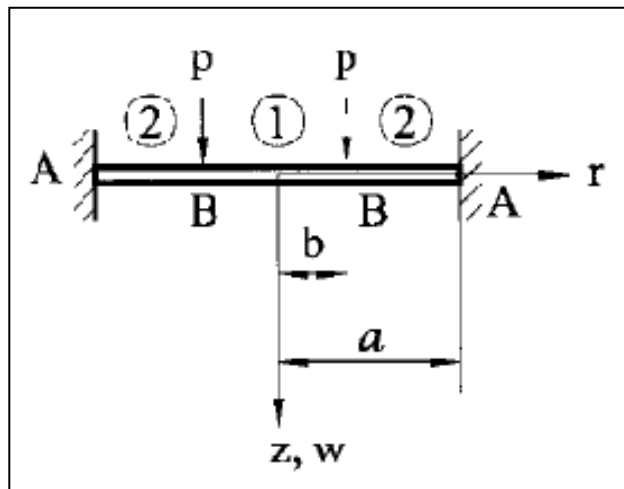
$$\mathbf{A} \times \mathbf{B} = (A_y B_z - A_z B_y) \mathbf{a}_x + (A_z B_x - A_x B_z) \mathbf{a}_y + (A_x B_y - A_y B_x) \mathbf{a}_z \quad (\text{A.2.11})$$

$$\mathbf{A} \times \mathbf{B} = (A_\theta B_z - A_z B_\theta) \mathbf{a}_r + (A_z B_r - A_r B_z) \mathbf{a}_\theta + (A_r \cdot B_\theta - A_\theta B_r) \mathbf{a}_z \quad (\text{A.2.12})$$

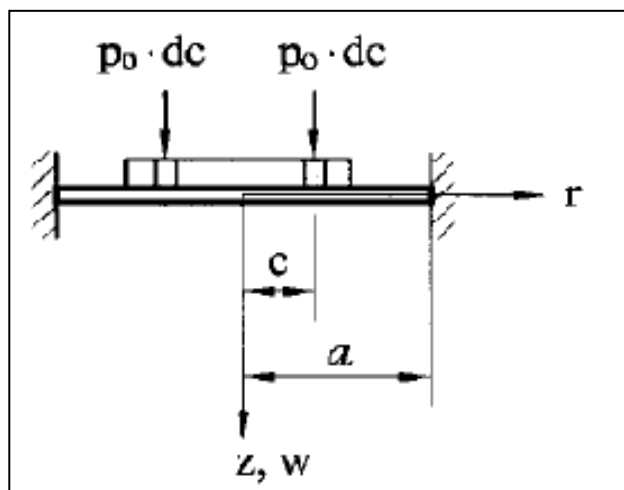
A.4 Thin plate analysis

A.4.1 Small deflection of clamped plate

Find the expression for small deflection of the clamped solid plate shown in Figure A.3-1(a) due to line load p distributed along a circle with radius $r = b$ [46] page106.



(a)



(b)

Figure A.4. 1: (a) Line load P , (b) Load distributed along inner parts of a concentric circle[46]

For the inner plate, $0 \leq r \leq b$

$$w = \frac{pb}{8a^2D} \left[(a^2 - b^2)(a^2 + r^2) - 2a^2(b^2 + r^2) \ln \frac{a}{b} \right] \quad (\text{A.3-1})$$

Using the method of supposition, the following procedures could drive out the equation (3-18).

The centre deflection, w_0 , is given by expression (A.3-1). Setting $b = c$ and $r = 0$, the centre deflection, w_0 , is obtained as follows [46] page 110:

$$W_0 = \frac{pc}{8D} (a^2 - c^2 + 2c^2 \ln \frac{c}{a}) \quad (\text{A.3-2})$$

Then, the centre deflection for the given loading is obtained from Eq. (A.3-2), replacing p by p_0dc and integrating from 0 to b . Thus:

$$W_C = \frac{p_0}{8D} \int_0^b (a^2 c - c^3 + 2c^3 \ln a) dc$$

$$W_C = \frac{p_0 b^2}{16D} (a^2 - \frac{3}{4} b^2 + b^2 \ln \frac{b}{a}) \quad (\text{A.3-3})$$

A.4.2 Large deflection of clamped plate

The theoretical analysis for large deflection of plates is complex and beyond the scope of this study. More details regarding this aspect can be found in the literature by Timoshenko [45] and Ventsel [46].

A.5 Driving circuit

An electromagnet is a type of magnet whose magnetic field is produced by the flow of electric current. The amplitude of current is controlled by the driving circuit. There are two types of electromagnetic coils in this project.

The resistance of the cylindrical coils is about 49 Ohms. The low frequency amplifier (LDS PA25E) could deliver enough current to meet the requirement of driving electromagnetic coils.

The resistance of the planar coils is about 0.7 Ohms. It is difficult for designers to build the low frequency amplifier whose output impedance is smaller than 1 Ohms. Thus the high power resistance (2 Ohms) could be the serial contented with planar coils. The TDA1519A is an integrated class-B dual output amplifier in a 9-lead single in-line (SIL) plastic power package. The device is primarily developed for driving 2 Ohms speakers. The circuit of power amplifier using TDA1519A could be obtained from the data sheet of production specification.

A.6 Experimental data of flow rate measurement

Figure A.6-1 shows that the experimental data of the flow rate measurement for the proposed single acting air pump. Using the experimental setups (see details Figure 4.4), the amplitude of the driving current is set as 0.23A while the frequency is fixed at 50m Hz. The flow rate of the proposed single acting air pump was measured by the flow meter (wavefront THOR D22/5B).

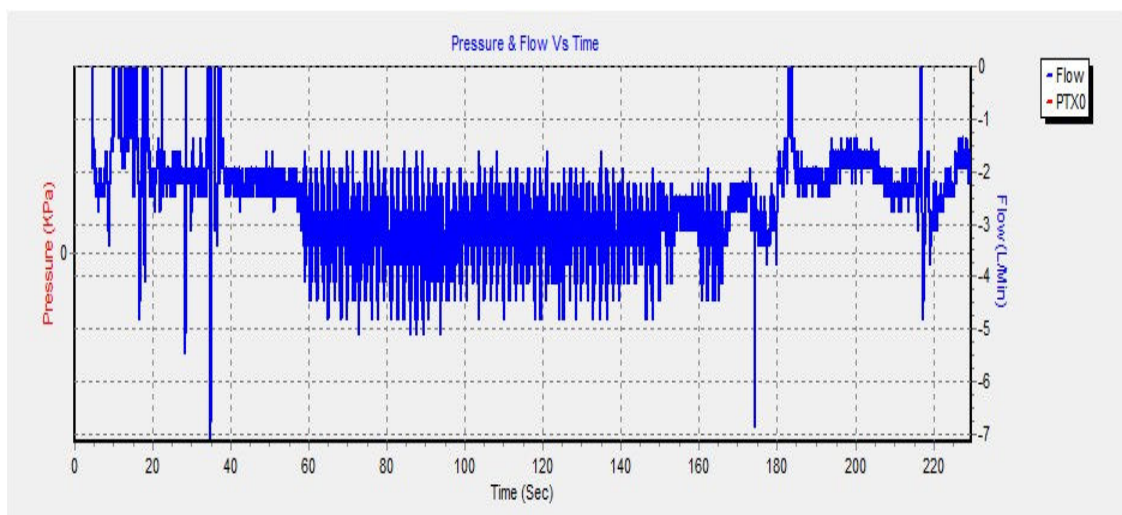


Figure A.6- 1 Flow rate (from 60 to 160 seconds, unit: L/min) of the proposed air pump (single acting)

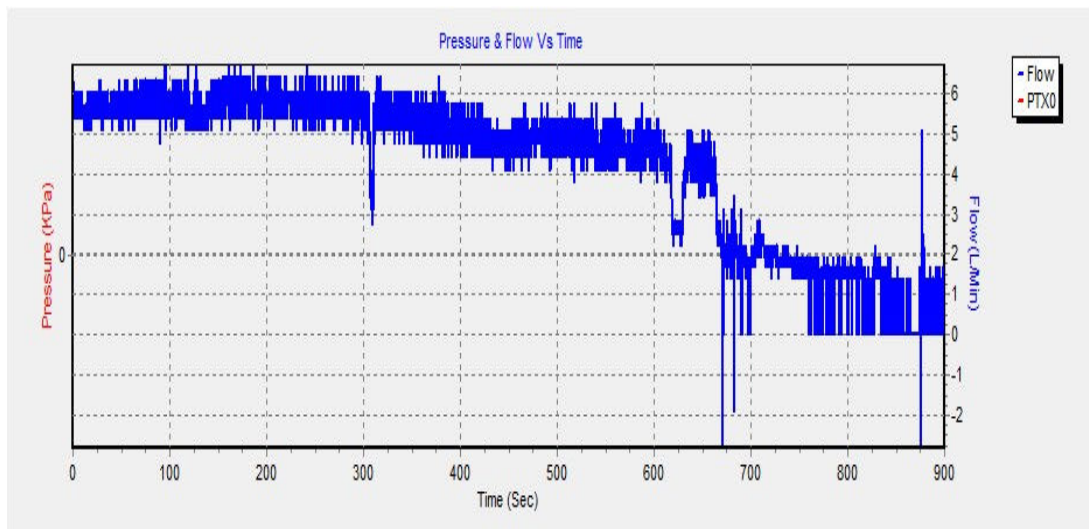


Figure A.6- 2 Flow rate (from 0 to 300 seconds unit: L/min) of the proposed air pump (double acting)

Figure A.6-2 shows that the experimental data of flow rate measurement for the proposed double acting air pump. Employing the experimental setups (see details Figure 4.4), the amplitude of driving current is set as 0.23A while the frequency is fixed at 60m Hz. The flow rate of the proposed double acting air pump was measured by the flow meter (wavefront THOR D22/5B).

A.6 Properties of PDMS

Figure A.6.1 shows the main properties of PDMS(Polydimethylsiloxane).

Test	Unit	Result
Mix Ratio		10:1
Color		Clear
Viscosity	centipoise or mPa.s	3900
Durometer, Shore A		50
Specific Gravity		1.03
Working Time at RT	min	>2 hours
Thermal Conductivity	Watt/meter-°K	0.2
	cal/cm·sec °C	4.3×10^{-4}
Linear Coefficient of Thermal Expansion	$\mu\text{m}/\text{m}\cdot^{\circ}\text{C}$ or ppm	310
UL Flammability Classification		94 V1, V0
UL Temperature Index, Electrical/ Mechanical	°C	130/130
Dielectric Strength	volts/mil	540
	kV/mm	21.2
Dielectric Constant at 100 Hz		2.7
Dielectric Constant at 100 kHz		2.7
Volume Resistivity	ohm-cm	1.2×10^{14}
Dissipation Factor at 100 Hz		<0.001
Dissipation Factor at 100 kHz		<0.001

Figure A.6. 1: Properties of PDMS (data from Dow Corning Corporation)

A.7 common materials and material properties

Figure A.7.1 shows that common materials and material properties.

Material	Thermal expansion coefficient [1/K]	Density [kg/m ³]	Resistivity [Ωm]
Copper	16.5×10^{-6}	8960	17.2×10^{-9}
Alumimium	23.1×10^{-6}	2700	28.1×10^{-9}
Silver	18.9×10^{-6}	10500	16.2×10^{-9}
Gold	14.2×10^{-6}	19300	22×10^{-9}

Figure A.7. 1: Common material and material properties

A.8 Matlab codes

Some Matlab codes of numerical calculations magnetic field and diaphragm deflection are shown in the following section.

A.8.1 Matlab codes for magnetic field of a circular electromagnetic coils

```
%using the x,y,z coordinate system
clear;
u0=1.2566e-6;
I=1;
z=4e-3;
R=10e-3;
cal=50;
step=R/cal;
[x1,y1]=meshgrid(-1.5*R:step:1.5*R,-1.5*R:step:1.5*R);

[kx1,px1]=size(x1);
[ky1,py1]=size(y1);

calno=360;
stepbeta=pi/calno;
beta1=0:stepbeta:2*pi;
[w1,v1]=size(beta1);

for t1=1:1:v1
    for n1=1:1:py1
        for m1=1:1:kx1
            Bzcir(m1,n1,t1)=(I/(4*pi))*u0*(R*R-R*cos(beta1(t1))*x1(m1,n1)-
R*sin(beta1(t1))*y1(m1,n1))/(((x1(m1,n1)-R*cos(beta1(t1)))^2+(y1(m1,n1)-
R*sin(beta1(t1)))^2+z.^2).^1.5);
        end
    end
end

Bzall1=sum(Bzcir,3);

figure(1)
surf(x1,y1,Bzall1);
axis tight;
view(60,30);
camlight left;
ylabel('Radiu of coil(meter)');
xlabel('Radiu of coil(meter)');
zlabel('Magnetic field(tesla)');
title(['Magnetic field z compoent distribution of circular, radiu=',num2str(R),'m',
gap=',num2str(z),'m']);
```

A.8.2 Matlab codes for diaphragm deflection

```
clear;
a=16e-3;
b=6e-3;
u0=1.2566e-6;
E=410e3;    %Young's Modulus of the silicone rubber
Poisson=0.5;    %Poisson ratio
diameter=32e-3;
diapht=0.27e-3;
height=6e-3; %
gamma=1.4;
P0=101325;
Tx=0;
Ty=0;
Br=1.1;
I=[0.1 0.2 0.3 0.4 0.5 0.6 0.7 0.8 0.85 0.9 1.0 1.1 1.2 1.3 ];
[c,d]=size(I);
k1=0.062;%paraemter of hole inside of plate case 6
mr=6e-3; %magnet radiu
mthick=2e-3;%magnet thickness
Am=pi*(mr.^2);
Vm=Am*mthick;
gap=3.75e-3;

copper_width=0.4e-3;
copper_space=0.6e-3;
interradiu=1.6e-3;
externalradiu=16.4e-3;
R=interradiu:copper_width+copper_space:externalradiu;
[c,s]=size(R);

calnox=50;
step=mr/calnox;
```

```

[x,y]=meshgrid(0:step:mr,0:step:mr);
[kx px]=size(x);
[ky py]=size(y);

calno=20;
stepbeta=0.5*pi/calno;
beta=0:stepbeta:0.5*pi;
[t1,w]=size(beta);

calnoz=20;
stepz=mthick/calnoz;
z=gap:stepz:gap+mthick;
[c,v]=size(z);

for t=1:1:w
    for r=1:1:s
        for j=1:1:v
            for n=1:1:py
                for m=1:1:kx
                    Bz(m,n,j,r,t)=-4*z(j)*(R(r)*R(r)-x(m,n)*R(r)*cos(beta(t))-
y(m,n)*R(r)*sin(beta(t)))/(((x(m,n)-R(r)*cos(beta(t))).^2+(y(m,n)-
R(r)*sin(beta(t))).^2+z(j).^2).^2.5);
                end
            end
        end
    end
end
Bzcirm=sum(Bz,5);

Bzc=sum(Bzcirm,4);

detz=(sum(Bzc,3));

detza=(sum(detz,2));

```

```

detBzct=(sum(detza));

Ft=-3*(1/(4*pi))*Br*Am*detBzct;

for i=1:1:d
    Ftotal(i)=I(i)*Ft;
end
V0=pi*a.^2*height;
D=E*diapht.^3/(12*(1-Poisson.^2));
ky=(a.^2-0.74*b.^2+b.^2*log(b/a))/16;
k=ky*b.^2/D;
for i=1:1:d
    defl(i)=Ftotal(i)*k;
end
figure(1)

plot(I,Ftotal);
title('Relationship between the force and current ');
xlabel('situation peak current(A)');
ylabel('force(N)');

```

Reference

1. Amirouche, F., Y. Zhou, and T. Johnson, *Current micropump technologies and their biomedical applications*. Microsystem Technologies, 2009. **15**(5): p. 647-666.
2. Krutzch W C, C.P., *Introduction: classification and selection of pumps*. 2001.
3. Laser, D.J. and J.G. Santiago, *A review of micropumps*. Journal of Micromechanics and Microengineering, 2004. **14**(6): p. R35.
4. Zhang, C., D. Xing, and Y. Li, *Micropumps, microvalves, and micromixers within PCR microfluidic chips: Advances and trends*. Biotechnology Advances, 2007. **25**(5): p. 483-514.
5. Iverson, B.D. and S.V. Garimella, *Recent advances in microscale pumping technologies: A review and evaluation*. Microfluidics and Nanofluidics, 2008. **5**(2): p. 145-174.
6. Gülich, J.F., *Centrifugal Pumps*. Second ed: Springer.
7. Wolfram, D. and T.H. Carolus, *Experimental and numerical investigation of the unsteady flow field and tone generation in an isolated centrifugal fan impeller*. Journal of Sound and Vibration. **329**(21): p. 4380-4397.
8. Choi, J.-S., D.K. McLaughlin, and D.E. Thompson, *Experiments on the unsteady flow field and noise generation in a centrifugal pump impeller*. Journal of Sound and Vibration, 2003. **263**(3): p. 493-514.
9. Younsi, M., et al., *Influence of impeller geometry on the unsteady flow in a centrifugal fan: Numerical and experimental analyses*. International Journal of Rotating Machinery, 2007. **2007**.
10. Takano, T., et al., *Impeller design for a miniaturized centrifugal blood pump*. Artificial Organs, 2000. **24**(10): p. 821-825.
11. Takano, T., et al., *Impeller inner diameter in a miniaturized centrifugal blood pump*. Artificial Organs, 2002. **26**(1): p. 67-71.
12. Wakui, D., et al. *EHD Micro Pump using Pyrolyzed Polymer 3-D Carbon Mesh Electrodes*. in *Micro Electro Mechanical Systems, 2009. MEMS 2009. IEEE 22nd International Conference on*. 2009.

13. Lee, C.K., A.J. Robinson, and C.Y. Ching. *Development of EHD ion-drag micropump for microscale electronics cooling*. in *Collection of Papers Presented at The 13th International Workshop on THERMal INvestigation of ICs and Systems, THERMINIC*. 2007.
14. Jen-Shih, C., et al. *Capillary/Narrow Flow Channel Driven EHD Gas Pump for an Advanced Thermal Management of Micro-Electronics*. in *Industry Applications Society Annual Meeting, 2008. IAS '08. IEEE*. 2008.
15. Lin, C.-W. and J.-Y. Jang, *3D numerical micro-cooling analysis for an electrohydrodynamic micro-pump*. *Sensors and Actuators A: Physical*, 2005. **122**(1): p. 167-176.
16. Komeili, B., et al., *Flow characteristics of wire-rod type electrohydrodynamic gas pump under negative corona operations*. *Journal of Electrostatics*, 2008. **66**(5-6): p. 342-353.
17. Tsubone, H., et al., *Flow characteristics of dc wire-non-parallel plate electrohydrodynamic gas pumps*. *Journal of Electrostatics*, 2008. **66**(1-2): p. 115-121.
18. Kazemi, P., P. Selvaganapathy, and C. Ching, *Electrohydrodynamic micropumps with asymmetric electrode geometries for microscale electronics cooling*. *IEEE Transactions on Dielectrics and Electrical Insulation*, 2009. **16**(2): p. 483-488.
19. Singhal, V., S.V. Garimella, and A. Raman, *Microscale pumping technologies for microchannel cooling systems*. *Applied Mechanics Reviews*, 2004. **57**(1-6): p. 191-221.
20. Affanni, A. and G. Chiorboli. *Numerical Modelling and Experimental Study of an AC Magnetohydrodynamic (MHD) Micropump*. in *Instrumentation and Measurement Technology Conference, 2006. IMTC 2006. Proceedings of the IEEE*. 2006.
21. Ghassemi, M., H. Rezaeinezhad, and A. Shahidian. *Analytical Analysis of Flow in a Magnetohydrodynamic Pump (MHD)*. in *Electromagnetic Launch Technology, 2008 14th Symposium on*. 2008.

22. Eijkel, J.C.T., et al., *A circular ac magnetohydrodynamic micropump for chromatographic applications*. Sensors and Actuators B: Chemical, 2003. **92**(1-2): p. 215-221.
23. Lemoff, A.V. and A.P. Lee, *An AC magnetohydrodynamic micropump*. Sensors and Actuators B: Chemical, 2000. **63**(3): p. 178-185.
24. Wang, L., et al. *A magnetohydrodynamic (MHD) microfluidic platform for cell switching*. in *Microtechnology in Medicine and Biology, 2005. 3rd IEEE/EMBS Special Topic Conference on*. 2005.
25. Ahn, C.H. and M.G. Allen. *Fluid micropumps based on rotary magnetic actuators*. in *Proceedings of the IEEE Micro Electro Mechanical Systems*. 1995.
26. Lei, K.F., et al., *A vortex pump-based optically-transparent microfluidic platform for biotech and medical applications*. Proceedings of the Institution of Mechanical Engineers, Part H: Journal of Engineering in Medicine, 2007. **221**(2): p. 129-141.
27. Woias, P., *Micropumps - Past, progress and future prospects*. Sensors and Actuators, B: Chemical, 2005. **105**(1): p. 28-38.
28. Ahmadian, M.T. and A. Mehrabian, *Design optimization by numerical characterization of fluid flow through the valveless diffuser micropumps*. Journal of Physics: Conference Series, 2006. **34**(1): p. 379-384.
29. Stemme, E. and G. Stemme, *A valveless diffuser/nozzle-based fluid pump*. 1993. **39**: p. 159.
30. Yamahata, C., et al., *A PMMA valveless micropump using electromagnetic actuation*. Microfluidics and Nanofluidics, 2005. **1**(3): p. 197-207.
31. Feng, G.H. and E.S. Kim, *Piezoelectrically actuated dome-shaped diaphragm micropump*. Journal of Microelectromechanical Systems, 2005. **14**(2): p. 192-199.
32. Cui, Q., C. Liu, and X.F. Zha, *Study on a piezoelectric micropump for the controlled drug delivery system*. Microfluidics and Nanofluidics, 2007. **3**(4): p. 377-390.
33. Kim, Y.S., et al., *Experimental and numerical studies on the performance of a polydimethylsiloxane valveless micropump*. Proceedings of the Institution of

- Mechanical Engineers, Part C: Journal of Mechanical Engineering Science, 2005. **219**(10): p. 1139-1145.
34. Bodnár, R., et al., *A polymeric paraffin actuated high-pressure micropump*. Sensors and Actuators, A: Physical, 2006. **127**(1): p. 88-93.
 35. Shin, D.D., K.P. Mohanchandra, and G.P. Carman, *Development of hydraulic linear actuator using thin film SMA*. Sensors and Actuators, A: Physical, 2005. **119**(1): p. 151-156.
 36. MacHauf, A., Y. Nemirovsky, and U. Dinnar, *A membrane micropump electrostatically actuated across the working fluid*. Journal of Micromechanics and Microengineering, 2005. **15**(12): p. 2309-2316.
 37. Astle, A.A., et al., *Theoretical and experimental performance of a high frequency gas micropump*. Sensors and Actuators, A: Physical, 2007. **134**(1): p. 245-256.
 38. Wu, J.D. and M.R. Bai, *APPLICATION OF FEEDFORWARD ADAPTIVE ACTIVE-NOISE CONTROL FOR REDUCING BLADE PASSING NOISE IN CENTRIFUGAL FANS*. Journal of Sound and Vibration, 2001. **239**(5): p. 1051-1062.
 39. Herbert P. Neff, J., *INTRODUCTORY ELECTROMAGNETICS*. 1991: WILEY. 72.
 40. SADIKU, M.N.O., *ELEMENTS OF ELECTROMAGNETICS*, ed. FOURTH. 2007, NEW YORK: OXFORD UNIVERSITY PRESS.
 41. William H. Hayt, J.J.A.B., *Engineering Electromagnetic*. p. page 225.
 42. Feustel, A., O. Krusemark, and J. Müller, *Numerical simulation and optimization of planar electromagnetic actuators*. Sensors and Actuators A: Physical, 1998. **70**(3): p. 276-282.
 43. de Bhailis, D., et al., *Modelling and analysis of a magnetic microactuator*. Sensors and Actuators A: Physical, 2000. **81**(1-3): p. 285-289.
 44. Chang, H.-T., *DESIGN AND MODELING OF A MEMS-BASED VALVELESS PUMP DRIVEN BY AN ELECTROMAGNETIC FORCE*. DTIP of MEMS & MOEMS, 2006.
 45. S.TIMOSHENKO, *THEORY OF PLATES AND SHELLS*. 1989.

46. Ventsel, E., *Thin Plates and Shells--Theory, Analysis, and Application*. 2001.
47. Wei-zang, C., et al., *The symmetrical deformation of circular membrane under the action of uniformly distributed loads in its central portion*. Applied Mathematics and Mechanics, 1981. **2**(6): p. 653-668.
48. Sherbourne, A.N. and W.C. Lennox, *Elastic large deflections of annular membranes*. J. Engng. Mech. Divis., Proc. ASCE, 1966. **92**(EM2): p. 75-99.
49. Kao, R. and N. Perrone, *Large deflections of axisymmetric circular membranes*. International Journal of Solids and Structures, 1971. **7**(12): p. 1601-1612.
50. Dutoit, B.M., P.A. Besse, and R.S. Popovic, *Planar multidipolar electromagnetic actuators*. IEEE Transactions on Magnetics, 2003. **39**(2 II): p. 1026-1034.
51. Kruusing, A., *Optimizing magnetization orientation of permanent magnets for maximal gradient force*. Journal of Magnetism and Magnetic Materials, 2001. **234**(3): p. 545-555.
52. Kruusing, A., *Actuators with permanent magnets having variable in space orientation of magnetization*. Sensors and Actuators, A: Physical, 2002. **101**(1-2): p. 168-174.
53. Dubois, M.R., H. Polinder, and J.A. Ferreira, *Varying magnetization orientation for permanent-magnet volume reduction in machines*. IEEE Transactions on Magnetics, 2003. **39**(3 II): p. 1793-1799.
54. Zhou, Y. and F. Amirouche, *Study of fluid damping effects on resonant frequency of an electromagnetically actuated valveless micropump*. The International Journal of Advanced Manufacturing Technology, 2009. **45**(11): p. 1187-1196.
55. Yufeng, S., et al., *Electro-magnetically actuated valveless micropump with two flexible diaphragms*. International Journal of Advanced Manufacturing Technology, 2006. **30**(3-4): p. 215-220.
56. Yamahata, C., F. Lacharme, and M.A.M. Gijs, *Glass valveless micropump using electromagnetic actuation*. Microelectronic Engineering, 2005. **78-79**(1-4): p. 132-137.
57. Doebelin, E.O., *MEASUREMENT SYSTEMS Application and Design*. Fourth ed. Mechanical Engineering. 1990: McGraw-Hill.

58. Ullmann, A., *The piezoelectric valve-less pump--performance enhancement analysis*. Sensors and Actuators A: Physical, 1998. **69**(1): p. 97-105.
59. Shoji, S., S. Nakagawa, and M. Esashi, *Micropump and sample-injector for integrated chemical analyzing systems*. Sensors and Actuators: A. Physical, 1990. **21**(1-3): p. 189-192.
60. Olsson, A., G. Stemme, and E. Stemme, *A valve-less planar fluid pump with two pump chambers*. Sensors and Actuators: A. Physical, 1995. **47**(1-3): p. 549-556.
61. Olsson, A., et al., *A valve-less planar pump isotropically etched in silicon*. Journal of Micromechanics and Microengineering, 1996. **6**(1): p. 87-91.
62. White, F.M., *Fluid Mechanics*. 384.
63. Ready, J.F., *Industrial Application of Lasers*. 1997, London: Academic Press.
64. David T.Eddington, W.C.C., and David J.Beebe, *Development of process protocols to fine tune Polydimethylsiloxane Material Properties*. 7th International Conference on Miniaturized Chemical and Biochemical Analysis Systems, 2003.
65. Murty, D.V.S., *TRANSDUCERS AND INSTRUMENTATION*. 1995, New Deihi: Prentice-Hall.